Advances in Mechatronics, Automation and Applied Information Technologies

Edited by
Q. Lu and C. G. Zhang

TRANS TECH PUBLICATIONS

Advances in Mechatronics, Automation and Applied Information Technologies

Edited by
Q. Lu
C. G. Zhang

Advances in Mechatronics, Automation and Applied Information Technologies

Selected, peer reviewed papers from the
2013 International Conference on
Mechatronics and Semiconductor Materials
(ICMSCM 2013),
September 28-29, 2013, Xi'an, China

Edited by

Q. Lu and C. G. Zhang

Trans Tech Publications Ltd
Kreuzstrasse 10
CH-8635 Durnten-Zurich
Switzerland
http://www.ttp.net

Volume 846-847 of
Advanced Materials Research
ISSN print 1022-6680
ISSN cd 1022-6680
ISSN web 1662-8985

Full text available online at *http://www.scientific.net*

***Distributed** worldwide by*

Trans Tech Publications Ltd
Kreuzstrasse 10
CH-8635 Durnten-Zurich
Switzerland

Fax: +41 (44) 922 10 33
e-mail: sales@ttp.net

and in the Americas by

Trans Tech Publications Inc.
PO Box 699, May Street
Enfield, NH 03748
USA

Phone: +1 (603) 632-7377
Fax: +1 (603) 632-5611
e-mail: sales-usa@ttp.net

Preface

It is our pleasure to welcome you to the 2013 International Conference on Mechatronics and Semiconductor Materials (ICMSCM 2013) in Xi'an, China. A major goal and feature of it is to bring academic scientists, engineers, industry researchers together to exchange and share their experiences and research results, and discuss the practical challenges encountered and the solutions adopted.

We hope you will have a technically rewarding experience, and use this occasion to meet old friends and make many new ones. Don't miss the opportunity to explore in Xi'an, China. And don't forget to take a sample of the many and diverse attractions in the rest of the China.

ICMSCM 2013 promises to be both stimulating and informative with a wonderful array of keynote and invited speakers from all over the world. Delegates will have a wide range of sessions to choose from and will have a difficult decision in deciding which sessions to attend.

This book covers these topics: Mechanics, Electronics and Industrial Informatics. We hope your experience with ICMSCM 2013 is a fruitful and long lasting one. With your support and participation, the conference will continue its success for a long time.

We would like to thank the organization staff, the members of the program committees and reviewers. They have worked very hard in reviewing papers and making valuable suggestions for the authors to improve their work. We also would like to express our gratitude to the external reviewers, for providing extra helps in the review process, and the authors for contributing their research result to the conference. Special thanks go to TTP Publisher.

We wish all attendees of t ICMSCM 2013 an enjoyable scientific gathering in Xi'an, China. We look forward to seeing all of you next year at the conference.

The Editors

Table of Contents

Chapter 2: Industrial Electronics, Communication, Sensors and Measurements

Chapter 3: Signal and Data Processing, Data Mining, Applied and Computational Mathematics

Chapter 4: Information Technology Applications in Industry and Engineering

Chapter 5: Semiconductors and Other Materials for Electronic Industry

CHAPTER 1:

Mechatronics, Automation and Control

Advanced Materials Research Vols. 846-847 (2014) pp 3-8

doi:10.4028/www.scientific.net/AMR.846-847.3

Input-Rate Based Adaptive Fuzzy Neuron PID Control for AQM

FAN Xunli[1,a] , Du Feifei[1] , XIE Zhenhua[2]

[1]School of Information Science & Technology, Northwest University, Xi'an 710127, China

[2]Qingdao Branch, Naval Aeronautical Engineering Academy, Qingdao 266041, China

[a] xunlfan@nwu.edu.cn

Key words: congestion control; fuzzy control; fuzzy neural; PID; self-adaptive

Abstract. Internet routers play an important role during network congestion. All the routers have buffers at input and output ports to hold the packets at congestion. Various congestion control algorithms have been proposed to control the congestion. Recently, some proportional-integral-derivative (PID) controller based algorithms have been proposed as Active Queue Management(AQM) schemes to address performance degradations of end-to-end TCP congestion control. However, most of the proposed PID-controllers for AQM are validated for their performance and stability via intuitive explanation and simulation studies instead of theoretic analysis and performance evaluation. But there are a few drawbacks of PID-controller based AQM algorithms leading to poor performance like causing data retention dropping and oscillation when the time delay is large, which means that the existing PID-controller can not meet the Quality of Service (QoS) requirements. To overcome the drawbacks of traditional PID, we analyze and enhance the PID-controller based AQM algorithm by regarding the TCP congestion control mechanism as an input-rate based Adaptive Fuzzy Neuron PID control algorithm(IRAFNPID) to avoid congestion in TCP/AQM networks. By means of simulations, we evaluate and compare the performance of traditional PID, single neural adaptive PID(SNAPID) and IRAFNPID, simulations with experiment data analysis and find that IRAFNPID has better convergence, stability, robustness, goodput and lower loss ratio.

1 Introduction

The essence of Internet congestion control is that a sender adjusts its transmission rate according to the congestion standard of the underline network. Network congestion takes place when arriving data exceeds available bandwidth, which may cause the degradation of link utilization, more round-trip time, and even make network inaccessible. But only increasing network resources can not solve the problem of traffic congestion effectively. Various kinds of congestion control algorithms have been put forward to control the congestion. Active Queue Management (AQM) has been proposed to convey congestion notification early enough to the senders, and accordingly, the senders are able to reduce the transmission rates before the queue overflows and avoid the packet loss. AQM has been a very active research topic[3-7]. The main target of AQM is to: 1) stabilize the queue lengths at a given target in order to make a good tradeoff between high goodput and low end-to-end delay; and 2) ensure high link utilization. Random Early Detection (RED) is a recommended congestion control mechanism[1]. In recent years, researchers design the TCP/AQM dynamic model using control theory, such as proportional integral differential controller(PID)[4,7], and neuron theory[2,8,9]. Traditional PID controller for AQM based on classical control theory is a typical representative, which was applied to solve congestion control problem of the intermediate nodes on the Internet, and the quality of network service was improved.

In this paper, a novel AQM scheme based on PID controller using input rate with adaptive and self-learning fuzzy neuron algorithm, suggests an input-rate based Adaptive Fuzzy Neuron PID control algorithm (IRAFNPID). The need for such an intelligent controller is justified because the Internet congestion control is complex and highly nonlinear. Compared with classical PID control algorithm, IRAFNPID can be more accurate in tracking target queue length, and the neuron adaptive learning strategy joined the routers with input rate can react more rapidly to network congestion, and is better adapt to the complicated network environment change.

2. Traditional PID Controller Scheme

The traditional PID controller is shown in Fig.1 and described by Equation(1).

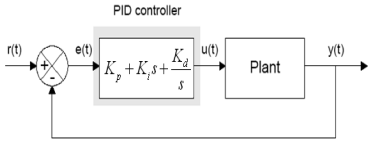

Fig.1 Traditional PID controller in *AQM*

$$p(k) = K_p e(k) + K_i \sum_{j=1}^{k} e(j) + K_d \left(\frac{e(k) - e(k-1)}{T}\right) \quad (1)$$

Where, Kp is the proportional gain, Ki is integration gain and Kd is derivative gain, which are the PID controller parameters respectively. T is the sampling time. p(k) is the packets dropping/marking probability, accordingly

$$e(k) = q(k) - q_0 \quad (2)$$

e(k) is the queue length error, q(k) is the queue length, and q0 is the target buffer occupancy.

3 Model of Adaptive Fuzzy Neuron PID Controller Based on Input Rate

Single neuron adaptive PID (SNAPID) is a kind of dynamic network structure comprised the PID control mechanism and neurons, which can adapt to the change of network environment with self learning and adaptive ability. The traditional PID controller parameters are not set according to the real-time adjustment. Therefore it cannot adapt to the complicated network environment. Neurons' self-learning capability can overcome the shortcomings of traditional PID. But the proportion coefficient of neurons in SNAPID is initially given, and cannot adjust itself online. To solve this problem, the paper puts forward an input-rate based adaptive fuzzy neuron PID(IRAFNPID) control scheme using routers input-rate to adjust the proportion coefficient of neurons dynamically, and to produce a better performance of convergence and robustness. The controller structure of IRAFNPID is shown in Fig.2.

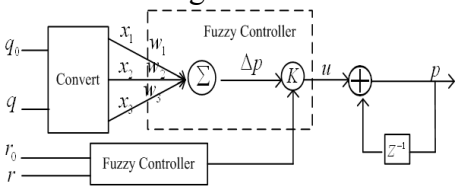

Fig.2 Fuzzy Control Based Rate of Neuron Adaptive PID Control

q0 is the target queue length, q is instantaneous queue length, r0 is routers expected input rate, r is routers instantaneous input rate, and p is packet dropping probability.

3.1 Model of Single Neuron Adaptive PID(SNAPID)

The input and output neuron mathematical model is described as Equation (3).

$$u(k) = K \sum_{i=1}^{n} w_i(k) x_i(k) \quad (3)$$

Where, K is the neuron proportion coefficient, xi(k) is the neuron input, wi(k) is weighted coefficient of xi, and u(k) is the neuron output, the single neuron input model is

$$\begin{cases} x_1(k) = q(k) - q_0 = e(k) \\ x_2(k) = e(k) - e(k-1) \\ x_3(k) = e(k) - 2e(k-1) + e(k-2) \end{cases} \quad (4)$$

The differential form of PID control can be expressed as:

$$p(k) = p(k-1) + K \sum_{i=1}^{3} w_i(k) x_i(k) \quad (5)$$

SNAPID controller's output depends on the weights wi(k). In order to make the intermediate node's instantaneous queue length q maintain in the near of q0. According to Hebb[4], the learning rule of a neuron is formulated by

$$w_i(k+1) = (1-c) w_i(k) + \eta e(k) p(k) x_i(k) \quad (6)$$

Where, η is the learning rate and η>0 and c is constant. In order to guarantee the adaptive neuron PID controller learning convergence and robustness, it adjusts the correction through Equation(7)[8].

$$\begin{cases} w_1(k) = w_1(k-1) + K_P e(k) p(k)(2e(k) - e(k-1)) \\ w_2(k) = w_2(k-1) + K_I e(k) p(k)(2e(k) - e(k-1)) \\ w_3(k) = w_3(k-1) + K_D e(k) p(k)(2e(k) - e(k-1)) \\ w_i(k) = w_i(k) / \left| \sum_{i=1}^{3} w_i(k) \right| \end{cases} \tag{7}$$

Where, Kp, KI and KD represent proportion, integral, and differential gain of the learning rate respectively.

3.2 The Improvement of Learning Rate

We should consider not only the error between instantaneous queue length q and target queue length q0 in the negative gradient direction, but also the trend of error function. In order to avoid the weights of learning process, slow down the rate of convergence, we add a momentum, which adds the previous weights to the current weights. The improved weights learning algorithm is the following.

$$\begin{cases} w_1(k+1) = w_1(k) + \eta_P e(k) p(k)(e(k) + \Delta e(k)) + \alpha(w_1(k) - w_1(k-1)) \\ w_2(k+1) = w_2(k) + \eta_I e(k) p(k) e(k) + \alpha(w_2(k) - w_2(k-1)) \\ w_3(k+1) = w_3(k) + \eta_D e(k) p(k)(e(k) - \Delta e(k)) + \alpha(w_3(k) - w_3(k-1)) \end{cases} \tag{8}$$

Where, $\Delta e(k)=e(k)-e(k-1)$, and α is correction coefficient.

3.3 Input-Rate Based Adaptive Fuzzy Neuron PID

SNAPID's neurons proportional coefficient K is set initial time, which can not adjust online. The experiment results show that the K is the sensitive parameters. When K is bigger, the system responds quickly which causes the big overshoot, even makes the system unstable. When K is small, the system responds slowly and the convergence speed is different. In order to make SNAPID proportion coefficient K adjust online, fuzzy control is introduced using routers' input rate r(k) and the expected input-rate r0 as input variables. To accommodate a data flow, input rate r(k) is measured by Equation(9).

$$r(k) = (1 - f')\frac{l_k}{T} + f'r(k-1) \tag{9}$$

Where, T is the sampling period, lk is the first k sampling cycle to the total number of data packets, which is a constant. Here it takes for 0.1, f is a factor which affects the measurement results.

Let re(k)=r(k)-r0, rec(k)=(r(k)-r0)-(r(k-1)-r0)=r(k)-r(k-1). For the fuzzy controller with two input variables, the fuzzy controller's output variable is the first k sampling period of IRAFNPID with learning rate η(k). So K(k)=η(k)K(k-1), re(k) is the first k sampling of queue transmission rate, and the expected rate differential rec(k) is re(k) change rate. The input variable re and rec are divided into five fuzzy set {NB,NS,Z,PS,PB}. The fuzzy function of input variable is shown in Fig.2. The output variable is divided into seven fuzzy set {SL, ML, BL, M, SH, MH, BH}, and the fuzzy function of output variable is shown in Fig.3.

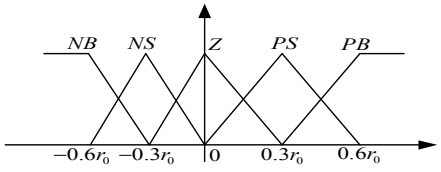

Fig. 2 The fuzzy membership function for input variables

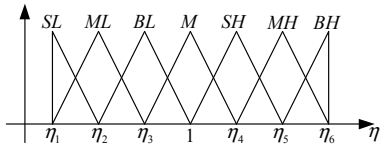

Fig. 3 The fuzzy membership function for output variable

Fuzzy controller control rule is expressed as:

IF re is rei and rec is recj, THEN ηij, i, j=1,2,…,5

According to the fuzzy control experience, the fuzzy control rules are illustrated in table 1.

Therefore, the first k sampling period of learning rate can be expressed as Equation(10).

$$\eta(k)=\frac{\sum_{i=1}^{M}\{y_i\mu(re_i)\mu(rec_i)\}}{\sum_{i=1}^{M}\{\mu(re_i)\mu(rec_i)\}} \quad (10)$$

Where, M is the total number of fuzzy rules, yi is the first i time rules of the output interval value, rei and reci are the ith fuzzy rules of the corresponding fuzzy set of re and rec. μ(x) is the first i set of the fuzzy membership function.

Table 1 Fuzzy control rule table

re \ rec	NB	NS	Z	PS	PB
NB	BH	BH	BH	BH	BH
NS	MH	MH	MH	BL	BL
Z	M	M	M	M	M
PS	ML	ML	ML	SH	SH
PB	SL	SL	SL	SL	SL

4 IRAFNPID Performance Simulation

We examine the sensitivity of control performance of PID, SNAPID, and IRAFNPID algorithms.

4.1 Simulation Parameters

The simulation topology is shown in Fig.4. We simulate the algorithms using NS2 tool[10].

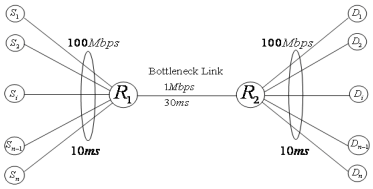

Fig. 4 Simulation Network Topology

Bottleneck link is located in router R1, R2, the link capacity is 1Mbps, and the link delay is 30ms. S is the source end which is connected to router R1, the link capacity is 100Mbps, and the link delay is 10ms. D is the destination end which is connected to router R2, the link capacity is 100Mbps, and the delay is 10ms. The queue management algorithm in router R1 uses PID, SNAPID, and IRAFNPID respectively, and the other nodes use DropTail algorithm. The buffer at the bottleneck has capacity of 300 packets and the target queue length value is set to 150 packets.

The parameters of PID controller are set as Kp=2.268×10-5, KI=4.193×10-5, KD=4.1225×10-7. Neuron proportion coefficient is K=6.4×10-4. IRAFNPID controller parameters of the learning rate and the proportion of neurons with SNAPID coefficient, the learning rate correction coefficient α=0.005, η1=0.5, η2=0.7, η3=0.95, η4=1.01, η5=1.04, η6=1.07, and r0 take for link capacity.

4.2 Performance Comparison of Constant Load

We examine the control performance in terms of instantaneous queue length, packet loss, link delay and throughput under two different traffic load conditions(N=150 and 300). The target queue length is 150Packets. The instantaneous queue length of three algorithms is shown in Fig.5 and Fig.6 respectively.

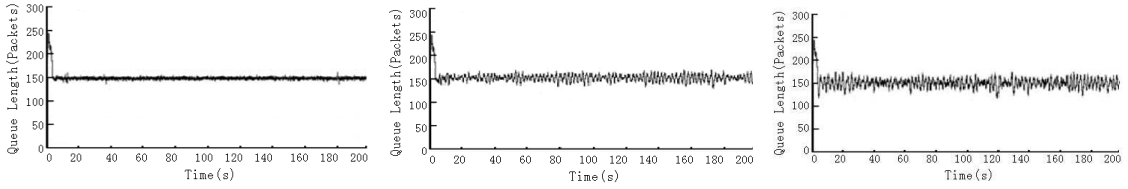

(a) The queue length of *IRAFNPID* (b) The queue length of *SNAPID* (c) The queue length of *PID*

Fig.5 Comparison of queue length for 150 sources

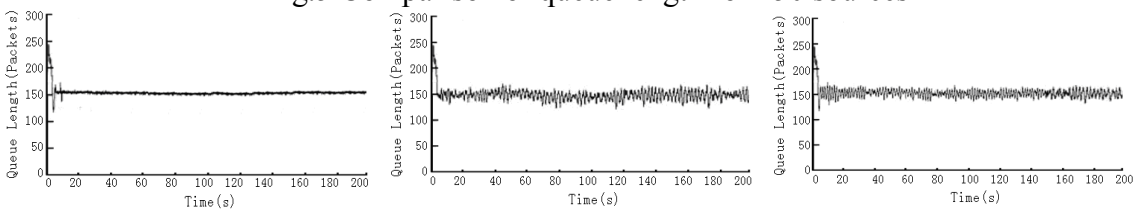

(a) The queue length of *IRAFNPID* (b) The queue length of *SNAPID* (c) The queue length of *PID*

Fig.6 Comparison of queue length for 300 sources

From the simulation results, it is clear that IRAFNPID shows good control performance independent of traffic load levels in terms of the queue length dynamics around packets.

4.3 The Steady-State Control Performance

4.3.1 Performance Metrics

Control performance of an AQM algorithm can be measured by two measures: the transient performance and the steady-state error control. Here we use the instantaneous queue length as a

performance metric for the transient performance. For the steady-state control performance, we use the quadratic average of control deviation(QACD),which is only applicable to PI and PID-controller and defined as follows.

$$S_e = \sqrt{\frac{1}{M+1}\sum_{i=1}^{M} e_i^2} = \sqrt{\frac{1}{M+1}\sum_{i=1}^{M}(q_i - q_0)} \tag{11}$$

Where q0 is the target queue length, qi is the ith sampled queue length; M is the number of sampling intervals.

4.3.2 Simulations of control performance

The steady-state control performance of IRAFNPID, SNAPID and PID-controller can be evaluated in terms of QACD at two different traffic load levels: 150, and 300 flows. Table 2 shows the mean of QACD of three algorithms under two different traffic loads. Table 3 shows the average rates of delay of three algorithms under several traffic load levels. IRAFNPID reduces the delay compared with traditional PID algorithm. Table 4 shows the average ratio of packet loss and Table 5 shows the average of goodput. It can be seen from the tables that goodput are comparable for all these schemes. IRAFNPID performs best in terms of packet loss is concerned followed by SNAPID controller. PID has more packet loss than either of the other schemes. In summary, IRAFNPID works same well as the other schemes for goodput, but has less delay and slightly higher packet loss than other schemes.

Table 2 Mean of *QACD* of *AQM* algorithms (packets)

No. Sources	*IRAFNPID*	*SNAPID*	*PID*
150	6.45	10.42	16.80
300	8.90	12.45	20.38

Table 3 Average delay rates of *AQM* algorithms in "ms"

No. Sources	*IRAFNPID*	*SNAPID*	*PID*
150	4.56	5.17	6.32
300	4.93	5.68	6.59

Table 4 Average packet loss ratio of *AQM* algorithms *"%"*

No. Sources	*IRAFNPID*	*SNAPID*	*PID*
150	6.52	7.89	8.67
300	9.36	11.48	13.23

Table 5 Average goodput of AQM algorithms *"kpbs"*

No. Sources	*IRAFNPID*	*SNAPID*	*PID*
150	7746.62	7743.32	7742.32
300	7866.62	7862.32	7860.32

4.3.3 Loss Ratio

Loss ratio is the rate of the number of packets dropped and the number of packets sent. In this experiment, the load varies from 50 to 300 TCP sessions and the results are shown in Fig.7. It is clear that the loss ratio of IRAFNPID is the lowest. We find that the performance of IRAFNPID is much better than SNAPID and PID because of the efficient management of the buffer space and the variation in the target value.

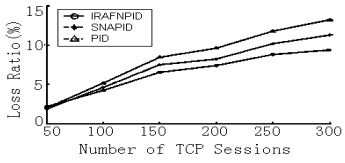

Fig.7 Comparison of Loss Ratio

5 Conclusion

The paper introduces a mode of input rate based adaptive fuzzy neuron PID controller, and uses routers' input rate to control neurons proportion coefficient adjusting online, and correct the neuron learning rate. Simulation results show that compared with PID and SNAPID, IRAFNPID has the advantage of faster convergence performance, robustness, better stability and goodput, and lower loss ratio.

Acknowledgement

This work was supported in part by Natural Science Foundation of China under Grant 61202393, the Scientific Research Foundation for the Returned Overseas Chinese Scholars, State Education Ministry, Natural Science Basic Research Plan in Shaanxi Province of China, and Scientific Research Program Funded by Shaanxi Provincial Education Department under Grant 12JK0935.

Reference

[1] S Floyd, V Jacobson, Random early detection gateways for congestion avoidance, IEEE/ACM Transactions on Networking, 1993, 1(4): 397-4133

[2] S Behrouz, M R Amir, E Mahdipour, A New Fuzzy Congestion Control Algorithm in Computer Networks, International Conference on Future Computer and Communication, 2010: 314-318

[3] K S Pramod, K G Santosh, Variable Length Virtual Output Queue Based Fuzzy Adaptive RED for Congestion Control at Routers, IC3 2011, CCIS 168, Springer-Verlag Berlin Heidelberg, 2011: 123–134

[4] X Liu, J Hu, S Wang, and et al, Research of AQM Strategy Based on Improved Neural Adaptive PID, International Conference on Computer Science and Information, Singapore, 2008: 147-151

[5] C Zhou, J He, Q Chen, A robust active queue management scheme for network congestion control, Computers & Electrical Engineering, 2013, 39(2): 285-294

[6] N Zhang, G M Dimirovski, Y Jing, AQM Algorithm Based on Kelly's Scheme Using Sliding Mode Control, 2009 American Control Conference, 1575-1579

[7] X Fan, J Wang, L Guan, and et al, Heuristic Active Queue Management with Hazard Rate Function, ICNC'11-FSKD'11, 2011: 2281-2285

[8] L Chong, M Abbas, A M Flintsch, and et al,A rule-based neural network approach to model driver naturalistic behavior in traffic, Transportation Research Part C, 2013, 32: 207–223

[9] Z. A Mohammed, A. S Shahad, Particle Swarm Optimization Based Fuzzy-Neural Like PID Controller for TCP/AQM Router, Intelligent Control and Automation, 2012(3): 71-77

[10] The Network Simulator (NS2), http://www.isi.edu/nsnam/ns/, 2012-11-10

Advanced Materials Research Vols. 846-847 (2014) pp 9-12

doi:10.4028/www.scientific.net/AMR.846-847.9

The Knowledge in Artificial Intelligence

Kunlong Zhang[1, a],Lixia Song[1,b]

[1] North China Institute of Science and Technology Beijing, 101601, China

[a] zhkl007@126.com , [b] Songlx100@sina.com

Keywords: Artificial intelligence, knowledge based intelligent systems, hybrid intelligent systems, Intelligent machines.

Abstract. The objective of this work was to investigate the concept of knowledge in order to obtain useful for the techniques of artificial intelligence and knowledge representation. several definitions of knowledge proposed by various authors are analyzed, compared and graded, they are then merged into a new definition, which is partially formalized tools logical-algebraic, and finally, discusses the possible links with the areas of intelligence artificial intelligence and knowledge representation.

1. Introduction

What is knowledge ? Philosophers have investigated for thousands of years on this issue, without going as far as I know , for a definitive answer. Then I will not be so presumptuous as to try to respond fully to this question : I will try rather to present some observations and reflections concerning the knowledge in a more organic way possible.

The objective of this study is to investigate the nature of the concept of knowledge (hereafter K , English knowledge) in order to obtain useful information for the techniques of knowledge representation (KR , from knowledge representation) or more generally artificial intelligence (AI). In these notes do not expose consolidated certainties , but ideas and arguments on which I'm still thinking about it. You can investigate the K from different points of view :

• formal logical : use the tools of mathematical logic to give definitions and formal proofs . This methodology is that the results of which are definitely less objectionable , but at the same time probably more limited;

• psychological and cognitive perform psychological experiments on a sample of subjects. The validity of this method is ensured by statistical considerations , but it takes a considerable effort ;

• philosophical- epistemological -IA : reflect, in an intuitive, on general considerations . It is without a doubt the point of view less "scientific" , but what I think is most suited to the initial phase of a study. It is those optics adopted here .

As mentioned, the K has long been an object of study of philosophers, without definitive results. In recent decades , thanks to the development of the industry of AI , and more in particular in the sector of the KR , the term " knowledge" is returned fashion , without that for this has come to a complete understanding of the phenomenon[1 , 2] .

This paper is structured as follows:In section 2, I present and discuss some definitions of K from the literature. In section 3, summarize the features in my opinion correct in a further definition. In section 4, I outline a possible formalization of the situation.In section 5 put in relation to the survey results carried out on K with the AI and finally.

2. Knowledge: some definitions

In this section are some definitions (or pseudo- definitions) of K found in the literature, mainly in the work of IA , and representatives of the most widespread opinions . I have divided these definitions into five categories as follows:

1) K = abstract data [3,4];
2) K = data and relations between them[5] ;
3) K = data related to the real world[6] ;
4) K = data to act [7];
5) K = property to explain the behavior[8] .

3. Knowledge : an attempt to define

Combining the latest definitions of the preceding paragraph has a fairly realistic, but in my opinion this framework can be made more clear and complete . In this section I make an attempt in this direction , proposing what later call " the definition of K" , but in reality is only a list of characteristics that K must have in my opinion . Here is the list :

• K is a characteristic that can be ascribed to an agent A1 , A2 attributed to another agent ;

• the assignment of K is an abstraction that allows to explain the behavior of A1, A2 .

• purposes A1 play an important role : A1 wants to understand , to explain the behavior of A2, and then attaches the K ;

• This assignment is perhaps not completely arbitrary , but it is certainly subjective;

• This assignment is not an atomic operation , as it can be decomposed into 2 most basic operations . First, the observer identifies herself in the agent A1 and A2 observed imagines perform the same actions (operation of identification), then A1 performs an introspection to explain to himself the behavior that he observed another agent A2 and imagine to play . In other words, it is as if A1 is saying, "If I were in A2 , and were to act like that, my actions could be explained by assuming that I have a certain K ";

• also the task of identification can be further analyzed : it is in fact a special case of the function of creating a counterfactual world . In the case of the function of identification , the counterfactual world created is one in which the viewer imagines himself to be the agent A1 A2 ;

• K to be learned (learned) : the only beings that are believed unanimously " have K" are human beings and K is a property that we humans learn by experience. As a result, the K is a dynamic property , evolving . However, it is important to note that learning does not start with a " clean slate " , but from a basic innate brain , obtained by the evolution of the species .

Prior to investigate the consequences of this definition of K on AI, I summarize the situation in a more formal way.

4. A more formal approach

The situation is shown schematically : *As* the agent ("s" is derived from "see") notes the agent *Aa* ("*a*" from "act"). *As* also identifies an environment in which *Aa* acts: such environment is denoted $E_{As}(Aa)$ ("E" from the English "environment"), to be read "the environment *Aa* by *As*."

As The agent observes the actions of *Aa*; these actions constitute the behavior of *Aa* observed *As*; behavior is indicated by $B_{As}(Aa)$ ("B" from "behavior"). In order to explain the behavior of *Aa*, *As* attributes K, denotabile with KAs (*Aa*) (K attributed to the *As* to *Aa*).

One might suppose that $K_{As}(Aa)$ depends only on the environment and the behavior, or, in symbols (indicating with attr function assignment of K):

$$K_{As}(Aa) = attr\,(E_{As}(Aa), B_{As}(Aa)).$$

But this is not true, as shown by the examples of the chess program and the thermostat are presented at the end of section 2. In fact (if the program that plays chess), if we consider another agent *Aa*', although that $B_{As}(Aa') = B_{As}(Aa)$ and $E_{As}(Aa) = E_{As}(Aa)'$, you can have that

$$K_{As}(Aa) \neq K_{As}(Aa'),$$

then to the $K_{As}(Aa)$ also depends on the agent *Aa*. Similarly (case of hermostat), if we consider two observers *As* and *As*', despite having $B_{As}(Aa) = B_{As'}(Aa)$ and $E_{As}(Aa) = E_{As'}(Aa)$, you can have that

$$K_{As}(Aa) \neq K_{As'}(Aa),$$

and then the $K_{As}(Aa)$ also depends on the observer. In summary, the $K_{As}(Aa)$ is therefore a function of the agent and the observer:

$$K_{As}(Aa) = attr(Aa, As, E_{As}(Aa), B_{As}(Aa)).$$

The formalization of the scenario proposed here is not complete, and certainly would require further work. However, the road is drawn and then here there is no continuation of this line; hint instead ties existing between the above and the AI industry.

5. Artificial intelligence

The definition of K with section 3 may seem correct, but it certainly raises doubts about its usefulness pratica.Comunque , the usefulness of this definition occurs if the endeavor to understand the work of AI , or KR.In this paragraph , first briefly summarize the procedure followed for the construction of a knowledge base (section 5.1) and then, in section 5.2 , illustrate the weaknesses of that procedure in the light of the definition of K presented in section 3.

5.1 The construction of a knowledge base

The KR has the aim of representing the knowledge that we humans use to perform certain tasks so that they are usable by a computer to play (or, if it is of the opinion Searle illustrated by the last quote of paragraph 2.5, simulate) our behavior. We analyze in detail the steps that are being taken in this work of representation :

1) the behavior of an agent *Aa* is observed . Using the terminology of section 4, it can be said that there is an agent *Aa*, acting in his room , another agent that identifies *As* the environment $E_{As}(Aa)$ and observes the behavior of *Aa*, $B_{As}(Aa)$;

2) the purpose of *As* is to explain the behavior of *Aa* and for this purpose he attributes to the $K_{AS}(Aa)$, ie the knowledge sufficient to explain his behavior. To do so , *As* first performs an operation of identification , that creates a counterfactual world (the world obtainable from " *As* if it were *Aa*, ..."), and then an operation of introspection.

5.2 The weaknesses of artificial intelligence

In the process described in section 5.1 we can identify some weaknesses :

• the environment $E_{As}(Aa)$ is a function of the observer *As*;

• the behavior $B_{As}(Aa)$ s a function of the observer *As*;

• the outcome of the allocation of K is not unique. In fact, this operation is inductive (induce a general rule from the observation of specific facts) and, for the principle of the poverty of the stimulus, the outcome of this assignment is not unique, as a stimulus for which you want to capture the regularity can be completed in infinite ways;

• the operation of construction of a world counterfactual (component , as already repeated several times , the operation of identification) is inherently problematic because it is not able to define all the conditions that must vary with respect to the real world (what that is named ceteris paribus - see [9]) ;

• the operation of introspection is obviously subjective (each performs it " his way "), but is also problematic because you can not be sure that what we think we " see" inside of us is correct ;

• are completely absent any form of learning and evolution of K : is the programmer (or knowledge engineer) that provides the K computer " beautiful and ready ." Visas and considered all of these issues , we can certainly detect that the objective of the KR is ambitious and because the methodology is questionable , and this perhaps explains why the KR and, therefore , the AI are far from having reached a stable condition and satisfactory.

6. Conclusions and Future Work

The questions raised in this paper are more numerous than an provided, these questions can assist a reflection, which places the investigation of K in a more general. There are several concepts that we human beings we commonly use, but they seem to not be defined formally, such as life, intentions or will. I believe that an integrated study of these concepts can provide more answers than unidisciplinare an approach similar to the one shown here.

In addition, the criticisms of the methodology of AI in the previous paragraph are not purposive, perhaps due to the fact that the approach adopted in the field of KR is the best available, at least for now. However, this work illustrates how an understanding of the "phenomenon knowledge" is limited and approximate and the questions proposed, together with the completion of the formalization of the scenario outlined in section 4, can be a useful agenda to improve this understanding.

Acknowledgements

This work described here is partially supported by “the Fundamental Research Funds for the Central Universities.

References

[1] Brachman, R. J. e Levesque, H. J., Readings in Knowledge Representation, Morgan Kaufmann, Los Altos, California[M]. 1985,

[2] Charniak, E. e Mc Dermott, D., Introduction to artificial intelligence, Masson, Addison-Wesley[M]. 1988,

[3] Wong, H. K. T., and Mylopoulos, J., 1977. Two views of data semantics: data models in artificial intelligence and database management, INFOR[C], 15(3): 344-383

[4] Wiederhold, G., Knowledge versus date. On knowledge Base Management Systems: 1986.77-82.

[5] Longo, G. O., From the Golem to Godel and return, Machines and Automata[C], 1995,75-106.

[6] Searle, J. R., The mind is a program, In The Science[J], 259(3), 1990: 16-21.

[7] Newell, A., The knowledge level. In Artificial Intelligence[J], 18(1): 87-127.

[8] Genesereth, M. R. and Nilsson, N. J., Logical Foundations of Artificial Intelligence, Morgan Kaufmann, Los Altos, CA. 1987.

Advanced Materials Research Vols. 846-847 (2014) pp 13-17

doi:10.4028/www.scientific.net/AMR.846-847.13

Design of Induction Heating power based on the power adjusting technique and the frequency tracing

WANG Yao-chen[a] ,HE Hui-wei[b],YAN Dong-chen[c] ,XIONG Jin-hui[d]

Electronic Engineering Department ,City University of Hong Kong,Hong Kong,999077,China

[a.] aaronchenwang@Gmail.com [b]. peterhehk@gmail.com

[c.] ydc903911814@gmail.com [d.] 363942836@qq.com

Keywords: power adjusting technique; frequency tracing; phase locked loop control; induction heating

Abstract. The ultrahigh frequency (more than 1MHz) of the HF Induction Heater need to be reached for surface-heat-processing of tiny mental components, which is not available by the traditional HF Induction Heater. To satisfy these requirements, by using the high-speed field effective transistor (FET) and high-speed phase-locked loops (PLL: MM74HC4046), the frequency of inverts for induction heater and the power can arrive at more than 1MHz and 5.5kW respectively at the same time. Additionally, it achieves the power adjusting technique and the frequency tracing. The experimental shows that this design can both achieve the high frequency and efficiency, and meet the requirement of the surface-heating-process of the tiny components.

Introduction:

Induction heating is a non-contact heating process, which uses high frequency electricity to heat materials that are electrically conductive. [1] Induction heating has the advantages of energy-efficient, high heating-rate, suitable factors of local heating, and less surface-oxide-layer，so induction heating has been widely applied nowadays. With the development of metal melting and the increasing requirements of metal surface heat treating, different kinds of inverters are widely used in induction heating applications, which lead to higher requirements to the inverter. Then different manufacturing engineering results in the different requirements to power and frequency of the inverter. Frequency varies from dozens of Hertz to several mega Hertz, while power varies from hundreds of watt to hundreds of kilowatt, and even to megawatt. The higher frequency of heating, the more concentrated of power, the shallower heating surface will be led to. The hardening for the surface of some small parts requires a frequency that reaches up to several megawatts, for example. In the early nineties， the GP series Vacuum tube H.F induction heating equipment, as the most popular H.F induction heating equipment , can achieve the high frequency(Power grade: 60 kW~1500kW, Frequency range: 20kHz~1500kHz) by GP series H.F. vacuum tube welder adopts vacuum tube[2] and ,at present, the inductive heating power sources with a frequency higher than hundreds of kilohertz and a power higher than thousands of watts are mainly manufactured by vacuum tubes. However, the vacuum tubes are not only large in size, but short in service life. The efficiency of them is also relatively low（less than 30%）.In 1996, shen chen and wu yaolin manufactured the MOSFET high frequency power supply(power:20kW, frequency:300kHz)[3] and shen jinfei and hui jing developed it in 2002(power:1kW, frequency:2MHz)[4]., However，, it is hard to achieve the high frequency together with the large power at the same time(Generally, it cannot meet 3kW AND 1MHertz in the meantime) and its low efficiency also cannot be ignored. So the inductive heating inverter for surface hardening made of complete semiconductors with a frequency of 1MHz and power of 5 kW is introduced. It applies the high-speed phase-locked loops (PLL: MM74HC4046), which leads to the realizing of frequency tracing and automatic power control (APC). The efficiency of this kind of inverter is higher than 80%.

2.Main Circuit of the Inverter

For the inductive heating powers with a relatively low power, series resonance has its own advantages.

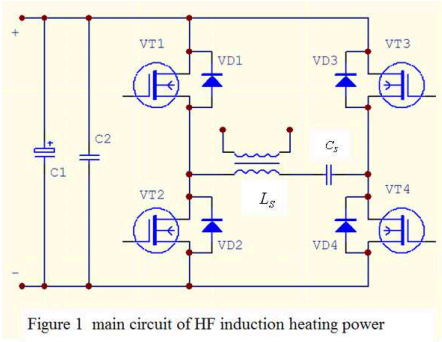

Figure 1 main circuit of HF induction heating power

Figure 1 shows the main circuit of it. A DC voltage is obtained from 220V power supply after uncontrolled rectifier and capacitor filtering. In order to achieve high frequency, the FET is used. Because of the limited current of a single transistor, each unit of H bridge circuit made of a 6-parallelled-FET unit is applied to increase the output power. To simplify the system, the method of adjusting power factor is applied to adjust the power. Although the efficiency is not very high, it can obviously simplify the complexity, reduce the cost, and enhance the reliability of the system, especially for some low powers.[5]

The inverter bridge is made from 4 groups of high-speed FET, from VT_1 to VT_4, and each FET is anti-parallel connected with a fast diode respectively. Figure 2 shows the wave shape of the voltage and current. At $t=t_0$, VT_1 and VT_4 are on, and a positive voltage is applied on the load network. At this moment, the current is still reversed and the follow current comes from the freewheeling diode VD_1 and VD_4. As the load is a resonant network and Q is much greater than 1, i_0 changes like a sinusoidal variation. At t_1, the current drops to zero, and the current through VT_1 and VT_4 gradually becomes positive and it is actually an increasing sinusoidal wave from 0. At t_2, VT_1 and VT_4 are turned off. Because of the continuity of the current, the resonant circuit produces a negative electromotive force, which keeps the current flowing. At this time, the freewheeling diode VD_2 and VD_3 are on and produce a circuit with the power source, which makes the load produce feedback energy to the power. During the period of freewheeling of VD_2 and VD_3, after a dead-time(FET spend more time on turning off than turning on. In order to make sure its safety, during a short time, all are opened, called "dead-time"), VT_2 and VT_3 are turned on. There is no current at all until t_3, and current is transferred from VD_2 and VD_3 to VT_2 and VT_3 respectively, which realizes the ZCS (zero-current-switching). At t4, VT_3 and VT_4 are turned off and current goes to VD_1 and VD_4. After the dead-time, VT_1 and VT_4 are turned on. At t_5, current starts to go through VT_1 and VT_4. The above processes form a whole cycle of the system. The resonant frequency f of the system is defined by the factors of the load network, that is：

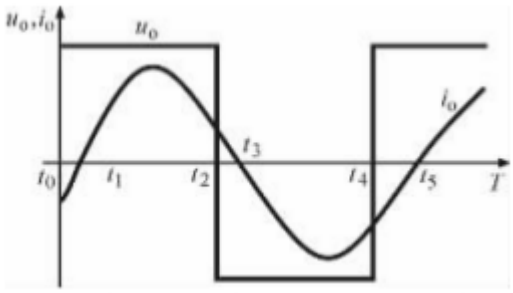

Figure 2 wave shape of current and voltage in the series resonance branch

$$f = \frac{1}{2\pi\sqrt{L_S C_S}}$$

where Cs equals the load capacitance of the resonant network and Ls is the inductance of the whole circuit, including the reflected inductance of the load.

The working frequency of the system, f_s, is a little bit higher than f_o.

3. Design of the Control Circuit

The resonant frequency of inverters for induction heating is greatly influenced by the load. Because of the differences in size of the parts and the environmental temperature, automatic tracing

of the frequency needs doing in order to get the best heating effect. Traditional method is to apply the SG3525[6]. Some other methods are also applied, for example, applying the PLL CD4046 or DSP. But for the frequency at megahertz high, the above ways can't work as usual. Thus, the design of using high-speed PLL MM74HC4046 as control circuit is applied. The highest frequency can reach up to 10MHz, with a very wide sweeping range. The frequency is automatically traced and phase adjustment can be also done in this way.

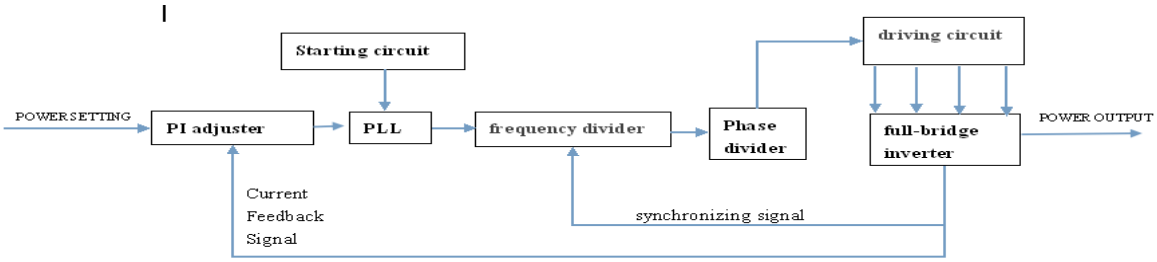

Figure 3 the chart of the control circuit.

Figure 3 is the chart of the control circuit. From the main circuit and the wave shape in figure 2, the load voltage leads the current an angle Φ. It is obvious that the larger the Φ, the smaller the active power of the output. Thus the output power can be controlled by changing the angle Φ.

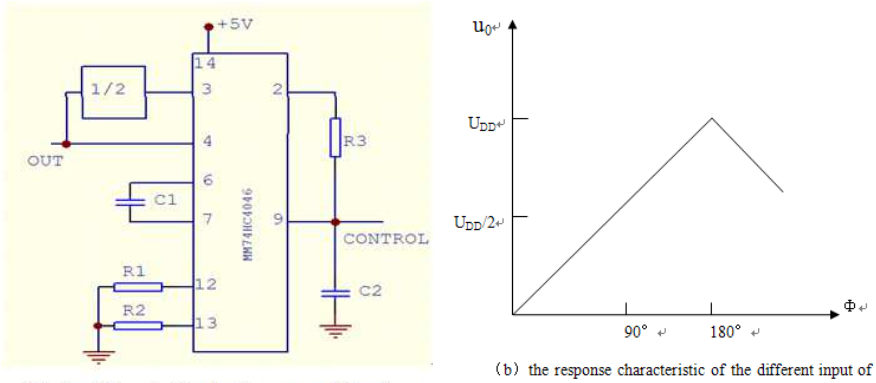

(a) circuit for controlling the frequency and phase

(b) the response characteristic of the different input of the Phase Comparator and u_0

Figure 4 Circuit for controlling the frequency and phase and the response characteristic

The operating frequency of MM74HC4046 is much higher than CD4046, but the internal structure and operating principle of them are almost the same. The power supply is +5V. Figure 4a shows the frequency control and phase adjustment circuit made by the PLL MM74HC4046. Firstly, the operating frequency range is defined by the possible load of the high frequency inductive heating power, and the central frequency and sweeping range can be defined then. The factor of C_1 and R_1 ensures the sweeping range, while R_2 defines the central frequency of the sweeping. The sinusoidal current of the load can be measured from the series resonance branch with the help of current transformer. After the wave shaping circuit, the square wave with the same phase as the sinusoidal wave can be produced and it is applied to the isochronous terminal of the PLL. The output signal of the PLL goes through the frequency divider and goes to the comparison terminal. The phase of these two signals are compared at the input terminal of the frequency discriminator of the PLL. If the phase difference equals zero, the average output voltage of the phase discriminator is zero. If the phase difference is 180°, the output is 5V. Figure 4b is the linear relationship between the output voltage u_0 and the phase difference. When the output square wave of the PLL is of the reversed direction as the resonance current, the pulse output of the phase discriminator exist a certain cycle ratio, which is filtered by the frequency divider low pass filter consists of R_3 and C_2. Then the filtered DC voltage adjusts the output frequency of the V_{OC}. If there is no other control signal, the output signal of V_{OC} will be synchronous with the resonance current, which means Φ equals zero.

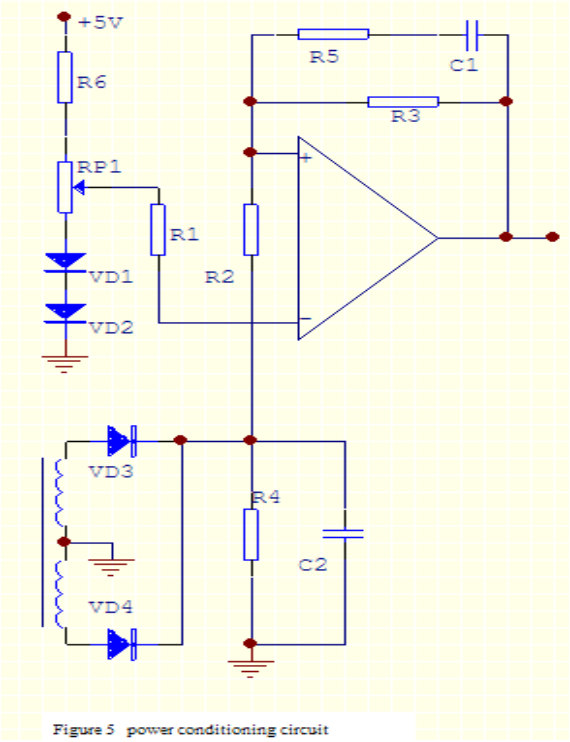

Figure 5 power conditioning circuit

When designing the circuit, the output voltage signal of the regulator u_0 is used to control the V_{OC} to achieve the goal of controlling the power. The power control is achieved by controlling the current. Figure 5 is the circuit of it. Power setting is determined by u_i, which is applied by the potentiometer and goes directly to the input of the operation amplifier. In order to guarantee the stable starting of the power, u_i has a minimum restriction, which is determined by the positive step-down of VD_1 and VD_2. The feedback voltage u_f is obtained from the load current going through the current transformer, after rectification and filtering. u_i is applied to the non-inverting terminal of the regulator, while u_f is applied to the inverting one. No matter what changes, the regulator can adjust u_0 automatically, until $u_f=u_0$ at last. The design can then change the way PLL works. The u_0 from the regulator will be used as the internal control signal of V_{OC}, which makes the operation frequency of the system f_s deviates from the resonance frequency f_0 and makes u_0 keep a certain phase difference Φ compared with load current i_0. The adjustment of u_i can then influence the angle Φ, thus control the power.

4.Design of Drive Circuit

In the high-speed induction heating power source, the signal transmission needs to be fast enough, the distortion of the wave needs to be small enough, and the drive power needs to be strong enough to guarantee the reliability of switching of the power part. The system applies the pulse transformer driving circuit, which can reach the highest transmission rate. Figure 6 shows the circuit of it. The phase-splitter circuit outputs two inverting signals with dead-time and applies them to the two grids of two MOSFETs respectively, which makes the MOSFETs on alternatively. The first stage of transformer produces a positive-negative polarity pulse voltage and after coupling, L_3 and L_4 will get a similar driving voltage as the primary voltage. It will drive the two electronic components of a single arm of the inverter bridge. The other arm of the bridge is of the same way, which makes the inverter bridge work safely when the phase is correct.

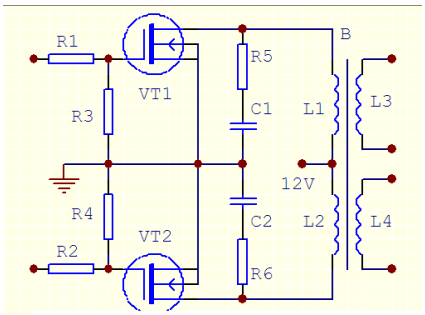

Figure 6 drive circuit

5.Experimental Results and Conclusions

According to the requirements of the experiment, design and manufacture a prototype of the high-speed induction heating power source. The actual input is 220V AC, the sweeping range is from 1.5MHz to 400kHz, the operating frequency is between 650 to 950kHz, the output power is between 0.3 to 5.5kW with adjusting continuance. The efficiency is around 82%. Figure 7 shows the experimental wave shape of load voltage u_0 and load current i_0 when the power output varies (Φ varies). The following statements are the conclusions.

- It is appropriate to apply the high-speed PLL MM74HC4046 to design the 10MHz high-speed induction heating power.

- The high-speed induction heating

- power of 5kW/1MHz under the suggested point of view is stable after half a year of bulk-production in Jintan Keyuan Electrical Alliances Co., Ltd

- The design has reference value when developing some ultrahigh frequency induction heating power.

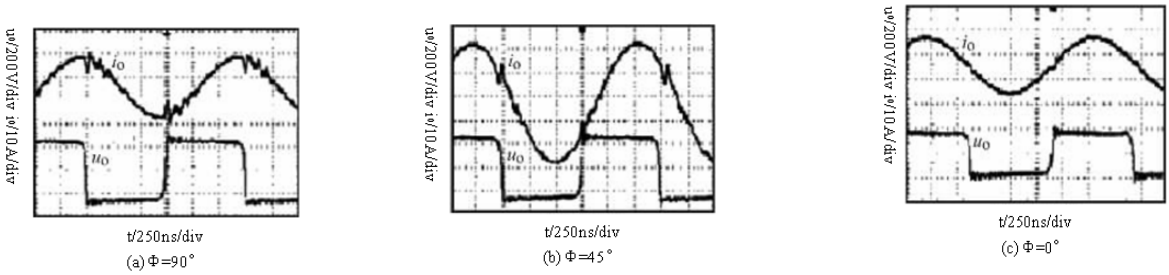

Figure 7 Experimental Results

References

[1]Stanley Zinn, S. L. Semiatin. ,Elements of Induction Heating: Design, Control, and Applications ASM International Press, 1988

[2]Lina C. ,GP Series Vacuum Tube Steel Pipe Welding Device, Baoding ZSHC Eletrical Press, 2009

[3] Chen S. ,Zhaolin W. ,20Kw/300KHz HF Induction Heating Power Supply Power ,Electronics Press ,30[2]pp.10-13 1996

[4] Jinfei S., Lei W. Jing H., 1Kw/2MHz Super HF Induction Heating Power Supply Power, Power Electronics Press ,36 [6]pp.13-15 2002

[5] Tianming P.,Modern induction heating equipment ,Metallurgical Industry Press, 1996

[6]Jing Z.,Bojin Q.,Wei Z.,Resonance Frequency Auto-tracing Technology Based on PI Control for IGBT Induction Heating Power Source,Power Electronics Press,37 [2]pp. 12-14 2003

Advanced Materials Research Vols. 846-847 (2014) pp 18-21

doi:10.4028/www.scientific.net/AMR.846-847.18

A developed adaptive tracking control technique for a four-rotor helicopter with external disturbance

Feifei Lu [1, a], Fuyang Chen*[1,b] and Ling Cai[1,c]

[1]College of Automation Engineering,Nanjing University of Aeronautics and Astronautics, China

[a]feifei_lu1@163.com, [b]chenfuyang@nuaa.edu.cn, [c]Cailing158@163.com

Keywords: Adaptive Compensation; Disturbance; Four-rotor Helicopter; Lyapunov Stability Theory.

Abstract. This paper deals with the tracking control problem of attitude angles for a four-rotor helicopter with external disturbance. A new direct adaptive compensation controller and its parameter adaptive laws are designed based on the Lyapunov stability theory, and the designed contorller can not only compensate the disturbance efficiently, but also can make the attitude angles of the four-rotor helicopter track a given reference output. By using the Barbalat lemma, the system's state tracking performance is proofed. Finally, the proposed adaptive technique is evaluated by a simulation example.

Introduction

Due to their novel appearance, simple structure, low cost, superior performance and unique flight control mode. Over the past few years, the control problems of four-rotor helicopters have gradually become a new study hotspot [1-3]. McKerrow[1] gives the dynamics modeling and structure of the four rotor UAV. Reference [2] proposes a new quaternion-based feedback control scheme for exponential attitude stabilization of a four-rotor aircraft. Adaptive control systems [4-8], for their capability of accommodating systems with parametric, structural, and environmental uncertainties, are widely employed to design of reconfiguration controller. Some adaptive compensation control researches have also been conducted for quadrotor helicopters [4-5], but most of them are aimed towards the uncertainties associated with quadrotor dynamics.

In this paper, we study the attitude tracking control problem for a four-rotor helicopter with outer disturbance based on reference [8], which proposes a standard model reference adaptive control (MRAC) approach. The new designed compensation controller and its adaptive law can compensate the disturbance excellently and quickly without the use of disturbance observer, it can also make sure the attitude angles track the reference ones asymptotically with a simple structure and parameter laws. The structure of this paper is organized as follows. System description and problems statement are given in Section 2. Section 3 describes the direct adaptive reconfiguration controller design process in detail. The digital simulation is presented in Section 4, followed by some conclusions in Section 5.

The Modeling of the Four-rotor Helicopter and Problems Statement

Four-rotor helicopter is an underactuated, dynamic vehicle with four input forces and 6 DOF motion. Ignoring the gyroscopic effect, bearing friction and atmospheric disturbance on the propellers, a simple model consists of three differential equations can be get. The thrust force generated by the front, back, left and right propellers is denoted as V_f, V_b, V_l and V_r respectively, and the thrust force generated by the front and back motors primarily actuate motions about the pitch axis while the right and left motors primarily move the hover about the roll axis.

From reference [7], we can get the model of the four-rotor helicopter:

$$\begin{cases} \dot{x} = Ax + Bu \\ y = Cx \end{cases} \tag{1}$$

$$A=\begin{bmatrix}0&0&0&1&0&0\\0&0&0&0&1&0\\0&0&0&0&0&1\\0&0&0&0&0&0\\0&0&0&0&0&0\\0&0&0&0&0&0\end{bmatrix},\ B=\begin{bmatrix}0&0&0&0\\0&0&0&0\\0&0&0&0\\-0.0327&-0.0327&0.0327&0.0327\\0.424&-0.424&0&0\\0&0&0.424&-0.424\end{bmatrix},C=\begin{bmatrix}1&0&0&0&0&0\\0&1&0&0&0&0\\0&0&1&0&0&0\end{bmatrix}.$$

with the sate $x=[y,p,r,\dot{y},\dot{p},\dot{r}]^T$, control input $u=[V_f,V_b,V_r,V_l]^T$ and output $y=[y,p,r]^T$, where y,p,r represent the yaw angle, pitch angle and roll angle respectively.

In this paper, we consider the four-rotor helicopter associated with external disturbance as follows

$$\dot{x}(t)=Ax(t)+Bu(t)+B_\omega\omega(t), \tag{2}$$

where $x(t)$ is the state space vector, $u(t)$ is the control input, $\omega(t)$ represents the bounded piecewise continuous external disturbance. $A\in R^{n\times n}$, $B\in R^{n\times m}$ and $B_\omega\in R^{n\times n_\omega}$ are unknown matrix.

The control objective is to design an adaptive feedback control law for the plant (2) such that all closed-loop signals are bounded and the plant state vector $x(t)$ tracks a reference state vector $x_m(t)$ asymptotically, which generated from the following reference model:

$$\dot{x}_m(t)=A_mx_m(t)+B_mr(t), \tag{3}$$

where $A_m\in R^{n\times n}$, $B_m\in R^{n\times l}$ are known constant matrices and all the eigenvalues of A_m are in the left-half complex plane, all columns of B_m are independent, and $r(t)\in R^l$ is bounded.

Define $\bar{\omega}=B_\omega\omega(t)$, the following standard assumptions are given

Assumption 1. $\{A,B\}$ is completely controllable. And there exists a matrix $K_1^*\in R^{n\times m}$ and $K_2^*\in R^{l\times m}$ satisfying

$$A+BK_1^{*T}=A_m,\ BK_2^{*T}=B_m. \tag{4}$$

Assumption 2. The external disturbance is a piecewise continuous bounded function. And there exists a matrix $k_3^*\in R^{m\times 1}$ satisfying

$$Bk_3^*+\bar{\omega}=0. \tag{5}$$

Direct Adaptive Compensation Controller Design

The direct adaptive controller is designed for system (2) as follows.

$$u(t)=K_1^Tx(t)+K_2^Tr(t)+k_3, \tag{6}$$

where $K_1^T=[k_{11},k_{12},\ldots,k_{1m}]^T$, $K_2^T=[k_{21},k_{21},\ldots,k_{2l}]^T$ and $k_3=[k_{31},k_{32},\ldots,k_{3m}]^T$ are the estimates of K_1^{*T}, K_2^{*T} and k_3^* respectively. Define the parameter errors and the tracking error

$$\tilde{K}_1^T=[\tilde{k}_{11},\tilde{k}_{12},\ldots,\tilde{k}_{1m}]^T=K_1^T-K_1^{*T},\tilde{K}_2^T=[\tilde{k}_{21},\tilde{k}_{22},\ldots,\tilde{k}_{2m}]^T=K_2^T-K_2^{*T},\tilde{k}_3=[\tilde{k}_{11},\tilde{k}_{12},\ldots,\tilde{k}_{1m}]^T=k_3-k_3^*. \tag{7}$$

$$e(t)=x(t)-x_m(t). \tag{8}$$

According to equations (2)-(5), we obtain

$$\dot{e}=A_me+B(\tilde{K}_1^Tx+\tilde{K}_2^Tr+\tilde{k}_3). \tag{9}$$

Select a Lyapunov function candidates as:

$$V_p=e^TPe+\sum_{i=1}^{m}(\tilde{k}_{1i}^T\Gamma_{1i}^{-1}\tilde{k}_{1i}+\tilde{k}_{2i}^T\Gamma_{2i}^{-1}\tilde{k}_{2i}+\gamma_{3i}^{-1}\tilde{k}_{3i}^2), \tag{10}$$

where $\Gamma_{1i}=\Gamma_{1i}^{T}>0$, $\Gamma_{2i}=\Gamma_{2i}^{T}>0$, $\gamma_{3i}>0$ and $P\in R^{n\times n}$, $P=P^{T}>0$ satisfies

$$PA_M + A_M^T P = -Q \tag{11}$$

for any constant $Q\in R^{n\times n}$, $Q=Q^{T}>0$. Then, according to (9) and (11), the time derivative of V_p is

$$\begin{aligned}\dot{V}_p &= 2e^T PA_m e + 2e^T PB\rho(\tilde{K}_1^T x + \tilde{K}_2^T r + \tilde{k}_3) + 2\sum_{i=1}^{m}(\tilde{k}_{1i}^T\Gamma_{1i}^{-1}\dot{\tilde{k}}_{1i} + \tilde{k}_{2i}^T\Gamma_{2i}^{-1}\dot{\tilde{k}}_{2i} + \tilde{k}_{3i}\gamma_{3i}^{-1}\dot{\tilde{k}}_{3i}) \\ &\le -e^T Qe + 2\sum_{i=1}^{m}2e^T Pb_i(\tilde{k}_{1i}^T x + \tilde{k}_{2i}^T r + \tilde{k}_{3i}) + 2\sum_{i=1}^{m}(\tilde{k}_{1i}^T\Gamma_{1i}^{-1}\dot{\tilde{k}}_{1i} + \tilde{k}_{2i}^T\Gamma_{2i}^{-1}\dot{\tilde{k}}_{2i} + \tilde{k}_{3i}\gamma_{3i}^{-1}\dot{\tilde{k}}_{3i})\end{aligned} \tag{12}$$

To make $\dot{V}_p \le 0$, we design the adaptive laws for k_{1i}, k_{2i}, k_{3i} as

$$\dot{k}_{1i} = \dot{\tilde{k}}_{1i} = -\Gamma_{1i}xe^T Pb_i,\ \dot{k}_{2i} = \dot{\tilde{k}}_{2i} = -\Gamma_{2i}re^T Pb_i,\ \dot{k}_{3i} = \dot{\tilde{k}}_{3i} = -\gamma_{3i}e^T Pb_i, \tag{13}$$

with this choice, equation (12) becomes

$$\dot{V}_p \le -e^T Qe \le -q_m\|e(t)\|^2 \le 0, \tag{14}$$

where $q_m>0$ is the minimum eigenvalue of Q.

Define the closed-loop signals vector $\tilde{e}(t)=[e^T(t), k_{1i}^T(t), k_{2i}^T(t), k_3^T(t)]^T$. $V_p>0$, $\dot{V}_p\le 0$ imply that its solution $\tilde{e}(t)$ is uniformly bounded, and in turn the boundedness of $\dot{e}(t)$ because of (9), namely $\dot{e}(t)\in L^{\infty}$. (14) implies $e(t)\in L^2$, applying Barbalat lemma, we conclude that $\lim_{t\to\infty}e(t)=0$.

Theorem 1: The adaptive controller (6), with the adaptive laws (13), applied to system (2) guarantees that all closed-loop signals are bounded and $\lim_{t\to\infty}(x(t)-x_m(t))=0$.

Numerical Simulation

The values of A_m, B_m in (3) are designed as:

$$A_m=\begin{bmatrix} 0 & 0 & 0 & 1 & 0 & 0 \\ 0 & 0 & 0 & 0 & 1 & 0 \\ 0 & 0 & 0 & 0 & 0 & 1 \\ -8.005 & 0 & 0 & -4.0025 & 0 & 0 \\ 0 & -94.8064 & 0 & 0 & -23.4048 & 0 \\ 0 & 0 & -94.8093 & 0 & 0 & -23.4048 \end{bmatrix},\ B_m=b_1,$$

where A_m is from an LQR design. B_m is the same as b_1 of the plant actuation matrix B.

Simulations are given with the following parameters: $B_\omega=B$, $\omega(t)=[1,2,3,0.1\sin(0.5t)]^T$, $t\ge 40$, $r=10$, $Q=10*I_6$. The initial values are set as $x(0)=x_m(0)=[0,0,0,0,0,0]^T$, $k_{1i}(0)=[0,0,0,0,0,0]^T$, $k_{2i}(0)=[5,5,-5,-5]$, $k_3(0)=[1,1,-1,-1]^T$. The design parameters for the adaptive laws are chosen as $\Gamma_{1i}=10*I_6$, $\Gamma_{2i}=10$, $\gamma_{3i}=20$.

With the initial values, the attitude tracking errors of the four-rotor helicopter are shown in Fig. 1.

From the simulation, it can be observed that there are transient tracking errors at the time instants when the external interference injecting to the system. But the tracking errors can go to zero asymptotically in a very short time.

Conclusion

In this paper, we design a new direct adaptive controller for a four-rotor helicopter subject to unknow external disturbance. The compensation controller and its adaptive laws can compensate the outer interference dramatically, and make sure a good tracking performance of the attitude angles. The simulation example illustrates the effectiveness of the proposed design. But there are still some

shortcomings. For example, although the tracking penformance is well, the transient response is unsatisfactory, which needs to be studied in the future.

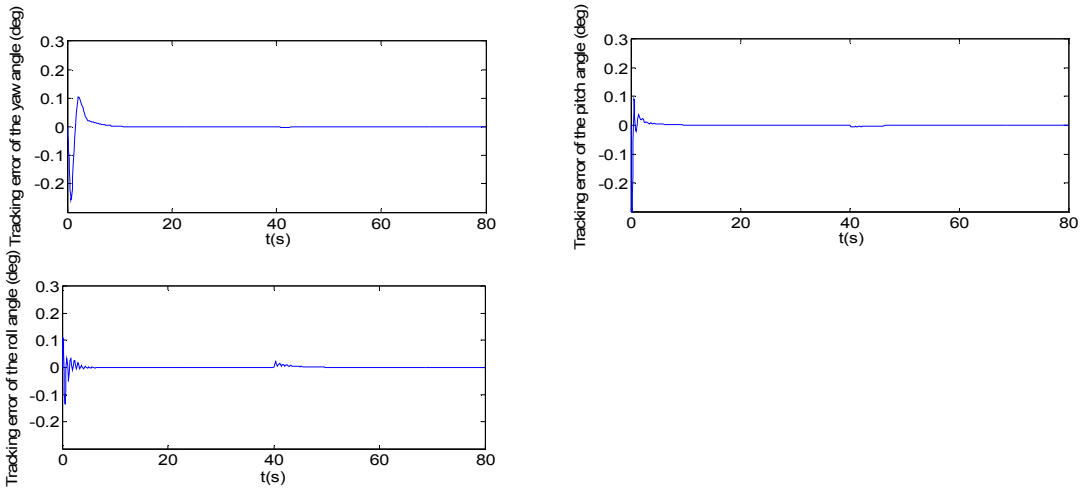

Fig. 1. The digital simulation results of the attitude tracking errors

Acknowledgements

The project is supported by National Natural Science Foundation of China (61074080). A Project Funded by the Priority Academic Program Development of Jiangsu Higher Education Institutions.

Corresponding Author

Feifei Lu, feifei_lu1@163.com, 15150553112.

References

[1] McKerrow P., Modelling the Draganflyer Four-Rotor Heli-copter[C], Proc. 2004 IEEE Int. Conf. Robotics and Automation. 2004: 3596-3601.

[2] A. Tayebi and S. McGilvray, "Attitude stabilization of a four-rotor aerial robot," in Proc. of the IEEE Conference on Decision and Control , Atlantis, Paradise Island, Bahamas, dec 2004, pp. 1216–1221.

[3] S. Bouabdallah and R. Siegwart, "Backstepping and Sliding-mode Techniques Applied to an Indoor Micro Quadrotor," in Proc. of the IEEE International Conference on Robotics and Automation, Barcelona, Spain, apr 2005, pp. 2247–2252.

[4] Chau T. Ton, William Mackunis, Robust Attitude Tracking Control of a Quadrotor Helicopter in the Presence of Uncertainty, 51st IEEE Conference on Decision and Control, (2012) 937-942.

[5] Huanye Liu, Jian Li, Jianguo Yao, Fei Hu, Backstepping Based Adaptive Control for a Mini Rotorcraft with Four Rotors, 2010 Second International Conference on Computer Modeling and Simulation, (2010) 472-476.

[6] G. Tao, S.H. Chen, X. D. Tang, S.M. Joshi, Adaptive Control of Systems with Actuator Failures, Springer, March (2004).

[7] Xinzhe Yang, Bin Jiang, Fuyang Chen, Ke Zhang, Multiple Observers Based Active Fault Tolerant Control for Quadrotor, ICIC express letters 4 (2010) 1-6.

[8] G. Tao, Adaptive Control Design and Analysis, John Wiley & Sons, (2003).

Advanced Materials Research Vols. 846-847 (2014) pp 22-25

doi:10.4028/www.scientific.net/AMR.846-847.22

Developing Simulation Model for Four In-wheel Motor Electric Vehicle Based on Simulink

Li Gang[1,2,a], Yuan Hang [1,b] , Shi Jing[1,c],Li Ning[1,d],Zhou Zhi-cheng[1,e]

[1]College of Automobile and Traffic Engineering , Liaoning University of Technology,Jinzhou Liaoning ,China

[2]State Key Laboratory of Automotive Simulation and Control, Jilin University,Changchun Jilin, China;

[a]lnitligang@126.com, [b]1016667641@qq.com, [c] 464408756@qq.com, [d]l_ning1979@126.com,

[e] 851353034@qq.com

Keywords: In-wheel Motor; Electric Vehicle; Modular Design;Dynamics

Abstract. The 15 DOF four in-wheel motor electric vehicle model is developed based on Matlab / Simulink. The model adopts modular design. The dynamic model equations, vehicle model diagram and the methods of each module modeling are presented. The model is verified by commercial software Carsim. The results show that the model is higher accuracy and it can be used for the control algorithm improvements and validation as a good platform.

Introduction

In the early time,The University of Japan has began to research the in-wheel motor electric vehicle. Both The University of Tokyo in Japan and Tokyo University of Agriculture and Technology built the 7 DOF vehicle model to study the stability of the four in-wheel motor electric vehicle[1-2].As described in [3],establish the four-wheel independent drive electric vehicle model with considering the round corner and suspension system of 18 DOF, among them the motor model is simplified to a second order transfer function. Literature [4] established a four-wheel independent drive electric vehicle model with considering suspension system of 15 DOF.In the motor model,the motor response approximation as a first-order lag characteristics,because it is modeling for hub motor,so considering the friction loss, has carried on the reset to drive efficiency.Both in literature [5] and literature [6],four-wheel independent drive,independent steering vehicle model is established for researching the electric vehicle, but they don't consider the vertical movement of electric vehicle. The paper builds a model for four in-wheel motor electric vehicle based on Simulink ,the model contains brushless direct current wheel motor model.The model considering the electric vehicle of the horizontal and vertical movement at the same time,in total of 15 DOF.In the paper gives the dynamic model equations, vehicle model diagram and the methods of each module modeling are presented. The precision of the model is verified by commercial software Carsim.

The vehicle dynamics model equation

Four in- wheel motor electric vehicle dynamics model including the vehicle longitudinal,lateral vertical, pitching, yawing and roll 6 DOF,4 wheel rotation DOF,4 wheel vertical movement DOF,1 front wheel angle DOF,in total of 15 DOF.Dynamic model coordinate systems are defined by the literature [7].Body dynamics equation of 6 DOF:

$$m\left(\dot{V}_x - V_y r + V_z \dot{\theta}\right) = F_{x1} + F_{x2} + F_{x3} + F_{x4} \tag{1}$$

$$m\left(\dot{V}_y - V_z \dot{\varphi} + V_x r\right) = F_{y1} + F_{y2} + F_{y3} + F_{y4} \tag{2}$$

$$J_r \dot{\gamma} = \frac{w}{2}\left(F_{x2} + F_{x4} - F_{x1} - F_{x3}\right) + a\left(F_{y1} + F_{y2}\right) - b\left(F_{y3} + F_{y4}\right) \tag{3}$$

$$m\left(\dot{V}_z - V_x \dot{\theta} + V_y r\right) = F_{s1} + F_{s2} + F_{s3} + F_{s4} - m_s g \tag{4}$$

$$J_{\varphi}\ddot{\varphi}=\frac{w}{2}(F_{s1}+F_{s3}-F_{s2}-F_{s4})+h_r(F_{y1}+F_{y2}+F_{y3}+F_{y4}) \quad (5)$$

$$J_{\theta}\ddot{\theta}=b(F_{s3}+F_{s4})-a(F_{s1}+F_{s2})+h_p(F_{x1}+F_{x2}+F_{x3}+F_{x4}) \quad (6)$$

Independent suspension beating the unsprung mass vertical dynamics equation of single wheel:

$$m_{ui}\ddot{z}_{ui}=k_{ui}(z_{ri}-z_{ui})-F_{si} \quad (7)$$

The equilibrium equation of the wheel movement:

$$T_{xi}-F_{xi}R-T_{bi}-M_f=J_{wi}\dot{\omega}_{wi} \quad (8)$$

The suspension force of the sprung mass:

$$F_{si}=k_{si_i}(z_{ui}-z_i)+b_{si}(\dot{z}_{ui}-\dot{z}_i)+f_i \quad (9)$$

Suspension and body connection points absolute position:

$$z_1=\frac{w}{2}\varphi-a\theta+z \quad z_2=-\frac{w}{2}\varphi-a\theta+z$$
$$z_3=\frac{w}{2}\varphi+b\theta+z \quad z_4=-\frac{w}{2}\varphi+b\theta+z \quad (10)$$

M is the total quality of the vehicles,ms is the sprung mass,mui is the unsprung mass of wheels,a is the distance from the center of mass of the vehicle to the front axle,b is the distance from the center of mass of the vehicle to the rear axle,w is wheelbase,R is wheel rolling radius,hr is the distance from the center of mass of the vehicle to the roll axle,hp is the distance from the center of mass of the vehicle to the pitch axis,Jθis the moment of inertia of pitch,Jφis the moment of inertia of roll,Jγis the moment of inertia of yaw,z is the vehicle sprung mass center height,zi is the height of the body and suspension points,θ is the pitching angle,φ is the rolling angle,γ is the yaw angle,Vx is the vehicle's portrait speed, Vy is the vehicle's side direction speed,Vz is the vehicle's sprung mass speed,ksi is the suspension stiffness,bsi is the suspension damping,kui is the vertical stiffness of the wheel,Fyi is the yawing force of the wheel,Fxi is the portrait force of the wheel,Fsi is the suspension force,Txi is the driving torque of the wheel,Tbi is the braking torque of the wheel,Mf is the rolling resistance of the wheel,g is acceleration of gravity,ω is the vehicle's travel speed.

The methods of each module modeling are presented of the vehicle model

The vehicle model adopts modular design,including driver module,steering system module,motor drive system module,braking system module, wheel dynamics module and vehicle dynamics module, etc.

A. Driver model

The simulation model is mainly used to verify the rationality of the control algorithm,the driver model adopt the simple PID model,mainly used for simulating the driver in the established simulation working condition of driving,braking and steering operate,to realize the PID control speed.

B. Steering system model

Based on the basic angle transfer characteristics of the steering system and considering tire's aligning torque has elastic additional influence on the steering system at the same time,according to the driver's steering wheel angle calculates left and right side of the front wheel angle.

C. Motor driving system module

In the motor driving system module,including motor model and four-wheel motor driving torque control allocation.In the motor system module,driving motor accepts the target driving torque signal Tedij is sent by the accelerator pedal by vehicle controller,output wheel driving torque Teij.Equal to equation (8),drive motor model described by following equations:

$$T_{eij}-T_{Lij}-r\dot{\omega}_{ij}=J_{wij} \quad (11)$$

$$T_{eij}=K_m i_{aij} \quad (12)$$

$$E_{ij}-K_e\omega_{ij}-Ri_{aij}=L_a\dot{i}_{aij} \quad (13)$$

D. Braking system model

Through the simulation from the brake pedal to the brake output torque's transmission characteristics, calculating the output braking torque of the four wheels.The braking system model adopts hydraulic braking system model,wheel cylinder pressure,the brake effective area and friction coefficient are multiplied by the effective radius of the brake force.,we can obtain steady braking torque.

E. Wheel dynamics model

According to equation (8),we know that we can calculate the wheel speed through the wheel angular acceleration's integral.The wheel angular acceleration can be calculated through the driving force of the wheel,braking torque,wheel's longitudinal force and rolling resistance.Rolling resistance according to the vehicle body feedback speed,with the experience formula to calculate.

F. Vehicle dynamics module

Vehicle dynamics module through the tire's longitudinal force, side force,applied force of the suspension system and air resistance calculate the vertical motion response,the longitudinal and lateral motion response of the horizontal motion and corresponding roll, pitch, yaw motion response of the vehicle.Using the dynamic equation (1)-(6) to build model.

G. Tire model

Tire model adopted the Magic Formula tire mode. Four wheel's tire force that including the longitudinal force,the lateral force and the aligning torque will be calculated by using Pacejka2002 tire model. Suspension system model

H. Aerodynamics module

According to the speed of the vehicle calculates the aerodynamic drag,which might be defined as in the following:

$$F_w = \frac{C_D A(3.6u)^2}{21.15} \tag{14}$$

Fw is the aerodynamic drag of the vehicle;CD is the aerodynamic drag coefficient of the vehicle;A is the windward area of the vehicle;u is the longitudinal velocity of the center of mass.

Model verification

For the above simulink electric vehicle simulation model has been established, the model's dynamic characteristics are verified by commercial software Carsim. According to parameters of the electric vehicle structure,parameters in Carsim need to reset. Verifying the work condition: The simulation speed is 80km/h,the road adhesion coefficient is 0.85.The results were shown as figure 1 to figure 4.

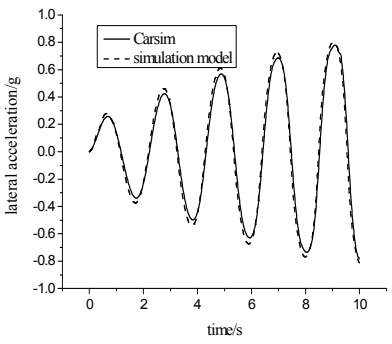

Fig.1.The contrast of lateral acceleration

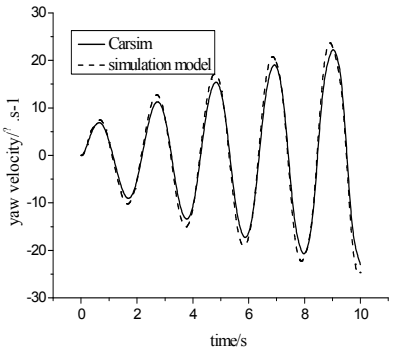

Fig.2.The contrast of yaw velocity

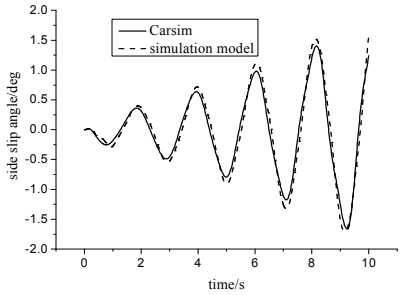

Fig.3.The contrast of side slip angle

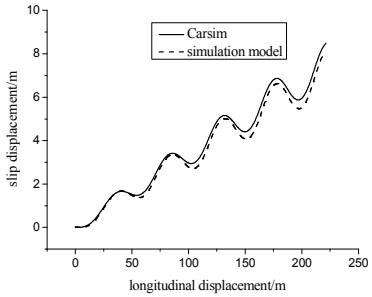

Fig.4.The contrast of vehicle trajectory

Due to analysis the simulation results from figure 2 to figure 6,we know when the lateral acceleration is smaller than 0.3g,the lateral acceleration,yaw velocity, sideslip angle,locus curve of the simulation model is similar to Carsim model,the main reason is when the lateral acceleration is small,suspension system has a little influence on the steering performance,therefore,linear suspension in the simulation model can well reflect the vehicle movement when the lateral acceleration is small.

Conclusion

Four in-wheel motor electric vehicle model is builded based on Simulink. The model is verified by commercial software Carsim,the model is higher accuracy and it can be used for the control algorithm of the four in-wheel motor electric vehicle improvements and validation as a good platform.

Acknowledgement

This work is supported by National Youth Natural Science Foundation of China (Project No. 51305190), Opened Foundation of State Key Laboratory of Automotive Simulation and Control （Project No.20111104）and Liaoning University of Technology Foundation(Project No.201108).

References

[1]Sakai SHin-Ichiro, Sado Hideo, Hori Yoichi. Dynamic driving/braking force distribution in electric vehicles with independently driven four wheels[J]. Electrical Engineering in Japan, 2002, 138(1): 79-89.

[2]Motoki Shino, Masao Nagai. Motion control of micro-scale electric vehicle by DYC considering lane marker information[C]‖Proceedings of the 8th IEEE International Workshop on Advanced Motion Control, Kawasaki, Japan , IEEE, 2004: 47-52.

[3]Jin li qiang. Dynamic model for simulation of EV with 4 independently-driving wheels[J]. Journal of System Simulation,2005,17 (12):3053-3066.

[4]Wang bo .Study on Experiment Platform of Four-Wheel-Independent-Drive EV and its Driving Force[D].Bei jing;Tsinghua University in China,2009

[5]Yang Guang fu .Research on anti-skid and Yaw Stability Control of 4WID/4WIS Electrical vehicle[D].Ji nan:Shandong University in China,2010

[6]Zong Chang fu, Liu Jing wen, Zheng Hong yu,ect.Modeling and Special Conditions Simulation of Electric Vehicle with 4WID /4WIS[J].Automotive Engineering,2011,33(10):829-833.

[7]Yu Zhi sheng.Automobile theory[M](The fifth edition).Bei jing in China:China machine press,2010

Advanced Materials Research Vols. 846-847 (2014) pp 26-29

doi:10.4028/www.scientific.net/AMR.846-847.26

Study of vehicle sideslip angle real-time estimation method

Xiaobin Fan[1,a], Pan Deng[1,b]

[1]School of Mechanical and Power Engineering Henan Polytechnic University, China 454000

[a]fanxiaobin@hpu.edu.cn, [b]SvenDeng@163.com

Keywords: vehicle; side slip angle; estimation; Kalman filter

Abstract: In the vehicle stability control and other active safety systems, vehicle sideslip angle real-time estimation is necessary. However, the direct measurement of sideslip angle is more difficult or too costly, so it is often used in estimating methods. The vehicle sideslip angle of closed-loop Luenberger observer and Kalman observer were constructed based on two degrees of freedom bicycle model, as well as the direct integration method for large sideslip angle conditions. The comparative study showed that Kalman filtering estimation method and Luenberger estimation methods have better estimation accuracy in small slip angle range.

Introduction

The vehicle is stabilized by the differential braking and produce steering yaw moment by vehicle electronic stability control system with real-time measurement of vehicle yaw rate and sideslip angle, and to determine whether the vehicle in reasonable limits.The yaw rate can be directly measured using inexpensive sensor, although you can use the side angle optical or GPS measurements to measure vehicle sideslip angle, but its cost, accuracy and reliability problems are still exist[1]. So people made a lot of sideslip angle estimation method[2].

Linear two degree of freedom vehicle model

In order to estimate the vehicle sideslip angle, at first the linear two-degree of freedom vehicle model is established which including yawing motion and lateral movement[3], as shown in Figure 1, and the dynamics motion equations of the vehicle are

$$\begin{cases} mV_x(\dot{\beta}+r)=F_{yf}+F_{yr} \\ I_{zz}\dot{r}=F_{yf}\cdot a-F_{yr}\cdot b \end{cases}, \text{ with, } \begin{cases} F_{yf}=C_{\alpha f}\cdot\alpha_f \\ F_{yr}=C_{\alpha r}\cdot\alpha_r \end{cases}, \quad \begin{cases} \alpha_f=\delta_f-\dfrac{V_y+a\cdot r}{V_x} \\ \alpha_r=-\dfrac{V_y-b\cdot r}{V_x} \end{cases}$$

From above the following equations are deduced

$$\begin{bmatrix} \dot{\beta} \\ \dot{r} \end{bmatrix}=\begin{bmatrix} \dfrac{-2C_{\alpha f}-2C_{\alpha r}}{mV_x} & -1+\dfrac{2C_{\alpha r}b-2C_{\alpha f}a}{mV_x^2} \\ \dfrac{2C_{\alpha r}b-2C_{\alpha f}a}{I_{zz}} & \dfrac{-2C_{\alpha f}a^2-2C_{\alpha r}b^2}{I_{zz}V_x} \end{bmatrix}\begin{bmatrix} \beta \\ r \end{bmatrix}+\begin{bmatrix} \dfrac{2C_{\alpha f}}{mV_x} \\ \dfrac{2C_{\alpha f}a}{I_{zz}} \end{bmatrix}\delta \tag{1}$$

Where, a and b are respectively distance of the centroid away from front axle and rear axle, $a=1.1\text{m}$, $b=1.5\text{m}$, L is wheelbase, $L=a+b$, $C_{\alpha f}$ and $C_{\alpha r}$ were front tire cornering stiffness and rear tire cornering stiffness, $C_{\alpha f}=C_{\alpha r}=43500\text{N/rad}$, m is the total mass of the vehicle, $m=1500\text{kg}$, I_{zz} is the automotive yaw moment of inertia, $I_{zz}=2800\text{kg}\cdot\text{m}^2$, V_x is the longitudinal speed, δ is front-wheel angle, β is vehicle sideslip angle, r is vehicle yaw rate.

Closed-loop state observer method

The vehicle sideslip angle is estimated by the lateral acceleration sensor and the yaw rate sensor based on the the linear two-degree of freedom vehicle model according to Figure 1. And lateral wind disturbance is applied in the front and rear, the road slope disturbance and uneven

pavement are the equation of state interference system noise ω. The lateral acceleration sensor noise and yaw rate sensor noise are measurement noise υ. According to the ideas of state estimation theory[4], the vehicle two degree of freedom model dynamics motion equations can rewrite as the state and measurement equations $\dot{\hat{x}} = A\hat{x} + Bu + L(y - \hat{y}) + w$, $y = Cx + Du + v$.

Where, $C = \begin{bmatrix} -\dfrac{C_{\alpha f} + C_{\alpha r}}{m} & \dfrac{bC_{\alpha r} - aC_{\alpha f}}{mV_x} \\ 0 & 1 \end{bmatrix}$; $D = \begin{bmatrix} \dfrac{C_{\alpha f}}{m} \\ 0 \end{bmatrix}$; $u = \delta$; $\hat{x} = \begin{bmatrix} \hat{r} \\ \hat{\beta} \end{bmatrix}$, $y = \begin{bmatrix} a_y \\ r \end{bmatrix}$.

Where, $\hat{x}$ is the state estimation vector; y is output vector; L is estimated gain matrix and its selection principle is: make the deviation $e = y - \hat{y}$ rapidly converges to zero, in which

$$L = \begin{bmatrix} \dfrac{\lambda_1\lambda_2}{C_{\alpha f}} \dfrac{(a-b)I_{zz}}{2(a^2+b^2)+4ab} - 1 & \dfrac{1}{V_x} \\ -\lambda_1 - \lambda_2 & \dfrac{m(a^2+b^2)}{I_{zz}(a-b)} \end{bmatrix} \tag{2}$$

Where, $\lambda_1$and λ_2 are closed-loop observer poles. ω, υ is the state noise and observation equations noise, and ω, υ is assumed as independent white noise. Namely $E[\omega\omega^T] = \begin{cases} Q & n = k \\ 0 & n \neq k \end{cases}$, $E[vv^T] = \begin{cases} R & n = k \\ 0 & n \neq k \end{cases}$, $E[\omega v^T] = 0$. The vehicle sideslip angle close-loop observer (Luenberger observer) diagram is shown in Figure 2.

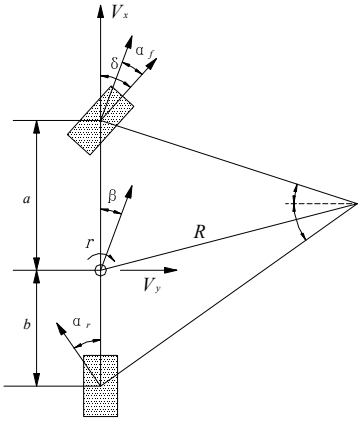

Fig.1 Linear 2-dof vehicle model

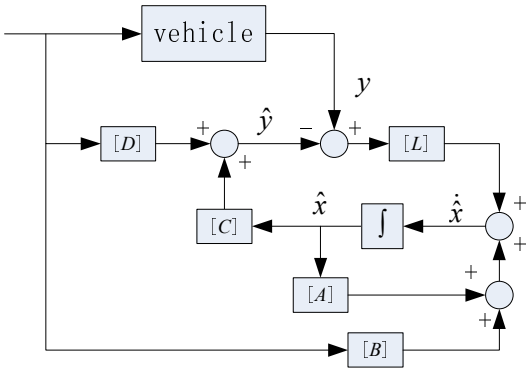

Fig.2 Sideslip angle loop observer

Kalman filter estimation method

Kalman filter is based on minimum mean square error for the estimation of the best criteria to derive a set of recursive estimation algorithm, the algorithm's basic idea is using signal-to-noise state-space model, the estimated value of the previous time and current time on the observed values to update the estimated state variables, the estimated value of the current time is obtained[5], it is very suitable for real-time processing and computing. Let the discrete state equations were described by the following stochastic differential equation: $x_k = Ax_{k-1} + Bu_{k-1} + w_{k-1}$. Defining the observed variables z, the observation equation is $z_k = Hx_k + v_k$.

The $\hat{x}_k^-$ is defined as the case of estimation of the state variables x_k at time k and at the time the observations z_k are unknown, and which is called a priori state estimation. The $\hat{x}_k$ is the estimation value of the state variables x_k with observation z_k is known, and which is referred to

as posterior estimates. The P_k^- and P_k are define as priori estimation error covariance and posteriori estimates error covariance, respectively. Kalman filter can be divided into time update process (forecast) and measurement update (correction) two parts. The next time priori estimation is obtain based on the current state of the system at time update process. The improved system posteriori estimates is obtain based on the combination of measurement and a priori estimate in measurement process. The filtering algorithm is: (1) Time update process: $\hat{x}_k^- = A\hat{x}_{k-1} + Bu_{k-1} + w_{k-1}$, $P_k^- = AP_{k-1}A^T + Q$. (2) Measurement update equations: $K_k = P_k^- H^T (HP_k^- H^T + R)^{-1}$, $\hat{x}_k = \hat{x}_k^- + K(z_k - H\hat{x}_k^-)$, $P_k = (I - K_k H)P_k^-$.

Direct integration method

If the vehicle hasn't nod angle and roll angle, and sideslip angle is very small[6], the vehicle body's slip angle is calculated by the following formula: $\beta(t) = \beta_0 + \int_0^t \dot{\beta} dt = \beta_0 + \int_0^t (\frac{\dot{V}_y}{V_x} - r) dt$.

According to vehicle four wheels model (Figure 3), the equation of motion for the vehicle is

$$\begin{cases} m(\dot{V}_y + V_x\omega_r) = (F_{xfl} + F_{xfr})\sin\delta + (F_{yfl} + F_{yfr})\cos\delta + (F_{yrl} + F_{yrr}) \\ I_{zz} \cdot \dot{r} = (F_{xfl} + F_{xfr})\sin\delta \cdot a + (F_{xfr} - F_{xfl})\cos\delta \cdot T_w / 2 + (F_{yfl} + F_{yfr})\cos\delta \cdot a \\ + (F_{yfl} - F_{yfr})\sin\delta \cdot T_W / 2 - (F_{yrl} + F_{yrr})b + (F_{xrr} - F_{xrl}) \cdot T_W / 2 \end{cases} \quad (3)$$

Where, T_W is the distance between the wheels，$T_W = 1.3\text{m}$。The formula (3) becomes as follows

$$\begin{cases} \dot{V}_y = A_{11} \cdot V_y + A_{12} \cdot r + D_1 \\ \dot{r} = A_{21} \cdot V_y + A_{22} \cdot r + D_2 \end{cases} \quad (4)$$

Where, $A_{11} = 0$, $A_{12} = V_x$, $A_{21} = 0$, $A_{22} = 0$,

$$D_1 = \frac{1}{m}(F_{yfl} + F_{yfr}) \cdot \cos\delta + \frac{1}{m}(F_{xfl} + F_{xfr}) \cdot \sin\delta + \frac{1}{m}(F_{yrl} + F_{yrr})$$

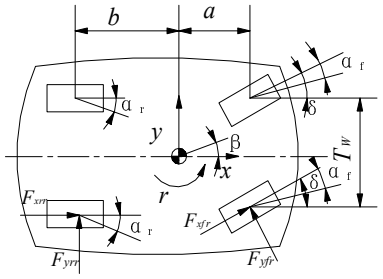

Fig.3 Vehicle four wheels model

$$D_2 = \frac{1}{I_{zz}}\big[(F_{xfl} + F_{xfr})\sin\delta \cdot a + (F_{xfr} - F_{xfl})\cos\delta \cdot T_w / 2 + (F_{yfl} + F_{yfr})\cos\delta \cdot a$$
$$+ (F_{yfl} - F_{yfr})\sin\delta \cdot T_W / 2 - (F_{yrl} + F_{yrr})b + (F_{xrr} - F_{xrl}) \cdot T_W / 2\big]$$

The formula (4) was discretized as

$$\begin{cases} V_{y,k+1} = (A_{11}T + 1) \cdot V_{y,k} + A_{12} \cdot T \cdot r_k + D_{1,k} \cdot T \\ r_{k+1} = A_{21} \cdot T \cdot V_{y,k} + (A_{22} \cdot T + 1) \cdot r_k + D_{2,k} \cdot T \end{cases} \quad (5)$$

Letting $r_{k+1} = 2 \cdot r_k - r_{k-1}$, and after it is substituted into Eq (5), we obtain

$$V_{y,k+1} = [r_k(1 - A_{22} \cdot T) - r_{k-1} - T \cdot D_{2k}] + A_{12}Tr_k + D_{1k} \cdot T \quad (6)$$

Direct integration method has small computational workload. When the signal quality is high it has good accuracy and does not require vehicle parameters, and there are good arguments robustness. However, the sideslip angle will obtain a greater deviation passing through the integrator with accumulation of the sensor signal weak errors.

The several estimation methods results contrast is shown in Figure 4 (a), which is on high coefficient of friction road surface and step input steering wheel angle($\mu = 0.8, V_0 = 60km/h$), where "Lbg" is the closed-loop observer Luenberger method. The several estimation results are compared in Figure 4 (b) under steering wheel angle sinusoidal input.

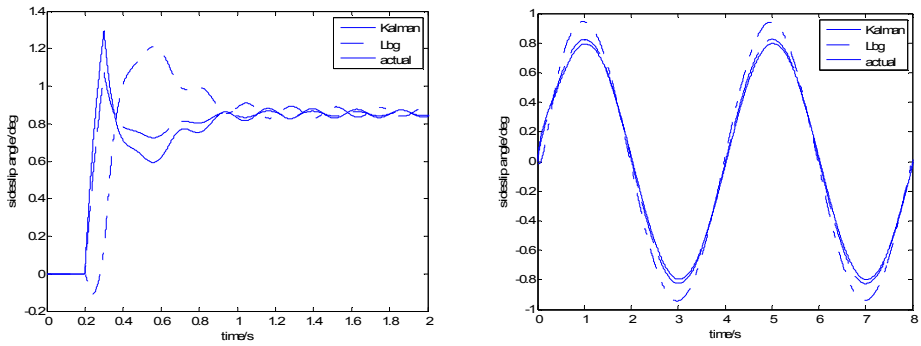

(a) (b)

Fig.3 Several side slip angle estimation results comparison

It has satisfactory estimation accuracy and good robustness using Kalman filtering method and the closed-loop state observer method within a small slip angle. The direct integration method is preferred under the large range side slip angle, but we should pay attention to cumulative errors of direct integration method.

Conclusions

Vehicle sideslip angle estimation are hot and difficult hotspot in vehicle chassis active control systems. The closed loop full state observer method, Kalman filtering observer method and direct integration method for vehicle sideslip angle estimation are introduced and studied and comparative study of estimation accuracy is outspreaded using various methods by simulation in this paper.

Acknowledgment

This research was supported by Henan Polytechnic University Doctoral Fund, P. R. China (No. B2010-12), the natural science fund of education department of Henan province (No. 2011B580001) and Henan Province Key Technology Research Project(No. 122102210045).

References

[1] Cheli F, Sabbioni E, Pesce M. A methodology for vehicle sideslip angle identification: comparison with experimental data, Vehicle System Dynamics, vol.45, no.6, pp. 549, 2007.
[2] R. Rajamani, Vehicle Dynamics and Control. New York: Springer-Verlag, 2005.
[3]Wong, J. Y. Theory of Ground Vehicles, John Wiley & Sons, New York, 2001.
[4] Andrzejewski, R., and Awrejcewicz, J. Nonlinear Dynamics of a Wheeled Vehicle, Springer-Verlag, New York, 2005.
[5] Mohinder, Grewal S., Angus P.A., Kalman Filtering Theory and Practice, Prentice Hall, 1993.
[6] Reza N. Jazar. Vehicle Dynamics: Theory and Applications. New York: Springer-Verlag, 2008.

Advanced Materials Research Vols. 846-847 (2014) pp 30-33

doi:10.4028/www.scientific.net/AMR.846-847.30

Sky-hook control of vehicle active suspension with electro-hydrostatic actuator

Farong Kou[1, 2]

[1]College of Mechanical Engineering, Xi'an University of Science and Technology, Xi'an, Shaanxi, 710054, China

[2]Automotive Engineering Research Institute, Shaanxi Automobile Group, Xi'an, Shaanxi, 710054, China

koufarong@xust.edu.cn

Keywords: Electro-hydrostatic actuator, Active suspension, Sky-hook control, Dynamic model, Experiment.

Abstract. A kind of vehicle active suspension based on Electro-Hydrostatic Actuator (EHA) is put forward. The suspension system consists of two parts: spring and actuator with controlled force. The actuator includes hydraulic cylinder, hydraulic pump, controller, etc. In this paper, a quarter-car dynamic model is exactly established involving bond graph models of EHA parts. Under the input conditions of the given road profile and designed sky-hook controller, The prototype and test rig of EHA active suspension are developed and bench tests are carried out. The simulation and experimental results show that sky-hook active suspension with EHA provides better ride comfort, handling and stability than passive suspension.

Introduction

The vehicle suspension isolates the car body from road disturbances for comfortable ride and controls vehicle body attitude. Vehicle suspension systems have been developed over the last 100 years to a very high level of sophistication. Complex kinematic configurations are designed to strike a balance between the complicated functions to be carried out by the suspensions. Most passive suspension systems mainly employ some types of springs in combination with hydraulic or pneumatic shock absorber. It is commonly accepted that passive suspensions have limited performance because their components can only store or dissipate energy. It cannot satisfy the comfort and handling requirements under varying road conditions. The idea of adding active components was introduced to improve vehicle handling and ride comfort [1].

The concept of active suspension was put forward in the 1950s .Active suspension employs pneumatic or hydraulic actuators which in turn create the desired force in the suspension system. In the study, a novel vehicle active suspension based on Electro-Hydrostatic Actuator（EHA） is proposed. The paper also investigates control methods on active suspension based on EHA. The paper develops sky-hook controller that is applied to the active suspension system with EHA. Based on a quarter-car dynamic model and developed suspension physical prototype, simulations and experiments for EHA suspension with designed sky-hook controller, under a certain road condition, are completed to confirm the validity of the proposed controller and suspension models. The response characteristics of vehicle active suspension system are studied.

Vehicle Active Suspension with Electro-Hydrostatic Actuator

The basic structure of vehicle active suspension based on EHA is given in Fig.1. The system consists of two parts: spring 7 and actuator with variable control force. The actuator is made up of hydraulic cylinder 5, hydraulic pump 4, controller 2 and BLDCM 3(Brushless Direct Current Motor). Hydraulic cylinder and spring are vertically connected respectively with sprung mass 6 and axle 8. And hydraulic cylinder is connected with hydraulic pump. Hydraulic pump is coupled with BLDCM by

shaft coupling and BLDCM is connected with accumulator 1. Controller is installed between BLDCM and accumulator [2].

In this paper, a quarter-car model with two degrees of freedom is exactly established involving mathematical models of EHA parts, which is shown in Fig.2. This model uses a power unit to create the control force between sprung mass and unsprung mass.

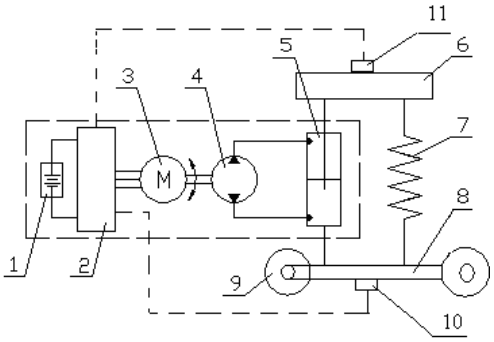

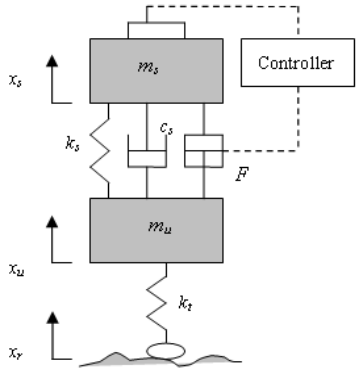

Fig.1 Vehicle active suspension with EHA Fig.2. A schematic diagram of a quarter-car model

According to bond graph principles, bond graph model of 2 DOF suspensions is established as shown in Fig. 4.

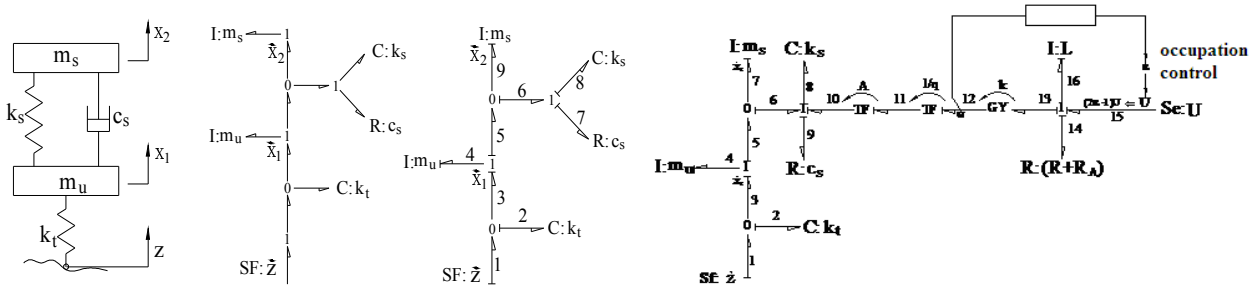

Fig.3 Bond graph models of passive suspensions Fig.4 Bond graph models of EHA active suspension

Main elements are dissipative element R, inertial element I and storage element C. The connections between these elements are implemented through junctions. There are two types of junctions: 1-junctions and 0-junctions which respectively correspond toseries connections and parallel connections. They express in fact the generalized Kirchhoff's laws. The transformers and the gyrators are used to go from a field of physics to another. Causal rules exist at the junctions. Only one port can fix the flow through a 1-junction. Only one port can fix the effort at a 0-junction. For instance, an effort source connected to a 0-junction fixes the effort at the junction; the rest of the system fixes the flows through this junction [3].

Sky-hook Control Simulation

Sky-hook control method was first proposed by Professor D.Kamopp in 1974. Because of its simple control algorithm, sky-hook control is widely used in active and semi-active suspension control[4-5]. Ideal sky-hook damping force is written as

$$F_s = -c_{sky} \cdot \dot{x}_2 \tag{1}$$

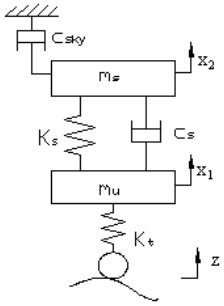

Fig.5 Ideal sky-hook control model

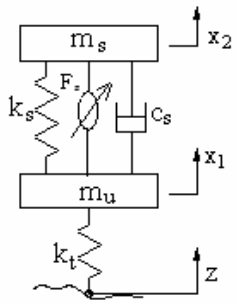

Fig.6 Practical sky-hook control model

Where $\dot{x}_2$ is the velocity of sprung mass, c_{sky} is sky-hook damping coefficient.

The ideal skyhook control model as shown in Fig.3. It envisages a move of the shock absorber system between vehicle body and the inertial coordinate. For an active suspension, the control force is required to produce, which is proportional to the actuator absolute speed.

Under the input of sine road with amplitude 0.03m and frequency 2Hz， the response characteristics of EHA sky-hook active suspension are simulated as shown in Fig.7 and Fig.8.

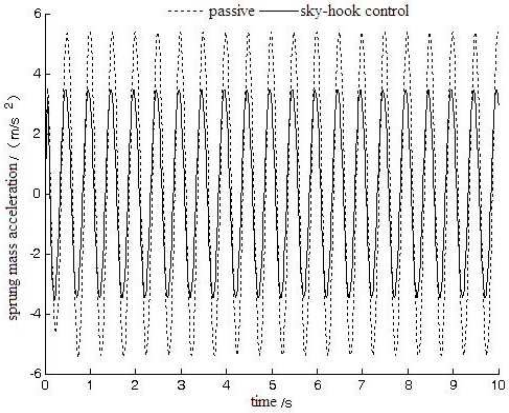

Fig.7 Sprung mass acceleration response

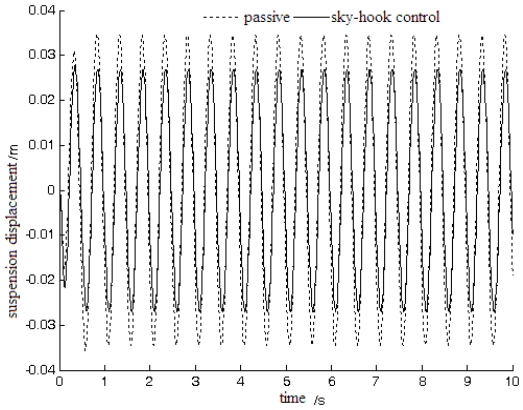

Fig.8 Suspension displacement response

Experimental investigation of EHA active suspension

To prove the effectiveness of proposed active suspension, according to simulation researchments, EHA active suspension prototype, vibration exciter and vibration bench are developed. A photograph of the schematic diagram and experimental quarter car rig are shown in Fig.9.

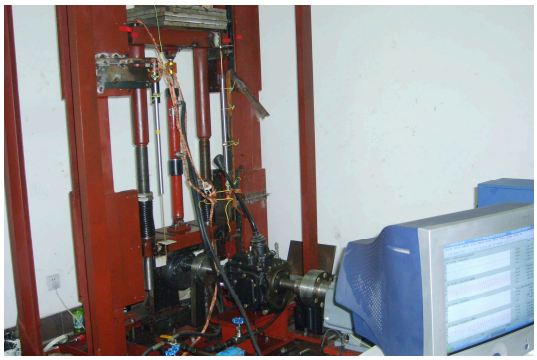

Fig.9 The experimental system of EHA active suspension

The mechanical cam vibration exciter is developed to generate sinusoidal signal, which is equal to simulation input. Experimental results are given in Fig. 10 and Fig. 11.

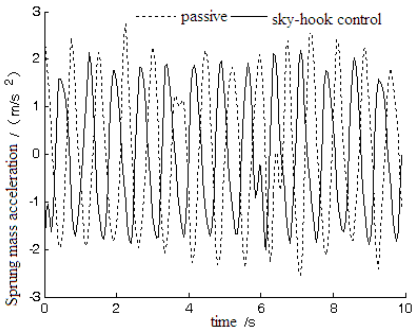

Fig.10 Time response of sprung mass acceleration

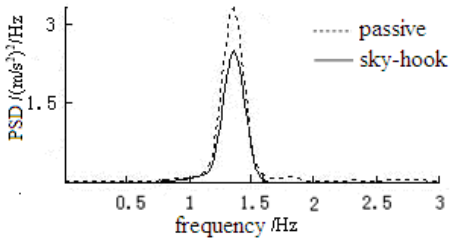

Fig.11 Power Spectrum Density of sprung mass acceleration

Experimental results show sprung mass acceleration for active suspension descends by 15.3%.

Conclusions

In the paper, a bond graph model with EHA active suspension is established to simulate vehicle behaviors and verify sky-hook controller. The simulation results show that EHA sky-hook controller is rather effective. On the base of EHA suspension system simulation, physical Prototype and test bench for active suspension were developed. Experimental results show that EHA active suspension apparently improves vehicle ride comfort.

Acknowledgements

This work was financially supported by the National Natural Science Foundation of China (Program No.51275403), Doctoral Fund of Ministry of Education of China (Program No. 20126121120003), the Post Doctoral initial funding of Xi'an University of Science and Technology (Program No.2013QDJ034),Scientific Research Program Funded by Shaanxi Provincial EducationD epartment (Program No. 2013JK1008).

References

[1] Daniel Fischer, Rolf Isermann: *Control Engineering Practice*.Vol. 12 (2004), p.1353-1363

[2] Farong Kou, Zongde Fang: *Machine tool and hydraulics*.Vol. 35(2007) p.129-131 (In Chinese)

[3] S. Lichiardopol, C. Sueur: *Journal of the Franklin Institute*. Vol. 347(2010), p.387-397

[4] Karnopp D Crosby M, Harwood R: *ASME J of Engineering for Industry*. Vol. 96(1974), p. 619-626

[5] Gopala Rao, L.V.V: *Journals of Sound and Vibration*. Vol. 323(2009), p.515-529

Advanced Materials Research Vols. 846-847 (2014) pp 34-39

doi:10.4028/www.scientific.net/AMR.846-847.34

Error source identification of machining accuracy of Five-axis Linkage CNC machine tools

GUO Zhiping, SONG Zhiyong, SHI Rongbo

AVIC Chengdu Aircraft Industrial (Group) Co. Ltd

Chengdu, Sichuan, China, 610092

E-mail:66837477@qq.com; cac_85@vip.163.com

Keywords: "S" test part;Machining accuracy;Error source identification;CNC Machine Tools

Abstract. The error sources of machining accuracy of CNC machine tools including geometric error, thermal error, system error and error of load control etc. The error source affect the relative position of the cutting tool and the workpiece by the dynamic motion, and then affect the machining accuracy of the workpiece. By trial cutting method, "S" test part is a new test part for detecting machining accuracy of five-axis linkage machine tools. Through experiment and simulation, identification of the error source of the machining accuracy and the regular of "S" test part surface errors, surface quality, results show that "S" test part can reflect the machining accuracy of CNC machine tool.

Introduce

Five-axis linkage CNC machine tools, with its high speed, high precision characteristics, are widely used in large aircraft structure part machining, to meet the development needs of "complex structure surface, high precision, high surface quality". Due to the CNC machine tools designed based on Cartesian coordinate system, the error accumulation among transmission chain, in order to ensure the quality of processing parts, it is necessary to make a comprehensive detection in machine tools precision at the CNC machine tools' debugging and acceptance-checking stage.

The error sources of machining accuracy of CNC machine tools including geometric error, thermal error, system error and error of load control etc. The error source affect the relative position of the cutting tool and the workpiece by the dynamic motion, and then affect the machining accuracy of the workpiece.

The machining accuracy detection, for the influence of machine tools dynamic characteristics and machining technology, etc, now mainly detected by trial cutting method, the usual implemented standards is "universal cutting test -- NAS series, metal cutting equipment specification" (referred to as "NAS979" standard), developed by the United States National Aeronautics Board[1]. This method's test cut is called "NAS" test part (shown in Fig.1a), limited by the test piece's itself characteristics, NAS979 test part's test results cannot reflect the need of complex shape parts, and is difficult to characterize the processing error in multi-axis coordinated motion, does not reflect the five axis linkage CNC machine's open-close angle conversion characteristics, also can't make integrate test on machining accuracy of five-axis CNC machine tools.

Presented in this paper, "S" shaped test part (shown in Fig.1b) can effectively solve the shortage of NAS979 standards, correctly realize the error source identification of machining accuracy of CNC machine tools [2].

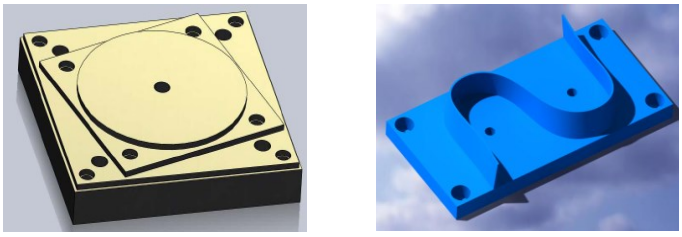

a) NAS979 test part b) "S" shaped test part

Fig.1 The test part model

Design of simulation platform

CNC machine tools processing error is mainly caused by the integral linkage of mechanical control system in the cutting process[3,4]. Machine tools' basic motion structure, servo system's coordination ability and performance are the main factors affecting machining accuracy. Therefore, to adopt the function errors-transfer modeling method for the analysis of the machine tools machining accuracy errors. As shown in Fig.2a is the motion association graph of machine mechanical system and control system, machine tools motion instruction pass by the way of position link, speed link, motor link, eventually driving machine link, to realize the CNC machine tools cutting movement. Each link can be represented through corresponding proportion, integral and differential G function, the main index of machine tools machining accuracy-influencing in each link has been listed in Fig.2a.

Fig.1b is the model of motion simulation established in MATLAB/Simulink, which based on the movement of machine tools moving association graph, to analyze machine tools motion's following error and motion matching under the influence of variable parameters. Due to the machine tools following error, multi-axis parameters mismatch and motion incoordination, eventually leading to the parts contour errors. Such as circular contour processing, each axis parameter matching exist small error in the radius direction, but when mismatch, it will make the processing contour oval. In corner milling, if the gain is too small, the axial dynamic performance will have to follow the damping, causing following error bigger and system response slow; if gain is too large, the system will less damping, follow error will cause the system to overcut. In order to obtain high contour precision at high speed, CNC machine tools system must be in the critical damping and gain matching.

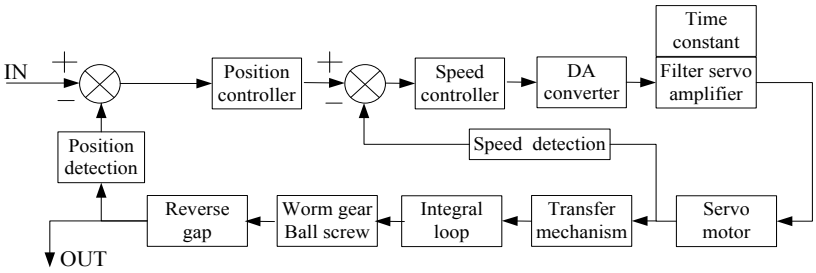

a) Association graph of the machine tools motion

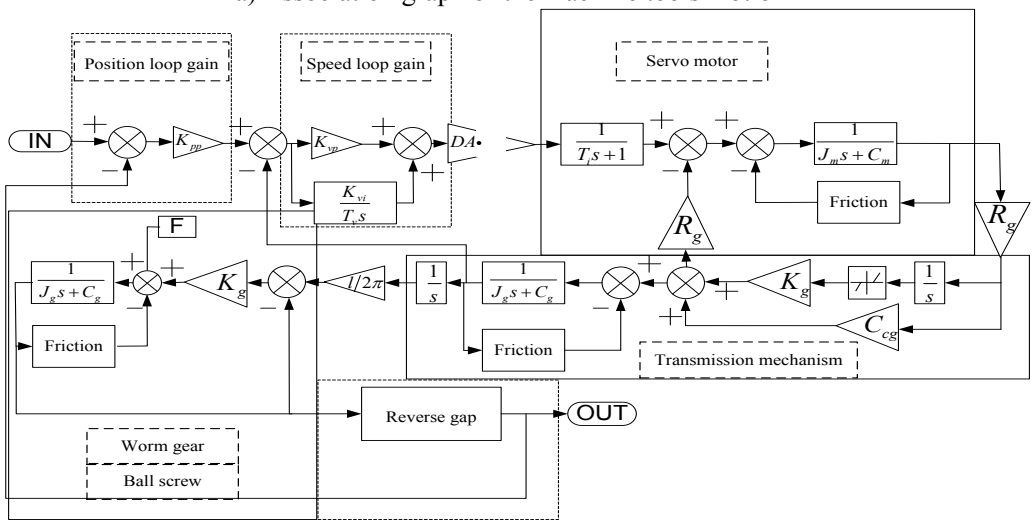

b) Control function of each link

Fig.2 Simulation model of CNC machine tools

Experimental design

From the analysis of simulation experiment can be found in the "S" test part can reflect main factors of the machining accuracy, assumed to be factors 1~7. Because the experimental conditions

are limited, cannot design a lot of experiment for each factor experiment, and the factor level change is too small, surface performance of the test part is not sensitive, therefore assume that the level of each factor change for two. According to the normal design of experiment, at least 128 specimen cutting, but using the orthogonal design table cutting experiment design, only need to do 8 times, after the experiment through the regression analysis of SPSS professional can analyze all factors and level of the error source.

In this paper, the experimental design is carried out by selecting factors: the position loop gain (five axis CNC machine tool matching uniform adjustment), axis-Y and axis-B acceleration. The level of experimental factors design as shown in table 1.

Table 1 The level of experimental factor

Factor \ Level	1	2
Position loop gain	+30%	-25%
Acceleration（Y/B）	-50%	+50%

Data processing

Experimental data processing. Fig.3 is the first experiment result, error measurement by three-coordinate measuring machine. Fig.3a shown 75 point position error, Fig.3b is three dimensional display of the position error, the surface of "S" test part in different colors to distinguish the error value and the negative image, to express distribution of the cutting error. "*" indicates the origin of measurement, "+" indicates the location of maximum error, "O" represents the maximum negative error position, in addition to Fig.3b gives each experimental measurements and super slip. From the Fig.3b can directly see the "S" test part central opening and closing angle conversion position prone to large negative error (the phenomenon of over cutting), as shown in the blue calibration region in the Fig.3b; in the "S" test part cutting end is easy to appear the large positive errors (undercut phenomenon), as shown in the red calibration region in the Fig.3b.

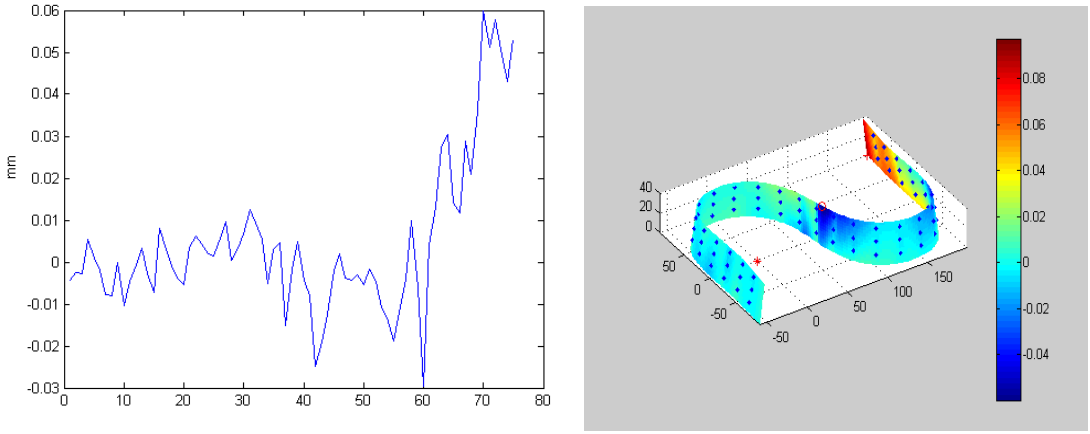

a）Point position error b）Three dimensional display

Fig.2 The first experiment result

Regression analysis

Multiple linear regression method is studied more arguments and experimental indexes, the main idea is to use linear experimental method is established between the cause variable and multi variables regression model[5]. The controllable variables into the hypothesis in the experimental process, i.e.$x_1, x_2, \ldots, x_n$. The multiple linear regression model can be expressed as equation 1:

$$y_i = \beta_0 + \beta_1 x_{i1} + \beta_2 x_{i2} + \cdots + \varepsilon_i \tag{1}$$

In the equation: y_i is the index of observation value; $\beta_0, \beta_1, \beta_2, \cdots$ is the linear regression coefficient; $\{ x_{in} \}$ is the controllable variables of the experiment examines; ε_i is the random errors in the process of experiment.

After the cutting experiment, measure error of "S" test part through three-coordinate measuring machine. According to the obtained experimental results of orthogonal test design, through the SPSS statistical software to do a special regression analysis, set up multi input (dynamic factor index) and the output (the error of "S" test part). Analysis of the experimental factors alone, coupling changes corresponding to the error. At the same time calculate the weight by the experimental factors on the error contribution through linear regression coefficient.

As shown in Fig.4a dotted curve indicates a cutting experiment method to the error, The solid curve indicates the error through linear regression coefficient calculated, comparing two curves, the tendency is consistent, the isolation of single factors using the method of multiple linear regression model to error is reliable. Fig.4a b, 4c, 4d is a phase separation results of experimental factors. Comparing the three figure can be seen, the error is rising in cutting of the "S" ending up position. In order to influence on the error description when change of factor level, injected new ideas "range" (errors of different level by the same factor difference), if a factor to the range is greater, mean change of the factors influence of the larger error of "S" test part. The range under the action of acceleration of axis-B calculated 1.239, acceleration of axis-Y acceleration calculated 0.6205, position gain calculated 0.5847. Therefore the acceleration of axis-B level changes to the error of "S" test part great influence, the acceleration of axis-Y acceleration time secondly, the position gain minimum.

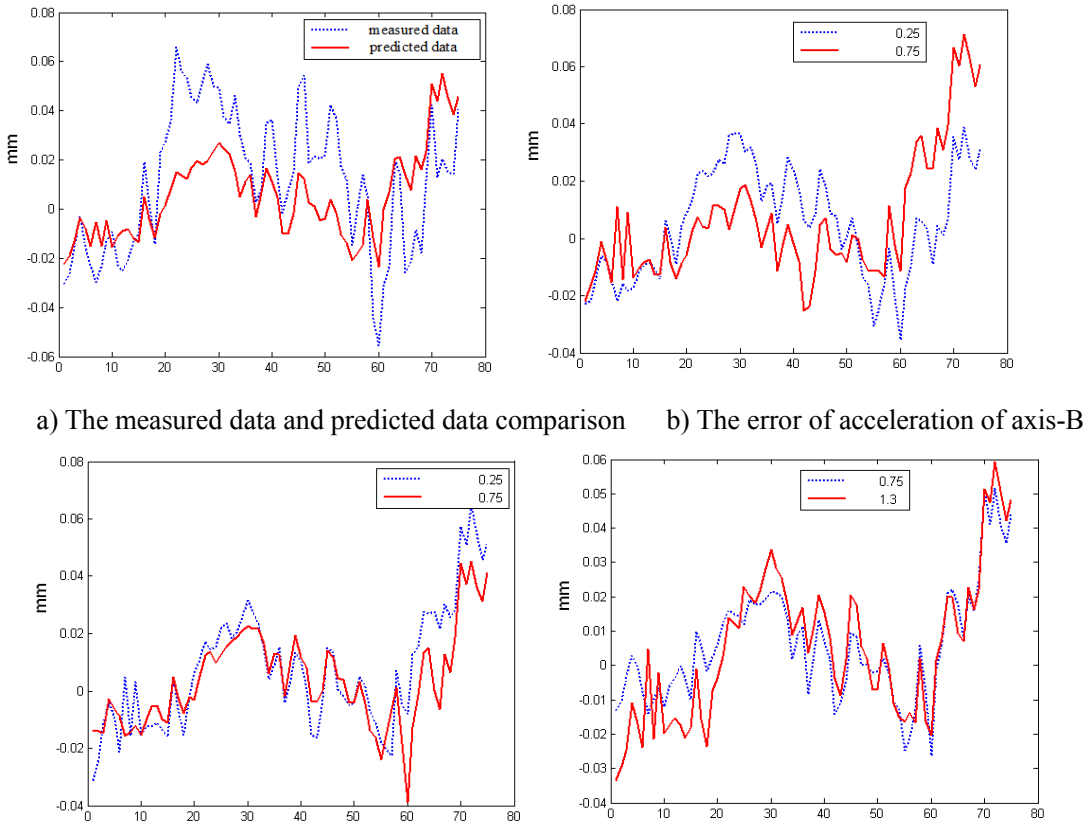

a) The measured data and predicted data comparison b) The error of acceleration of axis-B

c) The error of acceleration of axis-Y d) The error of position gain

Fig.4 The separation results of experimental error

Error source identification

Many factors influence the cutting of "S" test part, direct use of the neural network to identify the error source, the accuracy is not high[6]. First, using the fuzzy membership tracing out key error factors of "S" test part, and then combining BP neural network to identify the key factors.

Fig.5 gives algorithms of error source identification of the CNC machine tools.

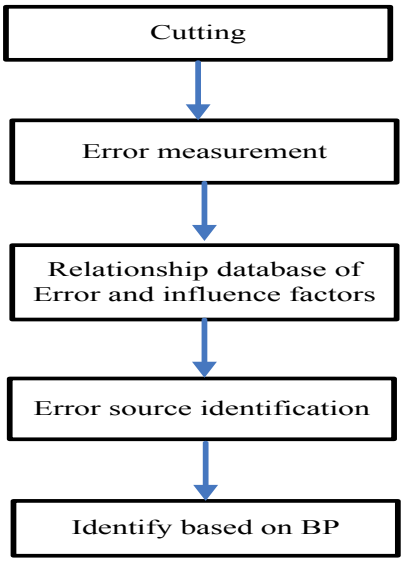

Fig.5 Algorithms of error source identification

According to the error distribution results, choose normal fuzzy membership function is calculated, as shown in equation 2, first establish the matrix $E_i = (a_{i1}, a_{i2}, \ldots$ corresponding to the change of errors of every dynamic factor (E_i representation error matrix, n representation number of the errors), calculate the cutting error into the equation 2, get out of the membership, as shown in equation 3.

$$\mu_B(x) = e^{-k(x-a)^2} \quad (k > 0) \tag{3}$$

In the equation: a is the error of E_i; x is the error of error matrix.

In order to determine the degree of similarity x and E_i, substitution the result of equation 3 into the equation 4, calculated the corresponding similarity value, in accordance with the closeness maximum principle, tracing the main dynamic influence factor of the CNC machine tools.

$$\sigma_H(E, X) = 1 - \frac{1}{n}\sum_{i=1}^{n}\left|\mu_E(x_i) - \mu_X(x_i)\right| \tag{4}$$

In the equation: $\mu_E(x_i) = 1$.

Establishment 3-layers BP neural network identification model based on MATLAB as shown in Fig.6, input is the points of "S" test part, output is the accuracy index. The neural network is trained by using sample, the training process continuously adjust the weights and thresholds of connection between the 3-layers, so as to realize the relationship between error of "S" test part and accuracy index size of machine. After training, input to the error of "S" test part, iterative identification through the network to produce the corresponding index value of accuracy.

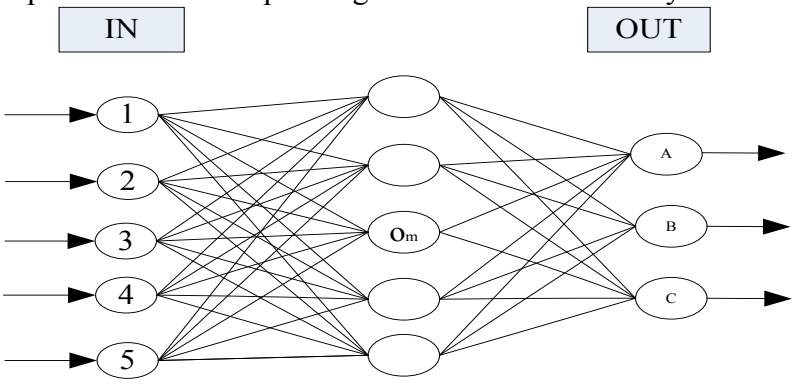

Fig.6 3-layers BP neural network identification model

Summary

In this paper, by trial cutting method, "S" test part is a new test part for detecting machining accuracy of five-axis linkage machine tools. Through experiment and simulation, identification of the error source of the machining accuracy and the regular of "S" test part surface errors, surface quality, results show that "S" test part can reflect the machining accuracy of CNC machine tool.

Acknowledgements

Supported by National Science and Technology major projects in China (2013ZX04001-021).

References

[1] NAS979: Uniform cutting test-NAS series, metal cutting equipment, 1969.

[2] Song, Z.Y., Cui, Y.W. S-shape detection test piece and a detection method for detecting the precision of the numerical control milling machine. US: 20100004777,2010,1,7.

[3] Dong Xie, Jiexiong Ding, Yanbo Huo, etc. Modeling of feed-rate predicition for small segment in high speed maching. ICEMI. 2011,Vol.2:176-180.

[4] Rongbo Shi, Jiming Yan, Zhiping Guo, etc. A New Test Part for Detecting Processing Accuracy of Five Axis CNC Machine Tools. Advanced Materials Research Vols. 468-471.

[5] Wang Xiushan, Yang Jianguo, Yu Yongchang. Research of thermal error modeling, measurement and compensation for Two turntable 5-axis NC machine tools. China Mechanical Engineering.2009,04.405-408.

[6] Zhang Hongtao. Research of dynamic real-time compensation error double turntable of five-axis CNC machine tool [D]. Shanghai Jiao Tong University, 2011.

Advanced Materials Research Vols. 846-847 (2014) pp 40-43

doi:10.4028/www.scientific.net/AMR.846-847.40

Research and Application of a New Constant Tension Control Device of the Carbon Fiber Warping Machine

Qin Jianfeng[1,a], Jiang Xiuming[1], Yang Jiancheng[1], Wang Huaqing[1], Yang Kai[1], Bai Yu[1], Hu Shuanghu[1]

[1] Advanced Mechatronics Equipment Technology Tianjin Area Major Laboratory, School of Mechanical Engineering, Tianjin Polytechnic University, Tianjin, 300387, China

[a]qinjianfeng5188@126.com

Keywords: Carbon fiber; warping; tension control; multilayer weaving

Abstract. This paper presents a new constant tension control device which is suitable for warping of the carbon fiber or the flake yarns which are zero twist, high tensile strength, low shear strength, high specific modulus and self-lubrication and can meet the requirements of the warp tension of the carbon fiber multi-layer weaving equipment which is in the process of development. The device can make yarn tension consistent in warping process. Especially with the decrease of the diameter of yarn tube, the tension of yarn sheet is consistent in warping process. In the process of warping the warp doesn't twist and wear is small. The experimental results show that the mechanism can realize accurate control on the tension of the single yarn and the yarn sheet, and is able to meet the requirements of the warp tension of the carbon fiber multi-layer weaving equipment which is in the process of development.

Introduction

With the rapid development of engineering and material science, the requirements of material performance have become more and more high. The carbon fiber composite materials because of its unique and excellent performance, is widely applied in aerospace and other fields [1, 2]. 3D woven carbon fiber is the rapid development of a new type of fabric structure and is a kind of the whole fiber reinforced skeleton interwoven by the continuous fiber in three-dimensional space according to certain rule and form [3].

Domestic carbon fiber three-dimensional multi-layer weaving equipment is in the stage of development which can reach up to 30 layers, especially the yarn count up to twenty thousand. For the reason that the bobbin creel let-off covers a big area and can't meet the requirement of multi-layer weaving, carbon fiber warping is the indispensable preparation process of carbon fiber multi-layer weaving.

Traditional warping tension device cannot meet the requirements of tension control of the carbon fiber [4]. To meet the requirements of the long yarn path and the consistency of single yarn and yarn sheet of the carbon fiber multi-layer weaving equipment [5], a set of carbon fiber warping tension control system is studied and designed in this article and the problems of the carbon fiber warping is overcame.

Technological process

The carbon fiber warping tension control device on the overall design in turn includes yarn sheet tension servo control device, single yarn unwinding device, yarn tension detection device, five roller tension device. Technological process can be described below. Firstly, the yarns are unwound from tangential bobbin creel, by changing the tension of the spindle tape the single yarn tension can be adjusted; Secondly, separating reed folds and arranges yarns, and then tension detection roller detects the initial tension of the yarn sheet. For the reason that with the diameter of yarn tube the initial tension of yarn sheet will increase and winding density will increase so that the difference among pan heads will be obvious and have much influence on property of the weaving. In view of

the problems mentioned above, in this article the servo control device of the yarn sheet is adopted to adjust the unwinding tension; Thirdly, the yarn sheet gets around the five roller tension device, among the five roller the first two (near tension testing institutions) as the active roller. Through changing the difference of the linear velocity between the active roller and the wind up roll, the sliding friction between the yarn sheet and the active rollers will emerge, so that the tension of yarn sheet will be increased. Eventually the tension of yarn sheet fulfills the requirements of carbon fiber warping tension; in the end, the yarn sheet is winded to the pad head with constant linear velocity. The working principle diagram of the tension control device of the carbon fiber warping machine is shown in Fig.1.

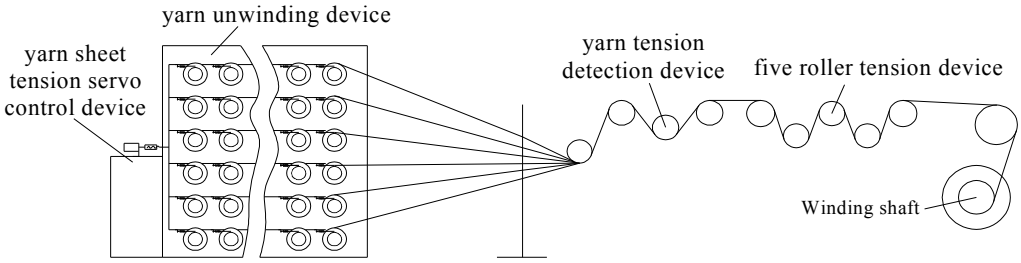

Fig.1The working principle diagram of the tension control device of the carbon fiber warping machine

Yarn tension control device

Yarn tension control device, in turn, consists of three parts. The first is the single yarn unwinding device, after getting around the guide rods, ceramic ring, and set plate, the unwinding single yarn obtain an initial tension; The second is the yarn sheet initial tension detecting and adjusting device, this device detect the initial tension of the yarn sheet and compare the value with the set value, and then control the servo motor to adjust the detecting value equal to the set value; The last one is the final tension device, after the yarn sheet going through the device ,the initial tension of the yarn sheet will be improved to the winding tension.

The single yarn unwinding device. This paper adopts a radial unwinding creel which can have a capacity of 120 bobbins. After unwinding from the yarn tubes, the yarns go through guide rod, ceramic ring, set plate and yarn guide roller. Under the winding of constant linear velocity and ignore the adhesion force during the process of yarn unwinding, etc, the single yarn tension can be calculated as follows:

$$F_0 = \frac{F_s \cdot \mathrm{D} \cdot (1 - \frac{1}{e^{\mu_0 \alpha_0}})}{d} \cdot e^{(\mu_1 \alpha_1 + \mu_2 \alpha_2 + \mu_3 \alpha_3)} \tag{1}$$

Where: F_s is the spindle tape tension; μ_0 is the friction coefficient of the spindle tape and the spindle seat; α_0 is the wrap angle of the spindle tape and the spindle seat; D is the diameter of the spindle disk; d is the diameter of yarn tube; μ_1 is the friction coefficient of the guide rods and the warp; α_1 is the warp angle of the guide rods and the warp; μ_2 is the friction coefficient of the ceramic ring and the warp; α_2 is the warp angle of the ceramic ring and the warp; μ_3 is the friction coefficient of the warp and the guide roller; α_3 is the warp angle of the warp and the guide roller;

The yarn sheet initial tension detecting and adjusting device. From the Eq. 1 we know that the initial tension of yarn sheet is that:

$$F_1 = \mathrm{n} \cdot F_0 \tag{2}$$

From the two equations, we know that the main variables affecting the initial tension of the yarn sheet is the tension of the yarn spindle tape and the diameter of yarn tube. In warping process, with the decrease of the tube diameter of yarn, the tension of the single yarn and the yarn sheet will increase gradually so that the winding quality and the winding density of the pan heads will be

influenced and the differences between the different pan heads will cause weaving opening is not clear. To solve this problem, this paper adopts the yarn sheet initial tension detecting and adjusting device. This tension sensor detects the initial tension of yarn sheet actively; the controller compares detection value with the set value and feedbacks to the servo motor to adjust the whole strain of the spindle tapes and adjust the detection value to the set value. The purpose of regulation is to ensure the ratio of the tension of the spindle tape and the tube diameter of yarn and the consistency of the initial tension of yarn sheet. Control block diagram, as shown in Fig. 2.

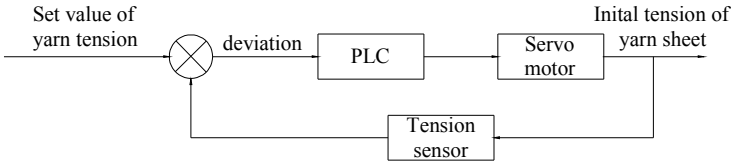

Fig. 2 The yarn tension control block diagram

The final tension device. Ordinary warp tension of warping mainly relies on the elastic deformation of the fiber that is achieved from the linear velocity difference of the winding roller and traction roller. Due to carbon fiber itself has a high elastic modulus and self lubrication, difference of tension directly projects on the winding length. The carbon fiber on the traction roller needs only a small force to slide so that relying on the elastic deformation to control the tension is not too big effect.

If warping tension is too small, the pan heads will be soft and the deviation of winding circumference will be big, during the weaving process, it is prone to defects cloth and cloth is not smooth, in addition the carbon fiber is a high tensile strength, so the carbon fiber is suitable for large tension warping. Creel unwinding tension or the tension of the yarn sheet is far less than the carbon fiber warping tension; the final tension device is adopted to increase the tension of warping. The final tension device is composed of five rollers, the first two rollers are active rollers which rotate to the opposite in the equal-sized speed, and the remaining three rollers is passive roller. The linear speed of the active rollers and the winding roller has certain differential, so when winding the sliding friction will be produced between the carbon fiber and the two active rollers. Due to the self-lubrication of the carbon fiber, mutual sliding will not cause damage to the carbon fiber, so the yarn tension will be increased. By changing the warp angle of the yarn sheet and the passive rollers, the tension of yarn sheet will be increased to the warping tension.

Moreover, the final tension device has the effect of uniform the tension of yarn sheet. Due to the existence of the sliding friction, after going around the passive rollers, the yarns with the smaller tension will be increased, so the difference of yarns will be decreased and the consistency of the warp tension will be better.

Experiment

In the experiment the parameters of winding process is adopted, such as the warping speed, yarn tension, traverse frequency, and so on, to achieve the best winding density and winding quality. The measuring tool of the experiment is Y2301 (DTM) digital yarn tension meter.

Fiber of the experiment. The T700-12 k carbon fiber.

Experimental results and analysis. After repeated warping experiment, testing on the carbon fiber weaving equipment and comparing the experimental results, the optimum technological parameters of the carbon fiber warping are completed, as shown in Table 1.

Table 1 Parameters of the carbon fiber warping

Warping speed	40 m/min	The number of yarn	45
Beam width	200 mm	the initial single yarn tension	450 CN
Yarn sheet width	198 mm	Yarn sheet tension	90 N
Reciprocating stroke	4 mm	Free yarn length	550 mm
Winding density	1.13 g/cm^3	Traverse frequency	0.25 HZ

Conclusions

A new constant tension control device of warping which is suitable for the carbon fiber has been developed based on the characteristics of carbon fiber, such as zero twist, high tensile strength, low shear strength, high specific modulus and self-lubrication.

This device can guarantee the consistency of yarn tension in the process of warping; the difference of pan head will not affect the usage and can meet the requirements of long-distance let off.

Acknowledgement

This research has been supported by the National 12th Five-technology Support Key Projects (2011BAF08B02).Qin Jianfeng also thanks Advanced Mechatronics Equipment Technology Tianjin Area Major Laboratory. The authors thank Jiang Xiuming for his valuable comments and helpful discussions.

References

[1] BOGDANOVICH A E, KARAHAN M, LOMOV S V, et al. Quasi-static tensile behavior and damage of carbon/epoxy composite reinforced with 3D non-crimp orthogonal woven fabric [J]. Mechanics of Materials, 2013, 62(14-31.

[2] FISHPOOL D T, REZAI A, BAKER D, et al. Interlaminar toughness characterisation of 3D woven carbon fibre composites [J]. Plastics, Rubber and Composites, 2013, 42(3): 108-14.

[3] NAUMAN S, CRISTIAN I, KONCAR V. Intelligent carbon fibre composite based on 3D-interlock woven reinforcement [J]. Textile Research Journal, 2012, 82(9): 931-44.

[4] SEVOST'YANOV P, NOVOSELOV K. Statistical modeling of warp thread tension in automatic control of warping [J]. Fibre Chemistry, 2008, 40(2): 152-4.

[5] HOERSTING K, WIENANDS C. Low Cost Tangential Bobbin Creel for Twist-Free Intermittent Reinforcement Fiber Placement [J]. Textile Research Journal, 1999, 69(6): 389.

Advanced Materials Research Vols. 846-847 (2014) pp 44-47

doi:10.4028/www.scientific.net/AMR.846-847.44

Development of High Speed Motor with Magnetic Bearing

Haibo Yu [1, a] and Kun Wang [2,b]

[1] China Electric Power Research Institute, No. 15, Xiaoyingdonglu, Qinghe, Haidian, Beijing, China

[2]Science and Technology on Inertial Laboratory, Fundamental Science on Novel Inertial Instrument & Navigation System Technology Laboratory, School of Instrument Science and Opto-electronics Engineering, BeiHang University, Beijing, China (Corresponding Author)

[a] buaayhb@163.com, [b] wangkunggg@163.com (Corresponding Author)

Keywords: magnetic bearing, high speed motor, rotor, wind abrasion

Abstract. In order to in-depth study the magnetic suspension molecular pump technology, a 4kW high speed magnetic motor was firstly developed. The magnetic motor includes 2 radial magnetic bearings, 2 axial magnetic bearing with five degrees of freedom. The wind abrasion and magnetic flux distribution in stators and the gap between the stator and the rotor were analyzed. Then the high speed magnetic motor prototype was introduced in detail. At last, the basic experiment result was present and the conclusions were given.

Introduction

In the past 10 years, research on magnetic suspension technology has become a significant subject in motor develops. High speed magnetic motors can be found as useful and energy saving tools in air conditioning compressor, sewage treatment plant, molecular pump technology and so on because of their small size, low-cost and no pollution [1]–[4]. Magnetic bearings offer many technical advantages for turbo machines such as oil-free operation, negligible friction loss, low acoustic noise, and extending a limit of rotational speed. For molecular pump rather high axial loads may occur and the reliability of axial bearings is extremely important [5]. In case the axial magnetic bearings are malfunctioning, the auxiliary mechanical bearings can hardly support the rotors due to the high speed and high axial force, which will result in unexpected damage to the compressors, even to the users. Presently most magnetically suspended compressors adopt active magnetic bearings (AMBs) [6]–[8], which have good controllability and damping properties. In order to complete the development of molecular pump, a lower powered high speed magnetic motor should be developed firstly to verify several key technologies. Therefore, this paper is focus on the development of a lower powered high speed magnetic motor.

The paper is organized as follows. Section 2 gives a detailed introduction of the magnetic designing of motor stator. Section 3 gives a description of the magnetic designing of the radial magnetic bearing and the axial magnetic bearing stator. Section 4 describes the composition of the high speed motor in practical. Conclusions and suggestions for future work can be found in last Section.

Design of Stator

We know that the smaller the rotor length is the higher the first bending frequency is. And the bigger the rotor diameter is the higher the first bending frequency is. However, because the AMBs and sensors should be installed, the rotor length can not be too short. Fig. 1 shows the relationship of the rotor diameter and length with the wind abrasion. We can see that the wind abrasion increase significantly with the increase of the rotor length and diameter. So the rotor diameter can not be too big either. Fig. 2 shows the relationship of the wind abrasion with the gap between the stator and the rotor. We can see that with the increase of the gap between the stator and the rotor the wind abrasion will be decrease.

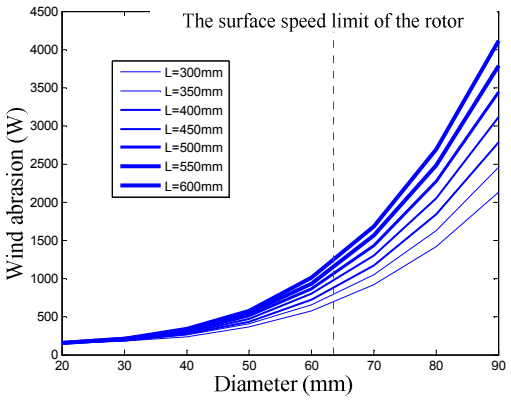

Fig. 1 The relationship of the rotor diameter and length with the wind abrasion.

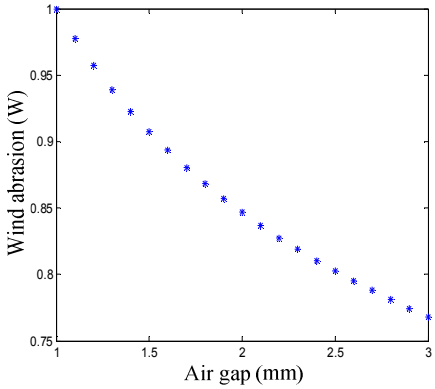

Fig. 2 The relationship of the wind abrasion with the gap between the stator and the rotor.

Based on the analysis of the wind abrasion, we designed the motor stator as shown in Fig. 3 and Fig. 4. Fig. 3 shows the simulation of magnetic flux density amplitude. And Fig. 4 shows the simulation of magnetic flux distribution. We can see that the flux density and the magnetic flux distribution are relative uniform. The simulation result can fit the design specifications.

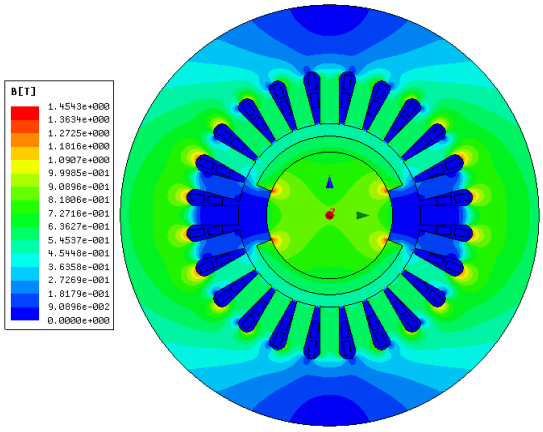

Fig. 3 The simulation of magnetic flux density amplitude.

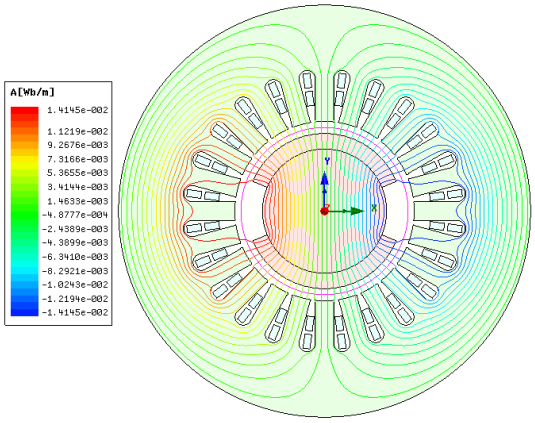

Fig. 4 The simulation of magnetic flux distribution.

Fig. 5 shows the radial magnetic flux distribution in the gap between the stator and the rotor. We can see that the magnetic flux distribution is relative uniform.

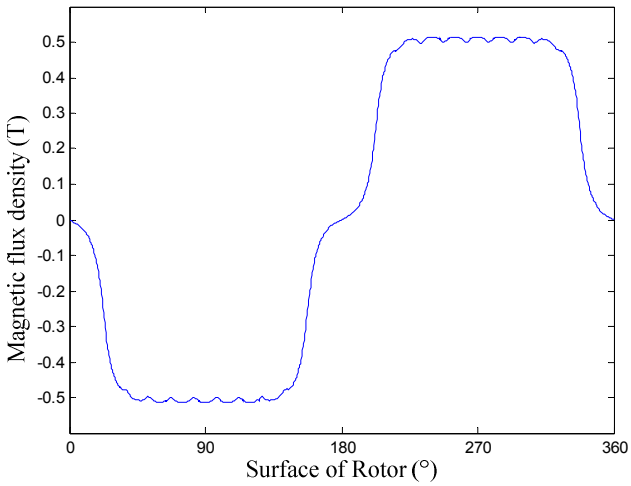

Fig. 5 Radial Magnetic flux distribution in the gap between the stator and the rotor.

Design of Magnetic Bearing

To reduce the develop difficulty, the high speed magnetic motor will be vertically installed that can make the debug easier. So there are some claims to radial magnetic bearing and axial magnetic bearing. Firstly, vertically installed can make the axial magnetic bearing symmetry because the rotor gravity can offset a part of axial load force. Secondly, the eddy current loss of radial magnetic bearing is more serious, and the skin effect is obvious. The bearing stiffness will decrease with the speed increased. Therefore, the load capacity of radial magnetic bearing should meet the requirements of the maximum radial force in the maximum speed of molecular pump. Finally, rotor suspension, which include begin to suspension and sudden failure to drop to auxiliary bearing in running then begin to suspension again, require the radial magnetic bearing have sufficient radial supporting force.

Fig. 6 shows the magnetic flux density of amplitude of the radial magnetic bearing stator in floating status. Fig. 7 shows the magnetic flux density of amplitude of the radial magnetic bearing stator in Max output supporting force status. Fig. 8 shows the magnetic flux density of amplitude of the axial magnetic bearing stator in Max output supporting force status. We can see that the simulation result can fit the design specifications.

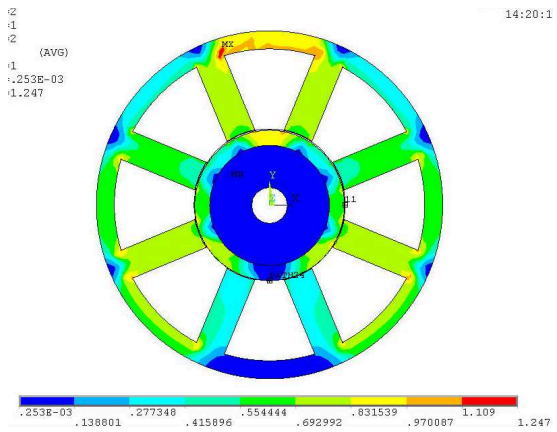

Fig. 6 The magnetic flux density of amplitude of the radial magnetic bearing stator in floating status.

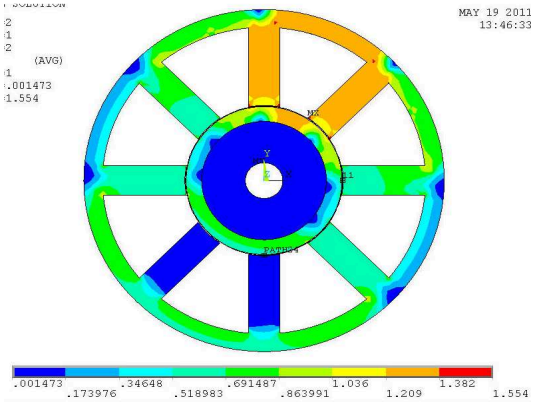

Fig. 7 The magnetic flux density of amplitude of the radial magnetic bearing stator in Max output supporting force status.

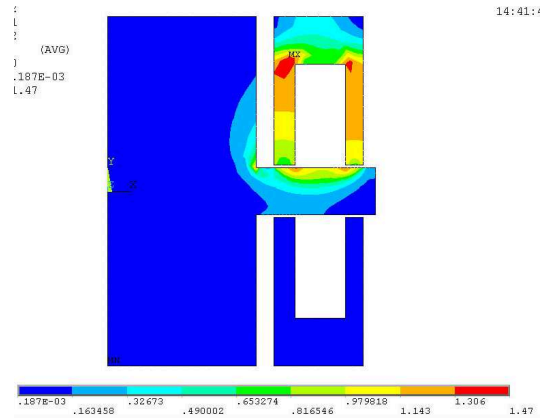

Fig. 8 The magnetic flux density of amplitude of the axial magnetic bearing stator in Max output supporting force status.

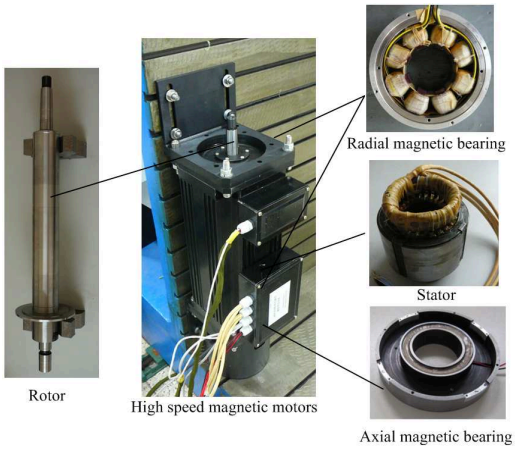

Fig. 9 The Prototype of high speed magnetic motor.supporting force status.

Development of the Motor

Fig. 9 shows the prototype of high speed magnetic motor, which mainly including 1 motor stator, 2 radial magnetic bearings, 2 axial magnetic bearing, rotor and some other parts such as sensors, auxiliary bearings, controller and so on.

The rated power of the high speed magnetic motor is 4kW. Rated rotation speed is 60000rpm. Rated voltage is 480V. Rated frequency is 1000Hz. The material of rotor is 40Cr. The total weight of the prototype is 30kg.

Basic Experiment

In order to improve current tracking speed, a current loop should be added on position loop. We directly added it to the duty cycle. This can make the position loop and current loop parameters independent. And it can also work in the condition of that the position loop and the current loop disconnected.

The experiment result is as follow. The radial float time from the starting to float to a predetermined position is 0.035s. The axial float time is 0.09s. The overshoot phenomenon is greatly reduced. The highest voltage used in the speed increasing of motor is 43V. The motor now can reach the highest rotation speed is 53200rpm.

Conclusions

A high speed magnetic motor based on the magnetic suspension technology was proposed and experimentally verified. The following results were obtained:

(1) The electromagnetic analysis and simulation of motor stator and magnetic bearing stator based on finite element method was presented.

(2) A prototype of high speed magnetic motor was developed in practical.

(3) The validity and feasibility of the prototype were tested by a series of basic experiments.

Future work will focus on the technology of flexible rotor. And improve the shortcomings on mechanics and control to realize the expected target.

References

[1] N.-C. Tsai and C.-W. Chiang: High-frequency linear compressor and lateral position regulation. IEEE Trans. Contr. Syst. Technol. vol. 20 (2012) p. 127–138

[2] P.-K. Budig: Magnetic bearings and some new applications. in Proc. XIX Int. Conf. Electrical Machines (ICEM)., Rome, Italy 2010 p. 1–7

[3] K. Hijikata, M. Takemoto, S. Ogasawara, A. Chiba, and T. Fukao: Behavior of a novel thrust magnetic bearing with a cylindrical rotor on high speed rotation. IEEE Trans. Magn., vol. 45 (2009) p. 4617–4620

[4] C. Bailey, D. Saban, and P. Pinto: Design of high speed, direct connected, permanent-magnet motors and generators for the petrochemical industry. IEEE Trans. Ind. Appl., vol. 45 (2009) p. 1159–1165

[5] C. H. Park, S. K. Choi, and S. Y. Ham: Design and control for hybrid magnetic thrust bearing for turbo refrigerant compressor. in Proc. 2011 Int. Conf. Automation Science and Engineering, Trieste, Italy (2011) p. 792–797

[6] S. Y. Yoon, Z. Lin, C. Goyne, and P. E. Allaire: Control of compressor surge with active magnetic bearings. in Proc. 49th IEEE Conf. Decision and Control, Atlanta, GA (2010) p. 4323–4328

[7] H. Walter, J. Denk, and D. Stoiber: Active magnetic bearing systems with standard drive technology for large turbo machines. in IEEE Petroleum and Chemical Industry Conf. (PCIC) Rec. (2010) p. 56–61

[8] D. Eaton, J. Rama, and S. Singhal: Magnetic bearing application and economics. in IEEE Petroleum and Chemical Industry Conf. (PCIC) Rec. (2010) p. 156–173

Advanced Materials Research Vols. 846-847 (2014) pp 48-51

doi:10.4028/www.scientific.net/AMR.846-847.48

Research of the Multilayer Carbon Fiber Loom's Shedding Device

Yang Kai[1,2] Yang Jiancheng[1,2] Wang Huaqing[1,2] Qin Jianfeng[1,2] Bai Yu[1,2]
Hu Shuanghu[1,2] Jiang Xiuming[2]

[1]School of Mechanical Engineering of Tianjin Polytechnic University

[2]Advanced Mechatronics Equipment Technology Tianjin Area Major Laboratory

Tianjin , 300387,China

584170006@qq.com

Keywords: Multiple openings, carbon fiber, multilayer loom.

Abstract. This paper designs a set of jacquard and dobby shedding device, it specially suitable for 30 layers carbon fiber weaving equipment, which meet the requirement of the special shed. Through to the main drive system design of the jacquard, the structural design and the kinematics analysis of tandem cylinder dobby shedding mechanism, so that the design reasonable. The experiments show that the opening device can well ensure the shedding action orderly, continuously and the shed clear, it can meet the requirements.

Introduction

The three-dimensional carbon fiber woven fabric is a strengthen frame system which is interwoven by continuous fiber bundles according to a certain rule in three-dimensional space. The fiber bundles which throughout the three directions made the fabric integrated and stable, so it can resist stress concentration of tensile, impact damage and crack propagation[1].

The multilayer (up to 30 layers) carbon angle interlock fabric is a good carbon fiber reinforced material[2]. Due to the complexity of this kind of fabric structure, and the carbon fiber bundle is no-twist, nonelastic, easy to be broken, easy splits leading to fluff[5], all of that can cause the shed unclear. So far, there is still no relevant domestic equipment can meet its weaving requirements of 30 layers angle interlock fabric[3]. This paper is derived from the national key scientific research project named the carbon fiber multilayer weaving equipment and technology research and development. In view of the particularity of the carbon fiber and the complex fabric structure, a new kind of shedding mechanism is designed.

Design of the Main Drive of Jacquard and Tandem Cylinder Dobby Shedding Mechanism

1.1 Design of the Main Drive of Jacquard

The mechanical model of lifting single harness cord shown in figure 1

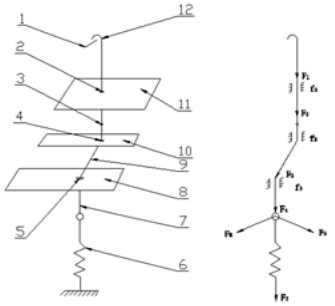

Figure 1 The mechanical model of lifting single harness cord

1. Griffe 2. Hole on the bottom plate 3. Neck twine 4. Hole on the upon demarcation strip 5.Hole on the comber board 6. The spring 7. Harness wire 8. The comber board 9. Harness cord 10. The upon demarcation strip 11. The bottom plate 12. Jacquard hook

The tension of single harness cord can be deduced according to the model, combining with the winch formula $T = T^{'} e^{-\mu\theta}$.

$$F_1 = (F_7 + KS) \times e^{f_1\alpha_1 + f_2\alpha_2 + f_3\alpha_3} + ma \tag{1}$$

In the type, f_1, f_2, f_3 are the coefficient of friction between the harness wire and the comber board , the harness wire and the upon demarcation strip ,the harness wireand and the bottom plate. α_1, α_2, α_3 are the wrap angles between the harness wire and the comber board , the harness wire and the upon demarcation strip ,the harness wireand and the bottom plate.K is the stiffness of the spring,S is the elongation of the spring.

According to relevant theory of the mechanical principle about dynamics,the torque of principal axis can be work out:

$$M = \sum_{1}^{n} F_i V_i \cos a_i / \omega + \sum_{1}^{k} M_i \omega / \omega \tag{2}$$

In the type, F_i is the forces acting on the ith motion part , V_i is the lifting speed of the ith motion part, α_i is the angle between F_i and V_i, ω is the rotate speedof the principal axis, M_i is the torque of the ith motion part,n and k are the number of ift-up and rotation motion parts.

According to torque,it can deducethe formula of the diameter of axle as follows:

$$d \geq \sqrt[3]{\frac{T}{0.2[\tau]}} \tag{3}$$

In the type,d *is* the diameter of the shaft,T is the torque on the shaft, $[\tau]$is the allowable torsional shear stress .

1.2The Design of the Tandem Cylinder Dobby Shedding mechanism

The Shedding mechanism model is shown in figure 2

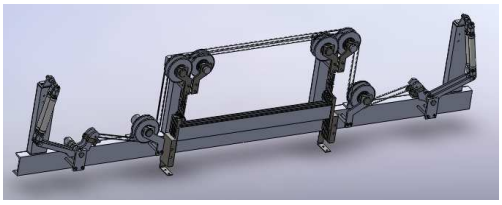

Figure 2 The structure model of the tandem cylinder dobby shedding mechanism

Optimization Design of the Tandem Cylinder Dobby Shedding Mechanism

The analysis process is shown in figure 3

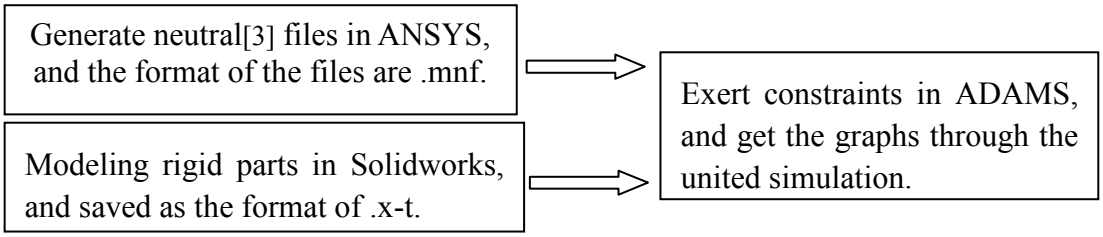

Figure 3 The integration analysis process

The figure 4 shown that all the parts imported into the ADAMS and exerted constraints

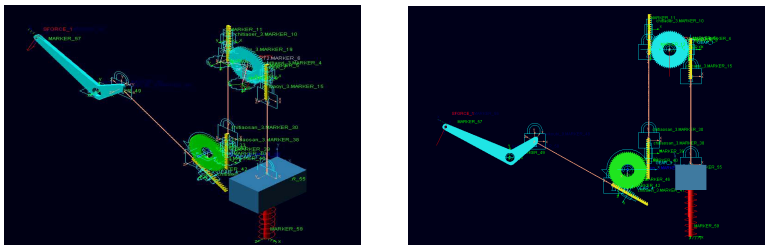

Figure 4 Diagram of the ADAMS model connections

Results of the Analysis

The analysis use a impulse of I = Ft to simulate the thrust of cylinder.The cylinder diameter is 6 cm, under the pressure of 4kg/cm^2, so the trust a cylinder providing is 1130N. Because the function time of the cylinder is 0.2s, the impulse a cylinder producing is I=Ft=1130×0.2=226N.s. And wire rope which is selected that the elasticity modulus is 140GPa. By changing the spring stiffness, obtained the best motion diagrams that are shown in figure 5

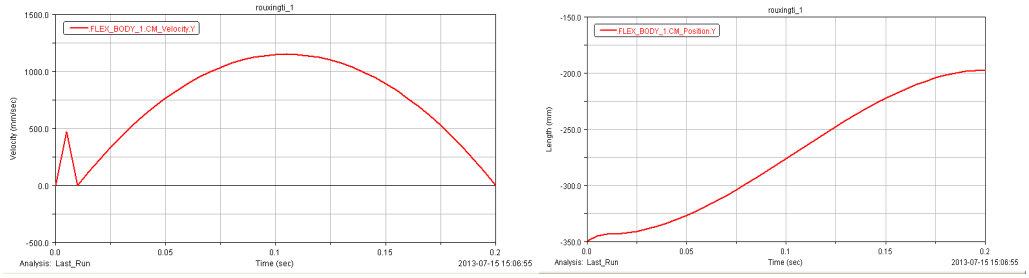

Figure 5 The curves of velocity and displacement changes of the heald frame

Through the velocity changes of the barycenter of heald frame, it can be known that the heald frame has a sudden change of velocity in a short time at start, and then the velocity decreases by the spring buffer system, at last the the curve changed as a rule of parabola. It is conform to practical situation. The curve of displacement of the barycenter of heald frame is smooth, it has an advantage to reduce the damage of the warps.

Conclusion

(1) Designing a set of jacquard and dobby shedding device which can specially suitable for the multilayer carbon fiber weaving equipment, and it can perfect meet the requirement of technology about carbon angle interlock fabric.

(2) The shed device can solve the problem of unclear shed which leaded by the carbon fiber bundle that has no-twist and easy splits leading to fluff .

(3) Making the design more optimal and reliable though the kinematics analysis of the dobby shedding mechanism.

(4) Practice shows that the device has good stability and can satisfy the requirements of the shed orderly, the shed clear.

Acknowledgments

This research has been supported by the National 12th Five-technology Support Key Projects(2011BAF08B02).Yang Kai also thanks Advanced Mechatronics Equipment Technology Tianjin Area Major Laboratory. The authors thank Yang Jiancheng for his valuable comments and helpful discussions.

References

[1] Writting by A.A.Tybaeba and translate by Chen Qishi,The motion and dynamics analysis about Jacquard harness wire and principal axis.

[2] MURATA KIKAI KK. Three-dimensional loom for weaving machine, has thread sending controller which regulates thread supplied to weft, warp and perpendicular thread from beam: JP, 2001064847-A[P],2003-06-30.

[3] Sun Yongde ,Wang Yangtao ,etc. The joint simulation based on ANSYS and ADAMS about flexible body [J]. The school of mechanical engineering of Harbin University of Science and Technology. 2008, 20 (17) : 4501-4504.[1] Zhang Li, Ma Chongqi, Cheng Qingji. New weaving method of 3d composite fabric. [J]. Tianjin Polytechnic University,2006,12:5-9.

[4] Shen Hui ,Wu Qintong. The mechanical structure and control system of 6144 needle jacquard machine[J].The limited company of hangzhou qi hui electronic jacquard machine , 2006, 27 (1) : 80-82.

[5] Zhang Fengfan, Shen Tunian. The technical problems that noteworthy in carbon fiber large-scale application[J]. treasure of carbon fiber in jiaxing liability co., LTD., 2006 (3) : 1-4.

Advanced Materials Research Vols. 846-847 (2014) pp 52-55

doi:10.4028/www.scientific.net/AMR.846-847.52

The Kinematics Simulation and Analysis of the Multilayer Carbon Fiber Loom's Beating-up Mechanism in ADAMS

Yang Kai[1,2] Yang Jiancheng[1,2] Qin Jianfeng[1,2] Wang Huaqing[1,2] Bai Yu[1,2] Hu Shuanghu[1,2]Jiang Xiuming[2]

[1]School of Mechanical Engineering of Tianjin Polytechnic University, Tianjin ,300387, China

[2]Advanced Mechatronics Equipment Technology Tianjin Area Major Laboratory ,Tianjin ,300387, China

584170006@qq.com

Keywords: beating-up mechanism carbon fiber multilayer angle interlocking construction rapier loom

Abstract: This article designs a new set of beating-up mechanism for the multilayer angle interlocking construction loom based on the requirements of special material of carbon fiber and weaving technology,and it can battening 30 layers carbon fiber at a beating-up.Through building the 3D solid models for linkage mechanism in SolidWorks, it show that the beating-up mechanism Run smoothly by the kinematics and dynamics analysis of different beating-up rule in ADAMS.

Introduction

The woven technology of the 3D angle interlocking construction is bundling the separate layers of warp and weft together by the Binder yarn and unified as a whole[2].The basic theory of this technology is the weave technology of the multilayer warp.Because this technology is not mature enough at home,and the development of high-tech in aerospace demands urgent needed of the carbon fiber[1],the study of carbon fiber multilayer loom's beating-up mechanism is particularly important.This research of beating-up mechanism belongs to heavy loom,the drawing mechanism and push rod mechanism have a large force to swinging rod when beating-up mechanism run to the extreme position,at the same time, the swinging rod mechanism will exert a larger torque because the drawing mechanism and push rod mechanism are not on a straight line.In this case, it is necessary to do kinematics and dynamics research for the beating-up mechanism (four-bar linkage) .

Design of the Multilayer Carbon Fiber Loom's Beating-up Mechanism

Building the 3d model for the beating-up mechanism in SolidWorks shown in the figure 1.

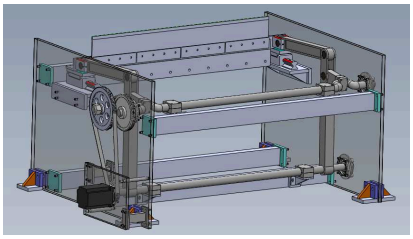

Figure 1 The 3D model of beating-up mechanism in SolidWorks

Optimization Design of Beating-up Mechanism in ADMAS

Using the algorithm of the Lagrange equation about the theory of the multi-rigid-body dynamics system in ADAMS to do dynamics analysis and calculation[3].it can determine the Descartes generalized coordinates of every parts through the Descartes generalized coordinates,and then using

the Lagrangian equation to complete the other coordinates to get a full-constrained system,exporting the variable which contain generalized coordinates and get the kinematic equations in the end.

Kinematics analysis is mainly analyse the displacement,velocity, acceleration and constraint forces[4] in fully constrained system,and the module of the ADAMS/View and ADAMS/Solver in ADAMS provide a variety of solvers that can offer the analysis of kinematics ,statics and dynamics. By solving the equations below can get the displacement,velocity, acceleration and constraint forces,etc.

$$\Phi(q,t)=0 \tag{1}$$

It can get the location of a part at a moment of t_0 based on the equation of Newton-Raphson[5], and the following is the equation.

$$\left.\frac{\partial \Phi}{\partial q}\right|_j \Delta q_j = \Phi(q_j, t_n) \tag{2}$$

In the equation, $\Delta q_i = q_{j+1} - q_j$, and the j represents the jth iteration.

It can get the velocity and acceleration by taking the first and the second derivative of the equation (2) at the moment of t_n.

$$\left(\frac{\partial \Phi}{\partial q}\right)\dot{q} = \frac{\partial \Phi}{\partial t} \tag{3}$$

$$\left(\frac{\partial \Phi}{\partial q}\right)\ddot{q} = -\left\{\frac{\partial^2 \Phi}{\partial t^2} + \sum_{k=1}^{n}\sum_{l=1}^{n}\frac{\partial^2 \Phi}{\partial q_l^{\,2}}\dot{q}_k\dot{q}_l + \frac{\partial}{\partial q}\left(\frac{\partial \Phi}{\partial t}\right)\dot{q}\right\} \tag{4}$$

The value of constraint force at the moment of t_n can be gotten by using the Lagrange equations .

$$\left(\frac{\partial \Phi}{\partial q}\right)^T \lambda = \left\{-\frac{d}{dt}\left(\frac{\partial T}{\partial \dot{q}}\right)^T + \left(\frac{\partial T}{\partial q}\right)^T + Q\right\} \tag{5}$$

Establishing dynamic differential equations by using the method of the Lagrangian multiplier in ADAMS.

$$\begin{cases} \dfrac{d}{dt}\left(\dfrac{\partial T}{\partial \dot{q}}\right)^T - \left(\dfrac{\partial T}{\partial q}\right)^T + \phi_q^T p + \theta_{\dot{q}}^T \mu - Q = 0 \\ \phi(q,t) = 0 \\ \theta(q,\dot{q},t) = 0 \end{cases} \tag{6}$$

In the type, $\phi(q,t)=0$ is a full-constrained equation, $\phi(q,\dot{q},t)=0$ is incomplete constrained equation, T is system energy, q *is* the array in generalized coordinates, Q is the array of generalized force, p is the full-constrained array of Laplace multiplier array μ is the incomplete constrained array of Laplace multiplier array, *M is t*he quality array, ν is the array of generalized velocity, I is the array of rotational inertia.

w —The array of generalized angular velocity

Building the model of the beating-up mechanism in ADAMS and exportting the model files in the format of .x_t, and then opening the files in the ADAMS directly. Defining the material properties of the parts in four bar mechanism,and inputting the mass,the moment of inertia and the other physical parameters according to steel type which is used.Defining the other parts which are not moving in simulation as the ground,so as to form a stable structure .As shown in the figure 2, adding the hinge pairs between 2 connecting rods, so it is for the connecting rods and the reed, and

then add the sliding pair to reed, at last ,adding a driving motor that the rotate speed is 1500r/min on the hinge pair near the end of the shaft.all of that accomplished can it start the simulation.

The pink part in the figure 2 is used to simulate the carbon fibers in the shed. Because the organization of carbon fiber is complex near the shed,it cannot build the 3d model for the shed as the same as the practic,with a flexible[7] rod instead of the carbon fibers in the shed can meet the requirements of the simulation.

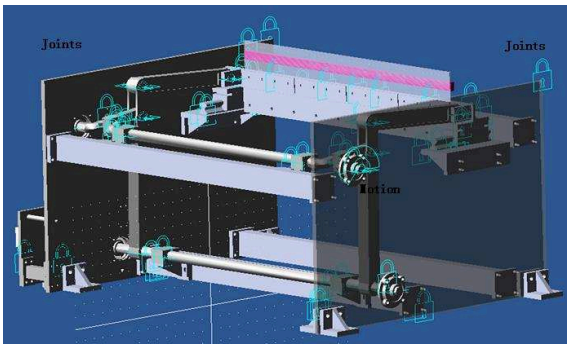

Figure 2 Model of the Beating-up Mechanism in ADAMS

Results of the Analysis

The graph of the reed's displacement and velocity shown in figure 3 as follow:

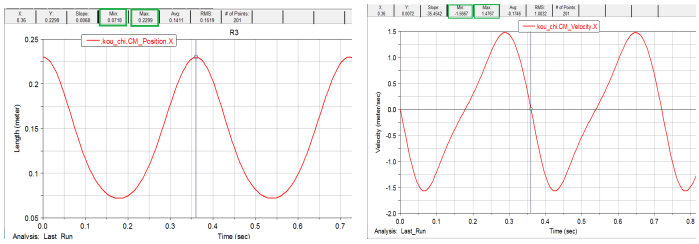

Figure 3 The graph of the reed's displacement and velocity in ADAMS

It can be seen from the figure 3 that the value of the reed's displacement is 0.2299m when the reed goes forward to one extreme position,and the value of the reed's displacement is 0.0718m when the reed goes backword to the other extreme position ,so the stoke of the beating-up mechanism is 0.1581m, it is corresponds to the stoke of 160mm that is required in the design.From the figure 2,it can get the the maximum speed is 1.4767m/s and the minimum velocity is1.5667m/s in a loop,and the results of the analysis within the range of the error.

Summary

Motion analysis is an important process in mechanism design,it can provide a powerful guarantee to optimize and improve the mechanism.Through the kinematics and dynamics analysis for the beating-up mechanism (four bar linkage) of multilayer carbon fiber loom can know more movement rule for the reed,and the design is reasonable based on the graph of the reed's displacement and velocity.

Acknowledgments

This research has been supported by the National 12th Five-technology Support Key Projects(2011BAF08B02).Yang Kai also thanks Advanced Mechatronics Equipment Technology Tianjin Area Major Laboratory. The authors thank Yang Jiancheng for his valuable comments and helpful discussions.

References

[1] Hou Jianrong,Han Xiao. The research of carbon fiber fabric weaving technology in china [J].Journal of high-tech fibers and applications, 2012, 8:37-43.

[2] Ji Yingchao,Jiang Fengqin, Geng Junxin. The research of production practice in carbon fiber weaving [J]. Journal of Textile Research, 2004, 4:25 to 28.

[3] Lu Ning, Chen Huanguo. The dynamics analysis and simulation of rapier loom's beating-up mechanism [J]. Advanced Textile Technology, 2012,2:33-38.

[4] KouJianBin. The dynamics analysis and virtual prototype design of the air-jet loom's beating-up mechanism[D].Shanghai: master's thesis of donghua university.

[5] Zhang Kai,Zhang Xiaozhang.Vibration control of rotational machines by means of active magnetic bearing[C]. Proceedings of the 7th Asia Pacific Conference on Control & Measurement,Tibet,China,2006:95-100.

[6] Lee S.H,Kim B.S,Lee M.G.A comparative study on damage detection in speed-up and coast-down process of grinding spindle-typed rotor bearing system[J].Journal of Materials Processing Technology, 2007:187-188.

[7] Janq G.H,Lee S.H.Free vibration analysis of a spinning flexible disk-spindle system supported by ball bearing and flexible shaft using the finite element method and substructure synthesis[J]. Journal of Sound and Vibration,2002:59-78.

Advanced Materials Research Vols. 846-847 (2014) pp 56-60

doi:10.4028/www.scientific.net/AMR.846-847.56

Artificial Intelligent Diagnosing Method Based on the Certainty-Speculated Reason of Pivot Factor

Tan,Wen Xue [1,2,a] Wu,Hua Rui [1,b *] Wang, Xi Ping [2,c]

[1.] Beijing Research Center for Information Technology in Agriculture, Beijing Academy of Agriculture and Forestry Sciences, National Engineering Research Center for Information Technology in Agriculture, Beijing,100097.

[2.] School of Economics and Management, Hunan University of Arts and Science. Changde, 415000, China.

[3.] College of Computer Science, Beijing University of Technology. Beijing, 100022, China.

[a]email: twxpaper@163.com; [b]email: wuhr@nercita.org.cn; [c]email: wxphuas@163.com

Keywords: Reason; Computer Diagnosing; Intelligent System; Expert system

Abstract. How to solve disease-diagnosing problem effectively by the aid of Artificial Intelligence Computer has been being a mainstream of Intelligent System researching and development. Heretofore, performance of the well-known native Uncertainty Reason Resolution method still is unsatisfactory to professionals. This paper pioneers the concept of Associative-Pivot Factor and its Certainty Index Speculation algorithm, and on this base designs A novelty Machine Diagnosing Algorithm based on the Certainty Reason of Associative-Pivot Factor. Results and analysis demonstrate that the method exhibit a better efficiency than man-expert individual and the native CF Method. Generally speaking, it manifests an accurate rate of diagnosis over 82% and possesses the capacity to expand diagnosing capability of man-expert.

1. Introduction

Along with the development of Artificial Intelligence (AI) application and agricultural information technology, Intelligent Disease Diagnosing System, which referred in the name of Disease Intelligent Aid System by some related literatures, has become a practical instrument used widely in the area of clinic diagnosis. It takes root in the computer technology and standardized expert experience knowledge, builds up human's diagnostic capability. For example, the Sheep Disease Intelligent System based on production rules which was proposed by [1], and the Grape Disease Diagnosis System based on Fuzzy Neural Network was discussed in [2].

On the one hand, Disease Intelligent Aid system, which based on digital technology and normalized expert experience knowledge, expands human's diagnostic ability, and it is widely used in diagnosing as a practical instrument. On the other hand, some systems, of which expert knowledge only based on the traditional Uncertainty factor-Inference (*U-Inference* for short) [3], obviously manifest 2 faults at least as follows.1.A low efficiency of Knowledge-Rule.2.The mechanism of traditional U-Inference based on the static Certainty Factor Vector while short of Correction or Speculation process disagrees with the human's habit of thinking and diagnosing, and always results in one-sided diagnosis, even misdiagnosis [4], [5], [6].

So, we try to overturn the situation by researching Artificial Intelligent Diagnosing Method Based on the Certainty Reason of Pivot Factor.

2. Preliminaries of Associative-Pivot Factor Uncertainty

Randomicity and chanciness, uncertainty are universe phenomena in the nature, and the same thing is in the area of disease diagnosing. Concepts of Uncertainty or Certainty are often used to measure indeterminate causality between cause and effect, which is taken into consideration when we select AI methods to lay foundation for intelligent Disease diagnosing mechanism**.**

[6] and [7] referred that many nature phenomena always have a stochastic-uncertainty accidental manifestation due to unknown factors or undeterminate observing factors. It is the same thing to diagnosing and symptom manifesting. In order to depict indeterminable-casual relation between

diseases and symptoms, the system introduced concepts of Certainty Index or Factor, which was processed into an index representing experimental knowledge certainty degree and being-true degree of observation.

After a long span of investigation, it is made clear that the native Certainty Factor method does not take it into account the associativity between the observed clinic symptoms and those so far not occurring and unobserved symptoms but which are listed in the standardized description of corresponding disease. Thus, a direct result is that some knowledge rules which should have been activated on reasoning have no access to be activated and applied, and misdiagnosis or diagnosis failure comes out. Addressing such a situation, the project crew proposed concepts as follows**.**

Definition 1.**Sample complexity** is defined as how many samples is needed to train a Machine learner to converge at an accurate hypothesis or to output a correct solution in a rather high probability.

Definition 2.**Computational complexity** is defined as how much computation workload is cost before a Machine learner converges at an accurate hypothesis or its convergent hypothesis is an optimal success in a rather high probability.

Definition 3.**Mistake bound** is defined as how many times of mistake classification is made by a Machine learner during classifying learning samples.

Definition 4.**Uncertainty Rule.** It refers to the knowledge rule denoted as (1) subject to (2), abbreviated as(2). *CF(E,H)* denotes the Certainty Factor depicting the knowledge intensity; the greater its value, then the more intensively the precondition denoted by *E* supporting the Hypothesis conclusion denoted by *H*. In other words, the bigger is the probability of conclusion *H* to be true. λ is a threshold of certainty, calculation of *CF(E,H)* referred in [8], [9].

$$if\ \ E_1(w_1)\ \ AND\ \ E_2(w_2)\ \ AND\cdots AND\ \ E_n(w_n)\ then\ \ H(CF(H,E),\lambda) \tag{1}$$

$$\sum w_i = 1, 0 \le w_i \le 1 (i = 1, 2, \cdots n) \tag{2}$$

Let E_i be a symptom of disease A, whose knowledge rule is as equation (1) and A is assigned with the biggest weight w_i of all the symptoms concerned in the rule.

Definition 5. This practical connotation is that E_i is decisive to confirmation of A, and if E_i has developed, the unobserved symptom E_j also will develop in succession if no further action is done to the subject, then define E_i to be a **Pivot Factor**.

Definition 6. In the case aforementioned, define E_j to be the Factor in association with Pivot E_i name it the **Associative-Pivot Factor**.

In a knowledge rule, a sequence of Associative-Pivot weights form a Associative-Pivot vector.

3. Theory of Certainty Factor Speculation

Definition 7. According to the description aforementioned, some steps should be constructed to speculate the certainty index of E_j which is a Associative-Pivot Factor in association with Pivot Factor E_i, not to let it be 0 and assign $CF(E_j)$ (CF_j for short) with some correction value by some speculation algorithm from observed evidence certainty vector $(CF_1, CF_2, ..., CF_k)$. If E_i is unobserved then it need a similar speculation. Define these steps and their corresponding process to be **Certainty Index Speculation**}, alias **Certainty Speculation**.

Let $CF_{speculate}$ be the output of speculation, the project crew proposes 3 methods of Certainty Index Speculation as follows.

$$CF_{speculate} = (\frac{1}{\sqrt{2}} \times \max(CF_1, CF_2, ..., CF_k) + \frac{1}{\sqrt{2}} \times \min(CF_1, CF_2, ..., CF_k)) / 2 \tag{3}$$

$$CF_{speculate} = \frac{\min(CF_1, ..., CF_n) + \sum_{k=1}^{n-2} CF_k \times w_k + \max(CF_1, ..., CF_n)}{w_1 + w_2 + ... + w_{n-2} + 2} \tag{4}$$

$$CF_{speculate} = \frac{(\sqrt{5}-1)\times \max(CF_1,...,CF_n)}{2} + (\sqrt{5}-3)\times \min(CF_1, CF_2, ..., CF_k) \quad (5)$$

Definition 8. Take the multiplication of cut-off-constant and the extremum of CF vector as and get the midpoint of both result as (3), which is called the **cut-off-midpoint-Speculate**. By this method, Speculation-value is only influenced by the extremum of observed CF indexes.

Definition 9. According to the front n CF Indexes of CF vector and $n-2$ weights and 2 constant weights, compute weighted mean-value of $n-2$ CF Indexes and get $CF_{speculate}$ as (4). Define such a speculation method to be **refined-mean-Speculate**.

With this means, we always get a median of confidence-interval between the lowest and the highest. Each of observed CF Index and the weight-vector of knowledge rule impacts $CF_{speculate}$.

Definition 10. If over-much variables restrict speculation value, reasoning process will be complex and low-efficient because of computation-workload. By a hint of golden-section-ratio and weighted-sum method, extract result of (5) and get speculation value, which is **golden-section-Speculate.**

Its computational complexity is between cut-off-Speculate and mean-Speculate, and $CF_{speculate}$ is only influenced by extremum of the observed CF sequence [10], [11], [12].

Which of 3 methods is best in respect of 3 kinds of complexity aforementioned? It is a puzzle. Data reveals that Facing different cases [13], they perform by a wide margin, which will be discussed in some following subsection.

4. Conclusion Certainty Integration

When the reason course ends, it is possible that there be multi rules to be activated and outputs be multi results. However, the system needs to give a macro conclusion as a response to user.

Definition 11. How to integrate a macro conclusion from results of all activated rules is an un-evadable subject matter. Define this fusing course of stand-alone results to be **Integration of Conclusion Certainty**.

Taking a hint from the conceptual similarity between certainty factor and set, researcher group devises an integration-method, where Certainty Factor is regarded as a set object, and is operated a set union operation and integrated several CF values of multi-rule into a macro conclusive CF value as equation (6) whose right function is an expression of (7),(8).

$$CF(\bar{E})\cdot\bar{w}^{(j)} \geq \lambda^{(j)} \ then \ H^{(j)}[CF(\bar{E}), \bar{w}^{(j)}, \lambda^{(j)}], 1 \leq j \leq m \quad (6)$$

$$f(CF(\bar{E}), \bar{w}^{(j)}, \lambda^{(j)}) = \sum_{j=1}^{C_m^1} CF(\bar{E})\cdot\bar{w}^{(j)} + \sum_{i<j\leq m}^{C_m^2} CF(\bar{E})\cdot\bar{w}^{(i)} \times CF(\bar{E})\cdot\bar{w}^{(j)} + f' \quad (7)$$

$$f' = \sum_{i<j<k\leq m}^{C_m^3} CF(\bar{E})\cdot\bar{w}^{(i)} \times CF(\bar{E})\cdot\bar{w}^{(j)} \times CF(\bar{E})\cdot\bar{w}^{(k)} - \cdots + (-1)^{m-1}\prod_{j=1}^{m} CF(\bar{E})\cdot\bar{w}^{(j)} \quad (8)$$

5. Experimentation Statistics and Analysis

Separate Sample Test. In the course of experiment, the Brindled Pig is singled out as a subject to experiment. The disease " Swine Dysentery " is highlighted as an example, of which the clinic manifestations are standardized and segmented into 8 atomic clinic items. A veterinary inputs the clinical symptom data sampled from diseased swine into both software prototypes, one of which based on *this method (this for short)* and the other based on the method proposed by [3] ([3] for short). Meantime, by diagnosing system several paper copies of the clinical report are printed and distributed to some human experts for diagnosing in order to determine the disease infecting the swine [6] and [14]. the information gleaned from the test is as follow.

Average of human experts' result is 0.69, which falls into the interval [0.65, 0.75]. Result of *This* are listed in Table 1. 5 knowledge rules about Swine Dysentery are activated on machine diagnosing,

each of which with a weighted vector of clinic characteristics, and the no. 5,6,7 symptoms are the *Associative-Pivot Factors* assigned with bigger weights. The *Mean-Speculation* method is used to speculate the *Associative-Pivot Factors*. The conclusion interval of *this* is about [0.69, 0.75]; it is best consistent with [0.6, 0.8] drawn by human experts. However, the result of [3] is [0, 0.53], last column of Table 1, and only is 1 rule activated. Mistake is obvious, while its reliability is very low.

Group Sample Test. This system, another system based on [3], and 3 human experts (denoted by John, Mike, Brand) respectively diagnose about 70 typical cases which are arranged and singled out from the recent medical records [15], [16]. Evaluation of performance is shown in Figure 1. It reveals that the diagnosis from the system with the highest accurate rate 82%, the lower misdiagnosis ratio 8% and uncertainty ratio 10%, and it demonstrates an overall diagnosing efficiency better than any individual human expert. Whereas, thing is nearly reverse as to the system based on [3].

TABLE 1. STATISTCIS CONTRAST

No. of Clinic	***CF***	**Weight matrix**					
0	1	1	2	3	2	4	4
1	0.9	3	3	5	3	3	1
2	0.8	11	16	4	3	1	3
3	0.6	15	16	5	3	3	5
4	0.9	5	8	7	9	7	11
*5	0	9	7	10	9	6	5
*6	0	7	4	9	7	9	3
*7	0	3	5	8	5	5	3
λ		0.6	0.5	0.55	0.75	0.6	0.6
Result of 6 rules							
***CF*(*D*, *L*)**		0.70	0.71	0.75	0.71	0.69	0.53

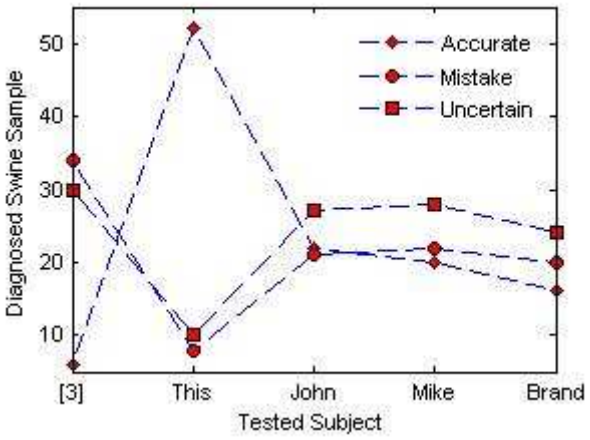

FIGURE 1.Evaluation of Diagnosis Performance

6. Conclusion

Because of overlooking the associability between the observed factors and prospective ones, and without certainty speculation the CF inference mechanism widely used in intelligent Diagnosing system often outputs a blank reply or a mistake diagnosis and manifests a low accuracy and efficiency on solving diagnosing problem. With focus of it, the paper proposes the concept of Associative-Pivot Factor and Certainty Index Speculation algorithm; designs an innovative method to solve computer diagnosing problem. At last, after constructing the prototype system of this innovative diagnosing algorithm, research group take the swine as the subject of test and practice ample test experiments. Results and analysis from the separate-group sample test reveals that its diagnosis accuracy ratio attain 82% and it possess a better overall diagnosing efficiency than any separate man-expert and the native Certainty Factor Diagnosing brought forward by [3]. On the whole, the favorable performance demonstrates the proposed scheme would become a promising AI diagnosing method.

Acknowledgments

This work is funded by Chinese National Science and Technology Support Program (2011BAD21B02; 2012BAD52G01); Hunan Provincial Natural Science Foundation of China (12JJ9020); Hunan Provincial Science and Technology Plan (2013GK3135).

References

[1] Hu Jian-dong, Yu Yong-chang. Technology of a fertilizing expert system PDA for crop growing, Transactions of The Chinese Society of Agricultural Engineering,vol.22(2006),149-155.
[2] XIAO Bing. A measure of non-linearity of partially non-linear regression models [J]. Journal of Hunan University of Arts and Science：Natural Science Edition,2013,1：10-13．
[3] WANG Da-feng, HE Yu-ping, DONG Hai-ping. Model transfer of on-line AOTF-NIR tobacco chemical composition models [J]. Journal of Hunan University of Arts and Science：Natural Science Edition,2013,1：78-81．
[4] Tan wen-xue, Wang xi-ping, Xi jin-ju, et al. Research on diagnosing disease method based on back propagation neural network. Computer Engineering and Design, Vol. 32 (2011),1070-1077.
[5] WANG Chuan-an, GE Hua, WANG Ya-jun. Study on the application of an optimal admission control policy in IPTV system[J]. Journal of Hunan University of Arts and Science：Natural Science Edition,2011,2：82-85．
[6] LIU Wei-feng, HE Xia. Some properties of interval grey numbers determinants based on the kernel and the degree of greyness of grey numbers[J]. Journal of Hunan University of Arts and Science：Natural Science Edition,2011,1：26-30．
[7] Liao Ying, Liang Jiahong, Liao Chaowei, et al. Research on the application of multi-combined technologies of fault diagnosis on missile seekers. Journal of Astronautics，Vol. 3 (2006), 30-36.
[8] YANG Chun-ying, HE Yi-yuan, GUO Mu-lin. Studies on morphological and chromosome karyotype of 2 pelteobagrus species in the Yuanshui and Lishui rivers of Dongting lake water systems in Hunan province[J]. Journal of Hunan University of Arts and Science：Natural Science Edition, 2011,4：57-61．
[9] Liu Shu-wen, Wang Qing-wei. Grape disease diagnosis system based on fuzzy neural network . Transactions of The Chinese Society of Agricultural Engineering, Vol. 18 (2006), 144-150.
[10] ZHU Yong-na. The asymptotic confidence estimation of Logistic distribution parameters with additional restrictions[J]. Journal of Hunan University of Arts and Science：Natural Science Edition,2011,4：26-28．
[11] Tianhong L. Integration of large scale fertilizing models with GIS using minimum unit, Environmental Modeling and Software, vol.18(2003),221-228.
[12] FENG Peng-hui, TAN Xi, LIU Guo-ying, PENG Chuan-wei. Fuzzy optimization based on genetic algorithm in simulation application of three-tank liquid level control system[J]. Journal of Hunan University of Arts and Science：Natural Science Edition,2012,2：46-50．
[13] LU You-xiang, DING Nai-hong, ZHANG Sheng-jun. Effects of different leaf redrying ways on quality of tobacco[J].Journal of Hunan University of Arts and Science：Natural Science Edition,2012,1：87-92．
[14] Chen Liping, Zhao Chunjiang, Liu Xuexin, et al. Design and implementation of intelligent decision support system for precision agriculture [J]. Transactions of The Chinese Society of Agricultural Engineering，2002，18(2)：145－159．(in Chinese with English abstract)
[15] LIAN Gao-jian, YANG Qian. Study of the effect of cysteamine on the change of mast cells number in chicken duodenum [J]. Journal of Hunan University of Arts and Science：Natural Science Edition,2012,3：33-35,45．
[16] LI Feng, ZHANG Yu, WANG Xing-ping. Bioinformatics analysis of Mus. IGF1 Gene promoter regions[J]. Journal of Hunan University of Arts and Science：Natural Science Edition,2012,3：40-45．

Advanced Materials Research Vols. 846-847 (2014) pp 61-64

doi:10.4028/www.scientific.net/AMR.846-847.61

Design of the Let-off Mechanism of Carbon Fiber Multilayer Diagonal Loom Based on Virtual Prototype Technology

Qin Jianfeng[1,a],Jiang Xiuming[1],Yang Jiancheng[1], Wang Huaqing[1], Yang Kai[1],Bai Yu[1],Hu Shuanghu[1]

[1] Advanced Mechatronics Equipment Technology Tianjin Area Major Laboratory, School of Mechanical Engineering, Tianjin Polytechnic University, Tianjin, 300387, China

[a]qinjianfeng5188@126.com

Keywords: carbon fiber multilayer diagonal loom; let-off mechanism; Virtual prototype technology.

Abstract. This paper presents a set of the let-off mechanism of carbon fiber multilayer diagonal loom, which can accomplish thirty layer fabric weaving. This mechanism can realize multi-layer positive warp let-off and negative warp tension control and can meet different fabric structure and different types of warp weaving requirements. According to the requirement of the multi-layer weaving and the characteristics of carbon fiber, 3 d virtual prototype model of carbon fiber multilayer diagonal loom is established by applying the 3 d design software Solidworks and using the mechanical analysis software ANSYS analyses the mechanical properties of the key parts in different working conditions. Virtual prototype design ensures the rationality and reliability of the design of the whole machine.

Introduction

In recent years, carbon fiber has become a hot topic. More and more carbon fiber composite materials because of its unique and excellent performance, is widely applied in aerospace and other fields [1, 2]. 3D woven carbon fiber is the rapid development of a new type of fabric structure and is a kind of the whole fiber reinforced skeleton interwoven by the continuous fiber in three-dimensional space according to certain rule and form [3]. However, carbon fiber multi-layer weaving equipment in our country is still in its infancy, in order to adapt to the needs of multi-level weaving equipment, this paper puts forward a set of let-off mechanism which is suitable with multi-layer weaving equipment.

Through in-depth analysis and studying the loom let off and the characteristics of carbon fiber, Using the theory of modern design method of textile machinery carries on the design of the let-off mechanism of carbon fiber multilayer diagonal loom based on using mathematical software to establish mathematical model of the tension of each layer of road rules of yarn, optimizes and chooses the motion of multi-layer warp, studies the key technology of carbon fiber let off, and realizes carbon fiber multi-layer weaving process of theoretical innovation. The design of the let-off mechanism of carbon fiber multilayer diagonal loom not only can provide the experiment platform the study of the theory of the carbon fiber weaving process and contribute to the research and development of new carbon fiber fabric, but also can make its directly used in production, liberate the workforce, improve the production efficiency and more likely can break the carbon fiber weaving equipment and technology blockade of the European and American countries.

Virtual prototype design in Solidworks

Let-off mechanism is mainly to achieve that in the weaving process, along with the formation of the fabric and away from knitting, weaving shaft releases corresponding length of warp and keep the warp tension to ensure the continuous of weaving. In actual production, the let-off amount range should be as large as possible in order to meet the needs of many varieties. In order to improve the quality of the products, the dynamic response of the let-off mechanism should be faster to timely follow the change of the tension and adjust the let-off amount; Warp send amount shall conform to the requirements of different weft density of fabric production [4].

Carbon fiber bundle is composed of a number of carbon fiber, the tensile strength is big, but because of the carbon fiber can't bear the larger radial friction and the carbon fiber bundle cannot twist when weaving, therefore in the process of the yarns running should try to reduce the sliding friction between the carbon fiber bundle and mechanisms and the carbon fiber bundle is flat twist [5].

According to the analysis of let-off mechanism and the performance of carbon fiber, using Solidworks combining top-down and bottom-up design method carries on the virtual prototype design of the let-off mechanism, it includes three parts, positive let off unit, Negative tension control unit and Yarn curl device. Fig. 1 is the virtual prototype model of the let-off mechanism of carbon fiber multilayer diagonal loom.

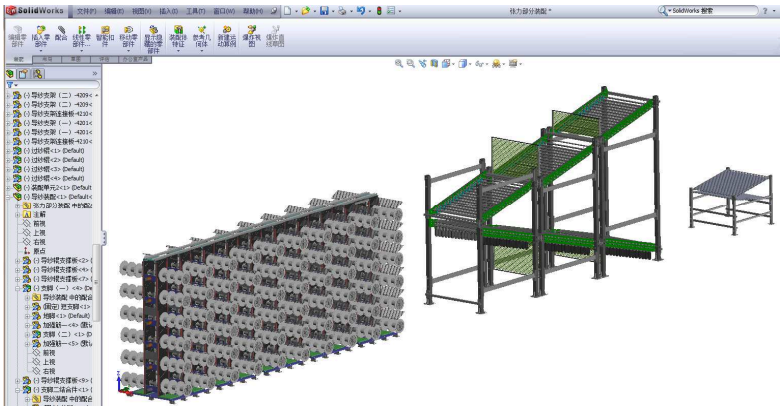

Fig. 1 The virtual prototype model of the let-off mechanism of carbon fiber multilayer diagonal loom

Mechanics analysis of key parts of let-off mechanism

The main shaft of carbon fiber multilayer diagonal loom let off is the key parts for let off tension control. According to the requirement of the host to let off par, Let off the rotation of the spindle to intermittent, And in order to guarantee the stability of the let-off system and the warp sheet fed yarn formation, Let off the largest cantilever part of spindle shape variables should be controlled within 0.5 mm, Using ANSYS software to the let-off mechanism of different diameter of axle spindle to check full load, Can be accurately obtained variable in the shape of the beam under different diameter.

Import the geometric model of the shaft. There are two kinds of methods to establish the model of part in ANSYS: (1) direct method, directly in the ANSYS according to the geometric shape of mechanical structure creates nodes and elements. Because of complex using of ANASYS software modeling, the direct method is applicable to simple mechanical structure system model. (2) Indirect method, first by the commonly used 3 d drawing software such as Solidworks and Pro/e model, etc. Again through model transformation, the geometric mode is imported to ANSYS. This way of operation can simplify the modeling process. Apply to import structure which is more complex mechanical structure system. After established the model geometry, meshing is determined by the boundary grid. Each line segment is divided into several elements. After determining the number and size of each edge elements, the interior of the ANSYS program can automatically generate the mesh. Automatically generate nodes and elements, and at the same time to complete the finite element model. The part after importing the ANSYS is shown in Fig. 2.

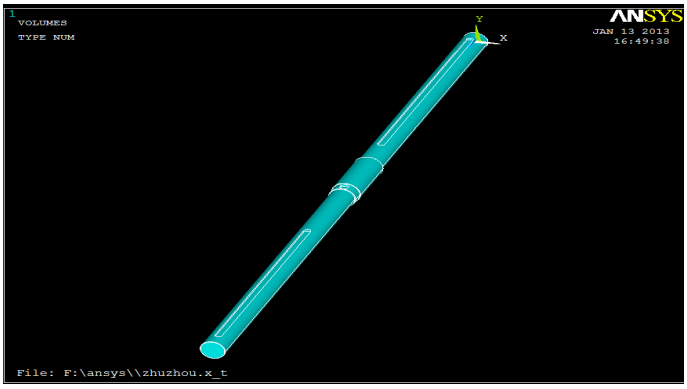

Fig. 2 Spindle parts ANSYS model

Meshing. Let off the spindle brand of 45 # steel. For material properties, Young's modulus is E = 2.09 e11 pa, Poisson's ratio u = 0.269 the density of 7890 kg/m3, According to the structure characteristics of the spindle, this model with solid element. The Structural Mess Solid Tet 10 node187, Using ANSYS grid partition function, various properties of meshing Settings, Grid can be divided into: Attribute assignment set, intelligent classification level control, Unit size control, Divide the shape set and meshing, Refine the grid control.ANSYS level of smart grid can be divided into 10 levels. The 10th level is the rough classification, the default level for level 6. The model grid level 6.

Boundary conditions and the results of analysis. Boundary constraints are an important step in the analysis of the finite element model. Through to the misalignment neck shaft parts imported into ANSYS is analyzed. Not the shape of the coaxial neck can be obtained under the maximum stress strain of the spindle. Fig. 3 is the analysis of the results of the shaft with diameter of 30 mm. Fig. 4 is the analysis of the results of the shaft with diameter of 40 mm. Fig. 5 is the analysis of the results of the shaft with diameter of 50 mm. Fig. 6 is the analysis of the results of the shaft with diameter of 65 mm.

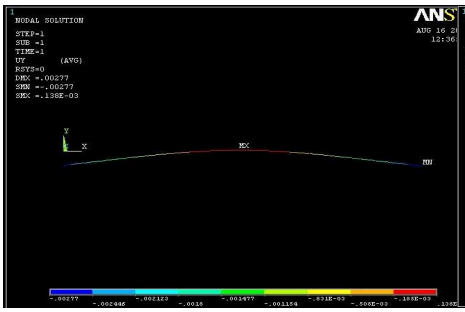

Fig. 3 Journal 30 mm analysis results

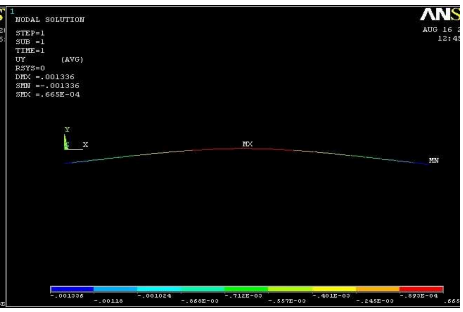

Fig. 4 Journal 40 mm analysis results

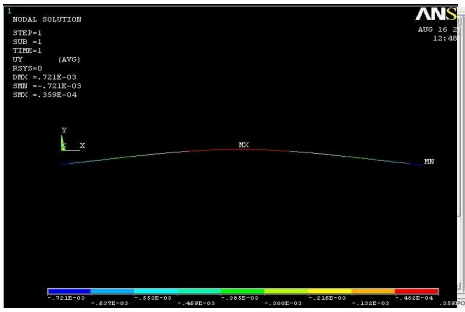

Fig. 5 Journal 50 mm analysis results

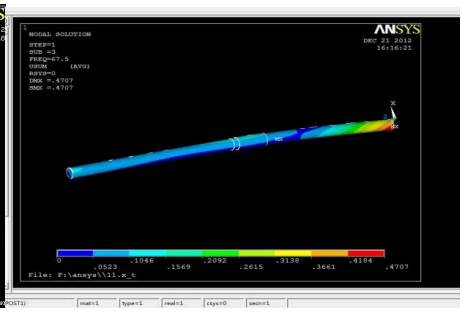

Fig. 6 Journal 65 mm analysis results

Analysis conclusions. Through the mechanical analysis of the shaft with different diameters, the deformation of the shaft with diameter of 65 mm is the smallest, 0.471mm < 0.5mm. It meets the design requirements, therefore, let off unit shaft diameter is 65 mm.

Conclusions

The let-off mechanism of carbon fiber multilayer diagonal loom is designed successfully; it can meet the fabric weaving of 30 layers.

Based on application of the modern design method and CAD/CAE tools, the virtual prototype model of the let-off mechanism is established and meets the actual needs of carbon fiber multilayer diagonal loom.

Acknowledgement

This research has been supported by the National 12th Five-technology Support Key Projects(2011BAF08B02).Qin Jianfeng also thanks Advanced Mechatronics Equipment Technology Tianjin Area Major Laboratory. The authors thank Jiang Xiuming for his valuable comments and helpful discussions.

References

[1] ZHANG J, FOX B L. Characterization and analysis of delamination fracture and nanocreep properties in carbon epoxy composites manufactured by different processes [J]. Journal of Composite Materials, 2006, 40(14): 1287-99.

[2] FISHPOOL D T, REZAI A, BAKER D, et al. Interlaminar toughness characterisation of 3D woven carbon fibre composites [J]. Plastics, Rubber and Composites, 2013, 42(3): 108-14.

[3] BEHERA B K, MISHRA R. 3-Dimensional weaving [J]. Indian Journal of Fibre & Textile Research, 2008, 33(3): 274-87.

[4] BILISIK K. Dimensional stability of multiaxis 3D-woven carbon preforms [J]. Journal of the Textile Institute, 2010, 101(5): 380-8.

[5] LAVIN J G. Chapter 5: Carbon fibres [M]. Woodhead Publishing Limited. 2001: 156-90.

Advanced Materials Research Vols. 846-847 (2014) pp 65-68

doi:10.4028/www.scientific.net/AMR.846-847.65

A simple, superior, practical design of brushless DC motor system

Xiaozhuang Gao [1, a], Peng Zhang [1,a] Wei Wang [1,a]

[1] Wuhan Ordnance NCO Academy of PLA,Wuhan

[a]email：gao_xzhwh@163.com

Keywords: brushless DC motor automatic control circuit

Abstract. The article mainly introduces the design and application of a small power brushless DC motor drive control system circuit, describes the special control function of the gate circuit chip, gives a typical application circuit, and explains.

Introduction

Brushless DC motor has the characteristics of small size, light weight, high efficiency, low noise and high reliability, so it is widely used in projects like radar servo system. Currently, the brushless DC motor system control circuit are generally composed of application specific integrated circuit (ASIC), FPGA, microprocessors, digital signal processor (DSP) and other form s of components, circuits of which are relatively complicated and costly. This paper provides a control circuit which is composed of four pieces of ordinary logic gate integrated circuit. With less components, fast logic operation, convenient debugging, stable and reliable performance, the composition of the brushless DC motor drive control system is greatly simplified, and price ratio increases. Thus, it is suitable for applications whose requirements of motor control are not very high.

1. System composition

The drive current of brushless DC motor（BLDCM）is hundred-percent alternating, so the electronic switch control circuit which provides alternating current is needed. Therefore, the application of brushless DC motor is a no closed loop automatic control system composed of electronic switch control circuit, brush DC motor, and position sensor, as shown in Figure 1. In the structure, brushless DC motor and the position sensor are devices, and the electronic switch control circuit is a circuit board. [1]

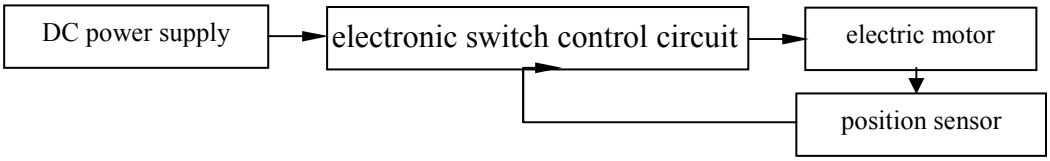

Figure 1 Block diagram

2. System function

It is not difficult to see from Figure 1, that the control system is the position sensor and the electronic switch control circuit. Position sensor converts the position signal of rotor to electrical signal, and then controls the communication of stator windings through the electronic switch control circuit. According to the principle of the motor, obviously, the control system constitutes a reversing device to ensure the normal operation of the motor, which makes the magnetic field generated by the stator winding and the rotor field generated by the rotor magnetic steel always maintain the angle of around 90 ° in electrical angle in space. Thus the maximum electromagnetic torque is generated to drive the motor to rotate. [2]

As shown in Figure 2, the electronic switch control circuit composed of a logic gate switch control circuit and a power driving circuit achieves two functions of the position signal processing and power logic switch. According to the position feedback signal, the logic gate switch control

circuit provides commutation driving signals to trigger the power driving tube through a certain logic operation, outputs square wave voltage required by the motor stator armature to make the winding phase current commutate according to a certain order with the changes of the rotor position, thus generating a leaping rotating magnetic field In the stator windings. According to the law of electromagnetic induction, energized stator windings will be affected by electromagnetic forces in the permanent magnets of the rotor, and drag the rotor to rotate in a certain direction. Since the conduction sequence of the power transistor is synchronized with the rotor position, it plays a role of mechanical commutator. [3] [4]

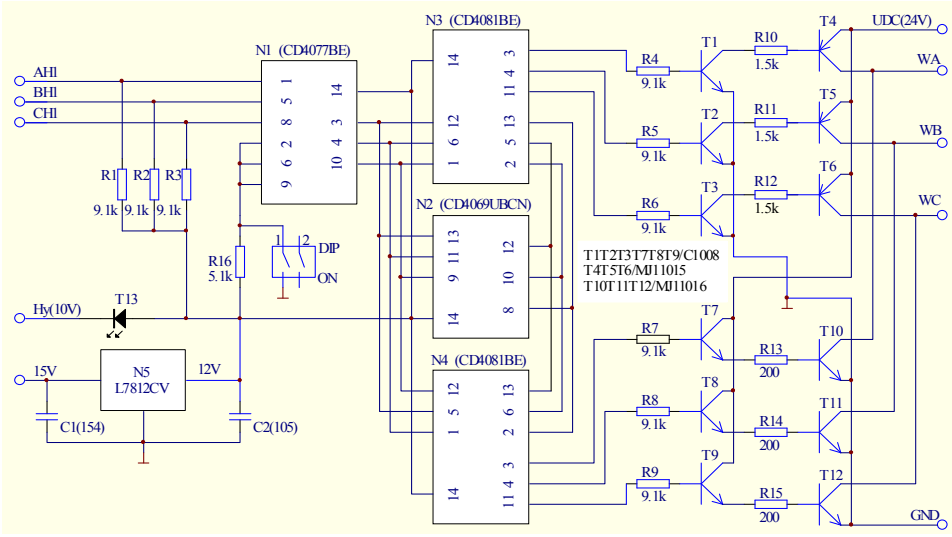

Figure 2 The control circuit diagram

Position sensor detects the magnetic pole position and speed of the rotor in the brushless DC motor. Permanent magnet brushless DC motor is a closed electromechanical integration system. It takes the rotor pole position signal as the commutation signal of the electronic switch control circuits to accurately detect the rotor position, and switches the power driving device in time according to the rotor position, which is the key to the normal operation of the brushless DC motor.

3. Operating principle

The three position signal AH1, BH1, CH1 generated by the position sensor are sent to the four exclusive NOR (XNOR) gate N1. The waveform of three signals output does not change after exclusive NOR with high level, and the signals are sent to six NOT gate N2 and four AND gate N3, N4. After reversed by N2, the output signals are sent to N3 and N4. Under the effect of a positive and a negative signal output by N1 and N2, N3 and N4 output six logic switch signals of different state, and then turn 24V AC into DC via pushing tube T1～T3, T7～T9 and power tube T4～T6,T11～T12, thus driving the brushless DC motor. The waveforms diagram is shown as Figure 3. [5]

Obviously, the electronic switch control circuit is essentially a self-control inverter. According to the different combination forms, logic gate control circuit outputs upper and lower MOSFETS these two groups of three-phase commutation logic signal under the bridge of in the position feedback signal, which turns the DC into AC, and outputs the three-phase AC required by the brushless DC motor, under the control of six power tubes. The output frequency is controlled by the rotor position signal. The frequency of motor input current is always synchronized with the motor speed, and the motor and the inverter do not generate vibration and desynchronizing.

Six power tubes adopt Darlington power amplifier tube, three MJ11015(PNP) and three MJ11016(NPN) each. The relationship between conduction sequence of each power tube and rotor position two-phase conducted by the three-phase six state brushless DC motor system is shown in Table 1, which complies with the principle of motor. [6]

The brushless DC motor using J46ZWS001 (J46ZWX01) type permanent magnet synchronous brushless DC motor, whose rated voltage is 24V, starting voltage is 2V, rated current is 1.84A, rated torque is 0.05N• m（490mN• m）,and rated speed is 6400r/min(6.24N• m).

The working voltage of N1, N2, N3 and N4 is 12V, which is provided by the three terminal regulator N5. N5 also provides working power for the brushless DC motor's position sensor, and the light emitting diode T13 cascaded in the circuit is used to indicate the position sensor working state.

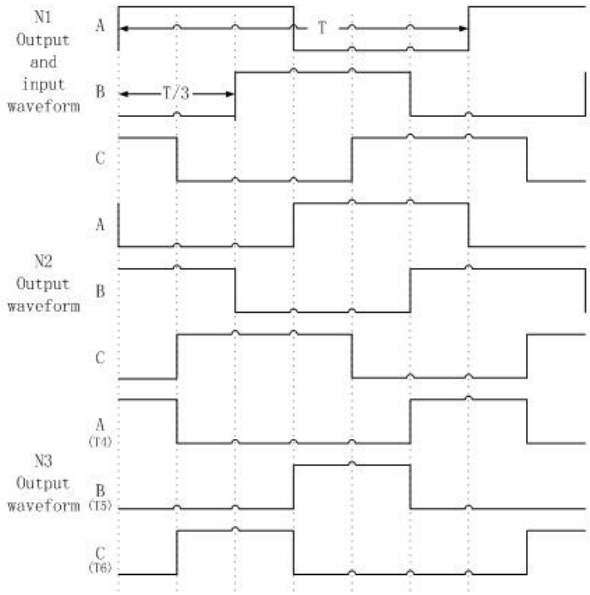

Figure 3 Waveforms diagram

Table 1 The relationship between conduction sequence of each power tube and rotor position

electrical degree	0°~60°	60°~120°	120°~180°	180°~240°	240°~300°	300°~360°
conductive power tube	T4T11	T6T11	T6T10	T5T10	T5T12	T4T12
conduction phase	A+B-	C+B-	C+A-	B+A-	B+C-	A+C-
instruction	+ shows that current flows in from head end, and flows out from back end. - shows that current flows in from back end, and flows out from head end					

The control circuit board uses 24V and 15V two kinds of DC power supply, and can also use 24V only. Because N5 uses L7812CV three terminal regulator, its input voltage can adopt any value in the range from 14.5V to 27V, output voltage is 12V, and output current is 1.5A. [7]

DIP switch can change the direction of rotation of the brushless DC motor. The principle of which is: When DIP switch sets "OFF", N1 outputs A, B, C three position sensor signal and three high level, and the phase of the original A, B, C three position sensing signal do not change after XNOR; While when DIP switch sets "ON", N1 outputs A, B, C three position sensor signal and three low level, and outputs the opposite phase of the original A, B, C three position sensing signal after XNOR. Through the reversion of N2 and conjunction of N3 and N4, the two states exchange the output signal of N3 with that of N4, as shown in Table 2, which makes the current direction of the power tube formed in the winding of the motor opposite. [8]

Table 1 The relationship between the DIP switch position and the logic output

DIP	N1 output	N2 output	N3 output	N4 output
OFF	A,B,C	$\bar{A}$, $\bar{B}$, $\bar{C}$	$\bar{C}B$, $\bar{B}A$, $\bar{A}C$	$B\bar{C}$, $A\bar{B}$, $C\bar{A}$
ON	$\bar{A}$, $\bar{B}$, $\bar{C}$	A,B,C	$B\bar{C}$, $\bar{A}B$, $C\bar{A}$	$\bar{C}B$, $\bar{B}A$, $A\bar{C}$

As the system works in one steering over a long period of time, once toggled at the first time the system works, the switch never need toggling anymore. If the system is used to frequently change the steering, then just use the control signal frequently change its steering to replace the switch.

a：output A phase signal (T4-c,T10-c)

b：output B phase signal (T5-c,T11-c)

c：output C phase signal (T6-c,T12-c)

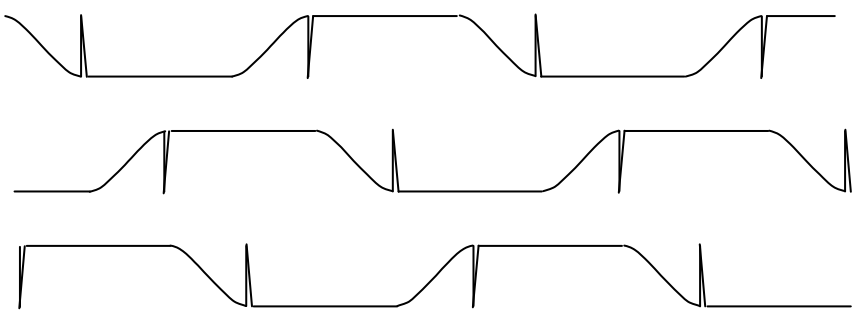

d：measured output waveform

References

[1] Brushless DC Motor Control System Changliang Xia Science Press Beijing 2009.2

[2] Small Power Permanent Magnet Motor Principle, Design and Application Jingwei Wei China Machine Press Beijing 2009.2

[3] Ho T. K., Hull J. J., Srihari S N. Decision combination in multiple classifier system. IEEE Trans on PAMI, 1994,16(1),66～75

[4] Gallant Stephen I. Neural Network Learning and Expert Systems. I Cambridge, Massachusetts, London, England The MIT Press 2010,195~198

[5] A.P.,Brits R. A clustering approach to incremental learning for feedforward neural networks Engel-brecht, Neural Networks, 2001. Proceedings. IJCNN'01. International Joint Conference on,2001,3:2019~2024

[6] A. Cha, H. M. RF Built-in Test and Enabling Technologies for Integrated Diagnostics. Proc of NAEC. 2005:207～211

[7] V. Szekeiy, M. Rencz. Thermal Monitoring of Self-Checking Systems. Journal of Electronic Testing: Theory and Application. 1998 (12), 81-92

[8] Erika F. Cota, Marcelo Negreiros, Luigi Carro and Marcelo Lubaszewski. A New Adaptive Analog Test and Diagnosis System. IEEE Transaction on Instrumentation and Measurement, 2000,49(2)

Advanced Materials Research Vols. 846-847 (2014) pp 69-72

doi:10.4028/www.scientific.net/AMR.846-847.69

Modeling and control of sludge pyrolysis in a fluidized bed reactor

LI Shi[1, a], ZONG Xiju[1,b] and HU Yan[1,c]

[1] School of Automation & Electrical Engineering, University of Jinan, Jinan 250022, Shandong, China

[a]cse_lis@ujn.edu.cn, [b]cse_zongxj@ujn.edu.cn, [c]cse_huy@ujn.edu.cn

Keywords: sludge pyrolysis, fluidized bed, internal model control, model predictive control

Abstract. This paper is concerns with the study of modeling and control of sludge pyrolysis in a fluidized bed reactor. Firstly, a mathematical model is established for sludge pyrolysis in a fluidized bed furnace, mass balance and energy equations are established. Then, the model is linearized at the steady-state point, two linear models are derived: state space model and transfer function model. The transfer function model is used in internal model control (IMC), where the filter parameter is selected and discussed. The state space model is applied in model predictive control (MPC), where controller parameters of prediction horizon length and control horizon length are discussed.

Introduction

Sludge is one of the most important wastes produced by waste water treatment plant. The common disposal processes for sludge include landfill, agricultural compost and incineration. However, conventional disposal methods have certain limitations, such as landfill volume, toxic metals in soil, air pollutants regulation [1]. Pyrolysis is the thermal decomposition of organic substances under oxygen lack. Pyrolysis involves a series of complex chemical reactions to decompose organic material. Sludge pyrolysis make mainly the products of oils, gases, char. The synthesized oil, char and gas can be used as alternative fuels, especially the synthesized oil, which can be reused as diesel fuel or industrial chemicals raw [2]. Compared with conventional disposals, sludge pyrolysis has lower pollutants and higher efficiency of energy recovery [3].

1 Mathematical model

Sludge pyrolysis in fluidized bed reactor. A fluidized bed reactor for sludge pyrolysis is presented in fig. 1. The inert gas N_2 is injected to guarantee an oxygen lacking environment. Sludge pyrolysis produce oil, gas, char and ash. Gas is separated from upper section and can be burned with char to supply pyrolysis energy. Sludge pyrolysis is endothermic. A heat input of fluidized bed reactor is installed to stabilize the temperature of sludge pyrolysis near 500°C, which is the optimal operation point [4].

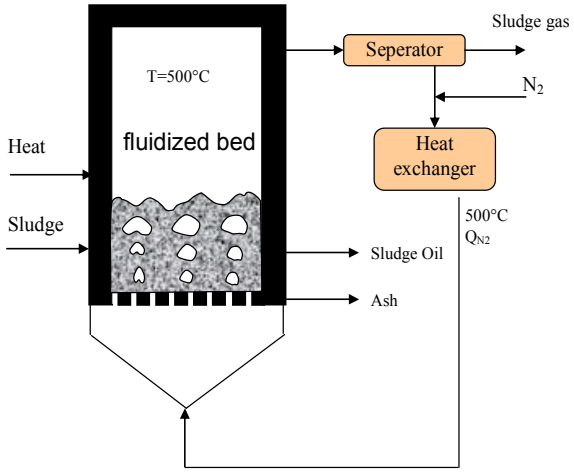

Fig. 1 Fluidized bed reactor for sludge pyrolysis

Nonlinear model. The fluidized bed reactor is supposed to be thermally isolated and perfectly mixed, i.e. the entering fuel is instantaneously mixed and uniformly dispersed in the furnace volume. Sand is supposed to be chemically inert. Sludge pyrolysis is supposed to be a simple reaction with second order.

$$sludge \rightarrow char + gas + oil + ash + \Delta H \tag{1}$$

where ΔH is the pyrolysis enthalpy, which is positive due to endothermic reaction. The reaction rate can be expressed as:

$$r = km^2 \tag{2}$$

where r is the reaction rate, m is the sludge mass in fluidized bed reactor, k is the reaction rate constant, which are based on the Arrhenius law:

$$k = k_0 \exp(-\frac{Ea}{RT}) \tag{3}$$

Mass and energy conservations are derived:

$$\frac{dm}{dt} = Q_b - k_0 \exp\left(-\frac{E_a}{RT}\right)m^2 \tag{4}$$

$$c_{ps}m_s\frac{dT}{dt} = c_{pN2}\rho_{N2}Q_{N2}(T_{in} - T) - \Delta H \times \left(k_0 \exp(-\frac{E_a}{RT})m^2\right) + H_{in} \tag{5}$$

Control objectives. The control objective is to stabilize the pyrolysis temperature at its optimal value of 500°C (773 Kelvin). Disturbances are sludge feed rate (Q_b), nitrogen flow rate (Q_{N2}) and temperature of nitrogen feed (T_{in}). The heat supply (H_{in}) is considered as the manipulating variable, and pyrolysis temperature (T) is the measured output.

2 Model linearization

Most control methods use linear model, which can be calculated by Taylor approximation of nonlinear model at steady-state point. The nonlinear model written by equation (4)-(5) can be expressed in a generalized form:

$$\begin{cases} \dot{x} = f(x,u) \\ y = g(x,u) \end{cases} \tag{6}$$

After linearization, linear state space model is obtained:

$$\begin{cases} \dot{x} = Ax + Bu \\ y = Cx \end{cases} \tag{7}$$

with

$$A = \begin{bmatrix} \frac{\partial f_1}{\partial x_1} & \frac{\partial f_1}{\partial x_2} \\ \frac{\partial f_2}{\partial x_1} & \frac{\partial f_2}{\partial x_2} \end{bmatrix} \quad B = \begin{bmatrix} \frac{\partial f_1}{\partial u} \\ \frac{\partial f_2}{\partial u} \end{bmatrix} \quad C = \begin{bmatrix} 0 & 1 \end{bmatrix} \tag{8}$$

State space model can be transformed to transfer function:

$$\hat{G}_p(s) = \frac{y(s)}{u(s)} = \frac{1.43(s+0.07)}{(s+0.12)(s+0.003)} \tag{9}$$

State space model and transfer function model will be used in controller design at following sections.

3 Internal model control

Internal model control (IMC) is a method that controller design can be acquired directly from mathematical model. IMC configuration is presented in fig. 2. IMC is constituted by controller and filter. Controller can be designed directly as an inverse form of process model; filter is normally one low-pass filter, which can attenuates mismatch of real process and mathematical model [5]. The IMC controller is written as follows:

$$G_c(s) = \hat{G}_p^{-1}(s)f(s) \tag{10}$$

Filter is normally designed as a low-pass filter of first order:

$$f(s)=\frac{1}{\lambda s+1} \tag{11}$$

where λ is the only parameter tuned in IMC design, the value of λ decides the performance of controlled system.

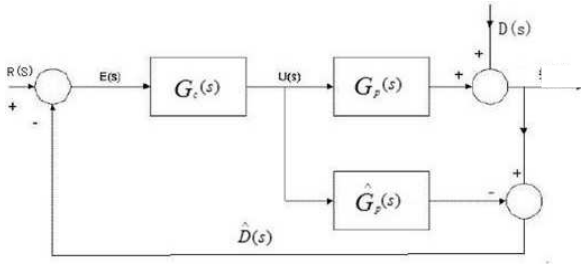

Fig. 2 IMC configuration

The simulation result of IMC controller is presented in fig.3. Results of three different values of filter parameter are compared. When λ increases, performance of controlled system becomes slower, in contrast, the system becomes more robust.

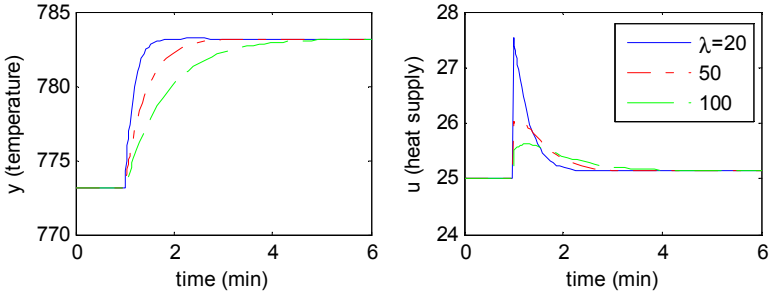

Fig. 3 Simulation results of IMC for different filter parameters (λ=20, 50, 100)

4 Model predictive control

Model predictive control uses a model to predict the model output in a finite horizon, the error between model output and desired value can be minimised by optimization method [6]. The optimization critere is normally expressed as:

$$J=\sum_{i=1}^{P}\left\|\hat{y}(k+i|k)-r(k+i|k)\right\|_Q^2+\sum_{i=0}^{M-1}\left\|\Delta u(k+i|k)\right\|_R^2 \tag{12}$$

The prediction horizon length is P, the control horizon length is M. Q and R are seperately the weights of outputs errors and control variables. At every step, MPC calculates the optimal sequence of control variable, which satifies the constraints:

$$\begin{aligned}&\min_{\Delta u_k,\cdots\Delta u_{k+M-1}} J\\ &s.t.\quad \text{model equations and constraints}\end{aligned} \tag{13}$$

where the model is state space model of equation (4)-(5). Constraints can be expressed as:

$$\begin{aligned}&y_{\min}\le\hat{y}_{k+i}\le y_{\max}\\ &u_{\min}\le u_{k+i}\le u_{\max}\\ &\Delta u_{\min}\le\Delta u_{k+i}\le\Delta u_{\max}\end{aligned} \tag{14}$$

Output feedback is normally applied to correct the error between model output and measured values:

$$\begin{aligned}&\hat{y}^c(k+i|k)=\hat{y}(k+i|k)+d_k\\ &d_k=y_k-\hat{y}(k|k)\end{aligned} \tag{15}$$

In the MPC design, prediction horizon length is P=5, control horizon length is M=1, the weighs are Q=1, R=0.1.

Fig. 4 presents the MPC results of tracking reference point for different prediction horizon length P. After 80s, the reference point is increased by 20, two different prediction horizon lengths are compared: P=1 and P=5. As P=5, the controlled system is more robust and the change of manipulated variable u is more realistic.

Fig. 5 presents the MPC results of tracking reference point for different control horizon length (M=1 and 3). The figure reveals that increasing control horizon length can accelerate the controlled system, but more M aggravates calculating burdens. Therefore, M is normally equal to 1 or 2.

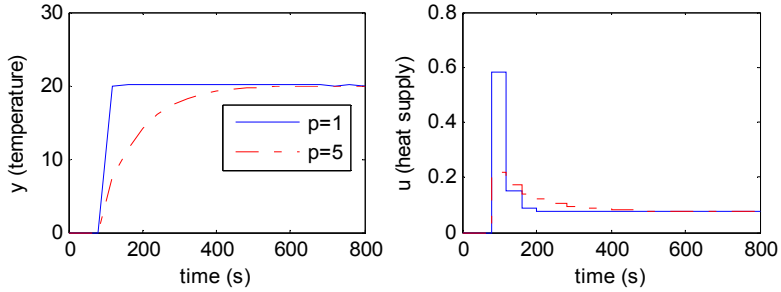

Fig. 4 Simulation results of MPC tracking the reference point at different P (P=1 and 5, M=1)

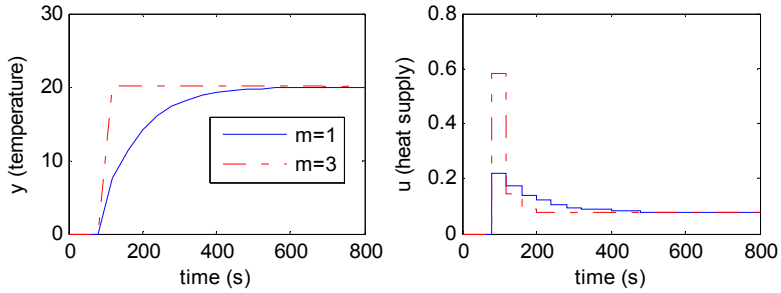

Fig. 5 Simulation results of MPC tracking the reference point at different M (M=1 and 3, P=5)

5 Conclusions

This paper proposes a nonlinear model of sludge pyrolysis in a fluidized bed reactor. The nonlinear model is linearized at steady-state point to obtain tranfer function model and state space model. Transfer function model is used in IMC design, where the filter parameter selection is dicussed. State space model is used in MPC design, the parameters of prediction horizon lenght and control horizon length are discussed.

Acknowledgements

This work is partially supported by National Natural Science Foundation of China (11201179), Shandong Provence Natural Science Foundation (ZR2011FQ004) and Scientific Research Foundation for the Returned Overseas Chinese Scholars, State Education Ministry (SQT1302).

References

[1] J. Werther, T. Ogada. Sewage sludge combustion. Progress in energy and combustion science, 1999, 25: 55-116.
[2] Y.Kim, W. Parker. A technical and economic evaluation of the pyrolysis of sewage sludge for production of bio-oil. Bioresource Technology, 2008, 99(5): 1409-1416.
[3] D. Fytili, A. Zabaniotou. Utilization of sewage sludge in EU application of old and new methods – A review. Renewable and Sustainable Energy Reviews, 2008, 12 (1): 116-140.
[4] B.W. Bequette. Process control: modeling, design, and simulation, Prentice-Hall, 2003.
[5] S.J. Qin, T.A. Bedgwell. A survey of industrial model predictive control technology. Control Engineering Practice, 2003, 11: 733-764.

Advanced Materials Research Vols. 846-847 (2014) pp 73-76

doi:10.4028/www.scientific.net/AMR.846-847.73

Model predictive control of circulating fluidized bed coal combustor

LI Shi, HU Yan and ZONG Xiju

[1]School of Control Science & Engineering, University of Jinan, Jinan, 250022, Shandong, China

[a]mrlishi@gmail.com, [b]cse_huy@ujn.edu.cn, [c]cse_zongxj@ujn.edu.cn

Keywords: circulating fluidized bed combustor, coal combustion, modeling, model predictive control

Abstract. This paper is concerns with the study of model predictive control of a circulating fluidized bed coal combustor. A nonlinear mechanical model is proposed based on a pilot plant and representative of the main combustion phenomena. The nonlinear model is linearized at the steady-state point, linear state-space model is obtained. Model predictive control (MPC) strategy is applied using linear model. Simulation results are presented and discussed.

Introduction

Starting in the 1980th the circulating fluidized bed technology has been widely used industrially for coal or waste materials combustion and biomass gasification. Due to the high complexity of the hydrodynamic behavior and chemical reactions schemes, the dynamical behavior of the circulating fluidized bed combustion is not well known. Conventional control strategies are difficult to deal with such process systems [1]. Model predictive control (MPC) is considered as one of the most attractive methods in process control, due to its inherent capability of treating multi-inputs multi-outputs systems with various kinds of constraints [2-4]. In this paper, a general approach is proposed for MPC design.

1 Mathematical modeling

Circulating fluidized bed Combustor. Fluidization operation consists in maintaining in suspension of homogeneous particles by a gaseous fluid with a fast velocity. In the circulating fluidized bed, which principle is presented in fig. 1, the gas is distributed through a distributor from the bottom of the furnace. The injected air flow rate is sufficiently rapid to carry away solid particles to the top of the furnace and assure the perfect mixing with particles and also a uniform furnace temperature. The particles movement is realized by gas bubbles surrounding the particles. The particles are almost constituted of sand, which stabilize the process temperature by inducing thermal inertia.

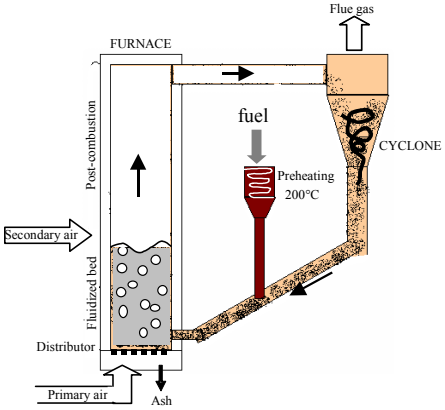

Fig. 1 Circulating Fluidized bed combustor pilot [5]

In the post-combustion area, gas reactions continue, and the introduction of a secondary air accelerates the moving up particles and gives more oxygen to guarantee the complete combustion of fuel. A cyclone separates the particles that are recycled to the bed, from the flue gas, which is getting out of the plant. Ash is removed from the distributor.

CFBC model. The circulating fluidized bed is supposed to be thermally isolated and perfectly mixed, i.e. the entering fuel is instantaneously mixed and uniformly dispersed in the furnace volume. Decomposition of coal in gaseous and particles elements by the process of devolatilization or pyrolysis is not taken into account in the model. Sand is supposed to be chemically inert. Coal particles are recycled by the cyclone with an efficiency factor θ.

The combustion reaction is:

$$C + O_2 \rightarrow CO_2 + heat \tag{1}$$

Oxygen is supposed to be sufficient so that the reaction is complete; otherwise carbon monoxide may be produced.

Based on these assumptions, three mass balances and two energy balances can be established.

$$\begin{cases} \dfrac{dm_C}{dt} = Q_e - r_C - (1-\theta)Q_s \\ \dfrac{dm_{CO_2}}{dt} = -Q^v \dfrac{m_{CO_2}}{V_R} + \beta r_C \\ \dfrac{dm_{O_2}}{dt} = f_{O_2}^w Q_{a0}^v \rho_{a0} - Q^v \dfrac{m_{O_2}}{V_R} - \gamma r_C \end{cases} \tag{2}$$

$$\begin{cases} \dfrac{dT_C}{dt} = \dfrac{1}{c_{pc} m_C}[c_{pc} Q_e (T_e - T_C) - c_{pc} r_C T_C - r_C \Delta H - A_f h (T_C - T_g)] \\ \dfrac{dT_g}{dt} = \dfrac{1}{c_{ps} m_s}[-f_{O_2}^w Q_{a0}^v \rho_{a0} c_{pg} T_g + \dfrac{c_{pg} Q_{a0}^v T_g^2}{V_R T_0}(m_{CO_2} + m_{O_2}) + c_{pg}(\gamma - \beta) r_C T_g + c_{pg} Q_{a0}^v (\rho_{a0} T_a - \rho_{g0} T_g) + A_f h (T_C - T_g)] \end{cases} \tag{3}$$

The reaction rate of the combustion, noted r_C is based on the Arrhenius law and can be expressed as:

$$r_C = k\, m_C m_{O_2} \text{ and } k = k_0 \exp(-\frac{E_a}{RT_C}) \tag{4}$$

The coal is recycled by a cyclone with an efficiency factor θ. The air flow rate and the coal feed rate entering in the cyclone are reconstructed as follows:

$$Q^v = Q_{a_0}^v \frac{T_g}{T_0} \tag{5}$$

$$Q_s = G_s A \frac{m_C}{m_S + m_C} \tag{6}$$

Control objectives. The control objective is to stabilize the furnace temperature at its optimal value of 850°C (1123 Kelvin). Disturbances are coal feed rate variations (Q_e), Temperature of coal feed (T_e) and temperature of air feed (T_a). The air flow rate ($Q_{a0}{}^v$) is considered as the manipulating variable, and gas temperature (T_g) is the measured output.

2 Model linearization

Due to mature and reliable linear theory, most control method is linear control, which is based on linear models. Nonlinear model can be linearized to obtain linear model, the most popular way is linearization at the steady-state point by Taylor approximation.

Suppose that the nonlinear model can be written as follows:

$$\begin{cases} \dot{x} = f(x,u) \\ y = g(x,u) \end{cases} \tag{7}$$

where x is system variables of n dimensions, u is input variables of p dimensions, y is output variables of m dimensions.

The objective of linearization at the steady-state point is to derive a linear model with such a form:

$$\begin{cases} \dot{x}' = Ax' + Bu' \\ y' = Cx' + Du' \end{cases} \tag{8}$$

Matrices of A, B, C, D can be calculated by equations as follows:

$$A_{ij}=\frac{\partial f_i}{\partial x_j}\Big|_{(x_0,u_0)} \quad B_{ij}=\frac{\partial f_i}{\partial u_j}\Big|_{(x_0,u_0)}$$
$$C_{ij}=\frac{\partial g_i}{\partial x_j}\Big|_{(x_0,u_0)} \quad D_{ij}=\frac{\partial g_i}{\partial u_j}\Big|_{(x_0,u_0)} \tag{9}$$

where $x'=x-x_0, u'=u-u_0, y'=y-y_0$, which indicate that the variables of linear model are deviations from steady-state point, x_0, u_0 and y_0 are steady-state point of nonlinear model.

Based on the equation (9), the nonlinear model (2)-(6) can be linearized to obtain a linear state-space model, which will be used in MPC design.

3 Model predictive control

Model predictive control uses a model (such as step response model, transfer function, state space model, ARX) to predict the model output in finite horizon in future, the error between model output and desired value can be minimized by optimization method. The optimization criterion is normally expressed as:

$$J=\sum_{i=1}^{P}\left\|\hat{y}(k+i|k)-r(k+i|k)\right\|_Q^2+\sum_{i=0}^{M-1}\left\|\Delta u(k+i|k)\right\|_R^2 \tag{10}$$

where $\hat{y}(k+i|k), r(k+i|k), \Delta u(k+i|k)$ are values of model output, reference point and control variable variation at k+i time, calculated by k time. The prediction horizon length is P, the control horizon length is M. Q and R are separately the weights of outputs errors and control variables. At every step, MPC calculates the optimal sequence of control variable, which satisfies constraints:

$$\min_{\Delta u_k,\cdots\Delta u_{k+M-1}} J$$
$$s.t. \quad \text{model equations and constraints} \tag{11}$$

where the model is state space model. Constraints can be expressed as:

$$y_{\min}\le\hat{y}_{k+i}\le y_{\max}$$
$$u_{\min}\le u_{k+i}\le u_{\max} \tag{12}$$
$$\Delta u_{\min}\le\Delta u_{k+i}\le\Delta u_{\max}$$

Output feedback is normally applied to correct the error between model output and measured values:

$$\hat{y}^c(k+i|k)=\hat{y}(k+i|k)+d_k$$
$$d_k=y_k-\hat{y}(k|k) \tag{13}$$

In the MPC design, prediction horizon length is P=5, control horizon length is M=1, the weighs are Q=1, R=0.1. The constraints are defines as follows:

$$\hat{y}_{k+i}\le 100$$
$$-20\le u_{k+i}\le 20 \tag{14}$$
$$-5\le\Delta u_{k+i}\le 5$$

Fig. 2 presents the MPC results of tracking reference point for different prediction horizon length P. After 0.2 hour, the reference point is increased by 20, two different prediction horizon lengths are compared: P=1 and P=5. As P=5, the controlled system is more robust and the change of manipulated variable u is more realistic.

Fig. 3 presents the MPC results of tracking reference point for different control horizon length (M=1 and 3). The figure reveals that increasing control horizon length can accelerate the controlled system, but more M aggravates calculating burdens. Therefore, M is normally equal to 1 or 2.

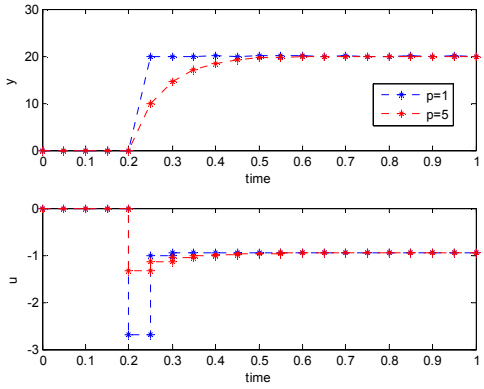

Fig. 2 Simulation results of MPC tracking the reference point at different P (P=1 and 5, M=1)

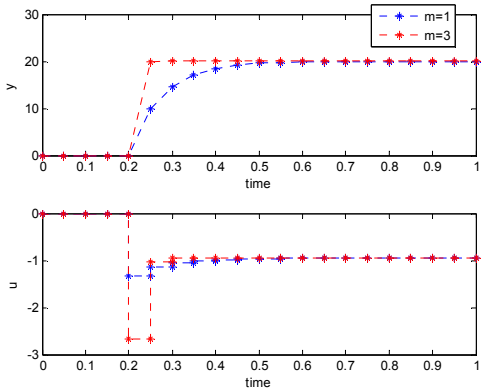

Fig. 3 Simulation results of MPC tracking the reference point at different M (P=5, M=1 and 3)

Conclusions

This paper proposes a nonlinear mechanical model of circulating fluidized bed combustor. The nonlinear model is linearized at steady-state point to obtain linear state space model, which is used in MPC design. The MPC with SS model and various constraints is applied and simulated in Matlab environment. The selection of prediction horizon length P and control horizon length M are discussed.

Acknowledgements

This work is partially supported by National Natural Science Foundation of China (11201179), Shandong Provence Natural Science Foundation (ZR2011FQ004) and Scientific Research Foundation for the Returned Overseas Chinese Scholars, State Education Ministry (SQT1302).

References

[1] G. Stephanopoulos. Chemical process control: an introduction to theory and practice, Prentice-Hall INC, Englewood Cliffs, 1984.

[2] B.W. Bequette. Process control: modeling, design, and simulation, Prentice-Hall, 2003.

[3] S.J. Qin, T.A. Bedgwell. A survey of industrial model predictive control technology. Control Engineering Practice, 2003, 11: 733-764.

[4] Allgöwer, F. & Zheng, A. Nonlinear model predictive conrol, 2000, Birkhäuser.

[5] P. Baussand, L. Lassagne, V. Jacob and P. Foster: Fresenius Envir. Bull, Vol.9 (2000), p. 544-551

Advanced Materials Research Vols. 846-847 (2014) pp 77-85

doi:10.4028/www.scientific.net/AMR.846-847.77

Attitude Protection Control for Side Stick-operated Aircraft

DONG Yiqun [1, a], ZHANG Lidong [1, b], ZHANG Yijun[1, c] and AI Jianliang [1, d]

[1]Department of Mechanics and Engineering Science, Fudan University, Shanghai China, 200433

[a]10110290003@fudan.edu.cn, [b]13110290005@fudan.edu.cn(correponding author),
[c]12210290016@fudan.edu.cn,[d] aijl@fudan.edu.cn

Keywords: Aircraft; side stick; attitude protection; Euler angles envelope; predictive control.

Abstract. A control framework to limit aircraft Euler angles (pitch/rolling) under adverse side stick command adding is introduced. Attitude envelope of the aircraft pitch/rolling angle is discussed based on geometrical position of the aircraft relative to the ground. Control law of is established by using linearized predictive control strategy. The simulation test presents the performance of attitude protection restricting the Euler angles within the required envelop at 1,000m. Based on the test work discussed herein, the control work proposed in this paper is believed to be applicable.

Introduction

An unintentional touch of stick input might unpredictably alter the flight attitude of the aircraft, which would cause the airplane to be Loss-of-Control (LoC). LoC has been the number one contributing factor to fatal airline accidents, and has resulted in more fatalities than any other factor during the past ten years [1-3]. On March 31st 2012, a JAL Japan Airlines Boeing 777-200, registration JA701J performing flight JL-82 from Shanghai to Tokyo with 296 passengers and 12 crew, was on approach to Haneda Airport at 16:10L when in the flare the aircraft caught a gust prompting the crew to go-around, the tail however contacted the runway surface leaving tracks of about 7 meters/23 feet length and about 50cm/1.6 feet width on the runway[1].On July 6th 2013, an Asiana Boeing 777-200, registration HL7742 performing flight OZ-214 from Seoul to San Francisco with 291 passengers and 16 crew, touched down short of runway 28L impacting the edge separating the runway from the San Francisco Bay 115 meters ahead of the runway threshold while landing on San Francisco's runway 28L at 11:27L, the tail plane, gear and engines separated. Three people are confirmed killed in the accident, 10 people are in critical condition[2].

All these accidents were related to the unexpected flight attitude in ground-proximity flight stage. As for civil aircrafts typically, they have long fuselage and wide wing span. A tiny change of the Euler angle of the aircraft will cause an obvious shift of the wingtips and other components. While in low altitude flight situations, these components are prone to interfere with the runway, which is unexpected and dangerous. Therefore, we decided to design an attitude protection control system to protect the aircraft from impact accidents, and guard the aircraft to land safely.

Control systems designed to protect aircrafts have been studied and employed for decades. With the rapid development of the active control technology, the stall/load-factor protection system has been applied in civil aircraft popularly. For instance, typical airliners like A320 series, B777 series are all equipped with mature protection system, which escorts the aircraft to fly safely. The design of AOA boundary limiter went through the stages from hard limit to soft limit. Early editions of F-8C plane adopted hard limit mode, then survival control system of F-4 equipped the single-stage polyline soft limit mode, and the AOA limiter of F-16 used two-stage polyline restriction scheme [6-9]. Whereas researches specific to attitude protection control were rarely published. We

thought the attitude protection shared many similar ideas with the AOA boundary limiter, but the slight modification may solve a thorny problem. The restriction of Euler angles can prevent the aircraft from interfering with the runway so as to protect the aircraft and passengers' life.

Based on the development of modern FBW control system [4,5], the side sticks control has been used broadly in civil aircrafts and is preferred by airplane manufactures like Airbus and COMAC China. The side sticks control has significant advantages like saving the valuable space in the cockpit and providing broader visual span for the pilots. Whereas there might be some innate drawback of side sticks. Generally, they do not provide direct feedback of the stick force, and the stick on each side works independently without mechanical interconnection. This might bring a challenge for the pilot to either perceive the real-time aircraft state, or the manual control status of other pilot, and a command signal-overlapping could happen. In adverse cases an abrupt change of the aircraft state would be encountered, as the command signals are literally being added from both pilots. Given such analysis, the adoption of side-stick control could worsen the already-problematic ground-proximity situation, and in this paper we try to address this issue. In our study, two approaches are included to address the side sticks command-overlapping problem. Prior to adoption of the two pilots' command signals, an adding logics is included to wash out unnecessary signals—an "unintentional touch" on the stick, for instance; also after the command signal is synthesized, inline control laws could be employed, so as to limit the aircraft state change within a reasonable threshold.

Attitude Envelope

Flight envelope is defined as a group of lines consist of flight points insuring the aircraft against dangerous situations. The flight control system may warn the pilots when the aircraft is approaching the threshold of the angle of attack, velocity, or flight height, etc. according to the envelope. In our study, a concept of the aircraft "attitude envelope" is adopted. Analogously, an "attitude envelope" imposes a restriction on pitch/rolling angle at each current flight altitude, which prevents the airframe from interfering with the runway.

The envelope for ground-proximity flight stage was elaborately designed. We believed that a reasonable attitude envelope should not only protect the objective aircraft from scratching with the runway but also reserve the maneuverability of the aircraft as far as possible. If we set the envelope only taking the tail and wingtips into account, other components would possibly hit the runway. On the other hand, if the constraint was too tight in order to avoid the impact, the aircraft will lose its maneuverability, which could lead to worse crash accidents for the aircraft cannot adequately turn off to evade the barrier. As a result, we must give consideration to both requirements when designing the attitude envelope.

To prevent the objective aircraft from interfering with the runway, $h*$ should greater than zero ($h*$ here is an 11-dimensional vector). Though we can obtain the scope of the safe Euler angles directly by solving the multi-dimensional inequalities, it is too cumbersome to implement the calculation. To simplify the problem, we reversed the known and unknown conditions. We calculated the attention points' height at each Euler angle at the selected flight altitude (by Eq. (2)). Then, we marked and picked out the numerical value of the Euler angle when the height of the lowest point equaled to zero. The picked out Euler angle value composed the scope of the safe Euler angles at the current altitude, namely, the rudiment of the attitude envelope.